A STUDY OF ORGANELLE Ca^{2+} DYNAMICS IN CARDIAC MUSCLE

By

DEBORAH FIDELIS REYNOLDS

Submitted in fulfilment of the degree
Doctor of Philosophy

to

University of Glasgow
Faculty of Biomedical & Life Sciences

February 2003

Abstract

Organelle Ca^{2+} dynamics of cardiac muscle were studied using fluorescent Ca^{2+} indicators and a bioluminescent Ca^{2+} probe, namely aequorin that was targeted to SR.

Enzymatically dissociated adult cardiac myocytes were subjected to prolonged incubation with acetoxymethyl (AM) derivatives of Fura-2, FuraFF and MgFura-2 which each have different Ca^{2+} affinities. This prolonged incubation allowed indicator loading into sub-cellular compartments. Permeabilisation with saponin and subsequent washout removed cytosolic component of the indicator. Results from the fluorescent indicator studies can be summarised as follows

1. Studies with Fura-2-AM loaded cardiomyocytes revealed the existence of a sub-cellular compartment or compartments, which exchanges Ca^{2+} passively with a very slow time course. The identity of this is unclear, although likely candidates include mitochondria and nuclear envelope
2. The signal from FuraFF-AM loaded cardiomyocytes appears to be almost exclusively from mitochondria with no contribution by SR.

Parallel studies were done with SR vesicles and mitochondria prepared from cardiac tissue. Mitochondrial signals were very similar to that from permeabilised cells. However, SR vesicles loaded with FuraFF-AM did not appear to be responsive to changes in external $[Ca^{2+}]$. The inability of AM loading to introduce dye with Ca^{2+} sensitivity into SR vesicles may be a consequence of low esterase activity. This may explain the lack of a clear SR signal in measurements from permeabilised cells.

An adenovirus vector was developed to allow over-expression of the bioluminescent Ca^{2+} sensitive protein aequorin specifically targeted to SR (Ad-CSQ-Aeq). Experiments were carried with these over-expressing cells in the presence of 5μM ruthenium red and therefore absence of RyR_2 Ca^{2+} flux. $[Ca^{2+}]_{CYT}$ was clamped at 162nM and 380nM. Under these conditions

$[Ca^{2+}]_{SR}$ was measured as 5.20 ± 0.230 x 10^{-4} M ($[Ca^{2+}]_{CYT}$ =162nM, *n*=6) and 1.21 ± 0.180 x 10^{-3} M ($[Ca^{2+}]_{CYT}$ =380nM, *n*=14).

The relationship between $[Ca^{2+}]_{SR}$ and rate of Ca^{2+} uptake in the absence of RyR_2 Ca^{2+} flux, revealed a non-linear lumenal dependence. High $[Ca^{2+}]_{SR}$ has a negative feedback effect upon SERCA2a resulting in a slower rate of Ca^{2+} uptake. The non-linearity of the lumenal dependence suggests a mechanism other than a simple trans-SR gradient.

Analysis of leak in the presence of 25μM thapsigargin and 5μM ruthenium red indicates a simple linear relationship between $[Ca^{2+}]_{SR}$ and the rate of Ca^{2+} leak. The kinetics of this relationship suggests a simple leak 'channel' or pathway, the identity of which is unclear. It is unlikely to be via RyR_2 or reverse mode of SERCA2a due to presence of inhibitors.

On the basis of a mean uptake and leak uptake curve an estimate of the equilibrium value of $[Ca^{2+}]_{SR}$ in absence of RyR_2 activity is approximately 960μM.

Declaration

The material contained within this thesis was carried out by myself. The material has not been submitted for the fulfilment of any other degree.

Some of the results obtained were published in abstract form and are detailed as follows.

Abstracts

Reynolds, D.F., Prestle, J., Sidler, T., Hasenfuss, G. and Smith, G.L. (2002) Measurement of intra-SR [Ca^{2+}] in isolated cardiac myocytes using a targeted aequorin probe. *J Physiol* **543P**. 60P

Reynolds, D.F. and Smith, G.L. (2001). Passive exchange of intracellular Ca^{2+} with a subcellular compartment in isolated cardiac myocytes. *J Physiol* **536P** 76*P*

Loughrey, C. M., Rankin, A., Reynolds, D. F., Hasenfuss, G., Prestle, J., Smith, G. L. (2002). FKBP12.6 overexpression alters the characteristics of SR Ca^{2+} release in permeabilised adult rabbit cardiac myocytes. *Biophys. J.* (Annual Meeting Abstracts) **82**: 66

Reynolds, DF, Smith, GL. (2001). Passive exchange of intracellular [Ca^{2+}] with a sub-cellular compartment in isolated cardiac myocytes *Biophys. J.* (Annual Meeting Abstracts) **80**: 588

Rankin,A., Reynolds, D.F., Maceachern, K.E., Hasenfuss, G., Prestle, J. and Smith, G.L. (2001) FK506-binding protein FKBP12.6 overexpression alters the characteristics of the Ca^{2+} transient and caffeine-induced Ca^{2+} release in adult rabbit cardiac myocytes. American Heart Association Scientific Sessions 2001. Abstract ID 109275

Seidler, T., Zibrova, D., Reynolds, D., Loughrey, C.M., Kania, A., Teucher, N., Wagner, S., Prestle, P., Kögler, H., Gerd Hasenfuss, G. and Smith, G.L FKBP12 Overexpression in Isolated Rabbit Cardiomyocytes Enhances Intracellular Ca2+ Transients, SR Ca2+ Content and Contractility. American Heart Association Scientific Sessions 2002. Abstract ID 104456

Abbreviations

AM	Acetoxymethyl
ANOVA	Analysis of variance
BAPTA	O,O'-Bis(2-aminophenyl)ethyleneglycol-N,N,N',N'-tetraacetic acid tetrapotassium salt, hydrate
BSA	Bovine serum albumin
$[Ca^{2+}]_{CYT}$	Cytoplasmic $[Ca^{2+}]$
$[Ca^{2+}]_{MIT}$	Intra-mitochondrial $[Ca^{2+}]$
$[Ca^{2+}]_{SR}$	Intra-SR $[Ca^{2+}]$
CaEGTA	Ca- ethyleneglycol bis(-aminoethylether)-N,N,N',N'-tetraacetic acid
CaUP	Ca^{2+} uniporter of mitochondria
cDNA	complimentary DNA
CICR	Ca^{2+} induced Ca^{2+} release
DHPR	Dihydropyridine receptor
E-C	Excitation-contraction
EGTA	ethyleneglycol bis(-aminoethylether)-N,N,N',N'-tetraacetic acid
ER	Endoplasmic reticulum
FCS	Foetal calf serum
FKBP	FK506 binding protein
FRET	Fluorescence resonance energy transfer
GFP	Green fluorescent protein
HEK 293	Hamster embryonic kidney 293 cells

HeLa	Cell line derived from a cervical carcinoma
HSR	Heavy SR vesicles
IP_3	Inositol 1,4,5 triphosphate
K_d	Dissociation constant
mAKAP	Anchor protein
MOI	Multiplicity of infection
NTA	Nitrilo-triacetic acid
PBS	Phosphate buffered saline
pfu	plaque forming units
PKA	cAMP dependent protein kinase
PP2a	Protein phosphatase 2a
RaM	Rapid mode of Ca^{2+} uptake
R_{max}	Maximum fluorescence ratio
R_{min}	Minimum fluorescence ratio
RuR	Ruthenium red
RyR	Ryanodine receptor
RyR_2	Ryanodine receptor isoform 2
RV	Right ventricle
SERCA2a	Sarcoplasmic/endoplasmic reticulum ATPase isoform 2a
SR	Sarcoplasmic reticulum
TG	Thapsigargin
YFP	Yellow fluorescent protein

Acknowledgements

I would like to thank everybody in Professor Godfrey Smith's group for all of their help (and for humouring me and laughing at my jokes!) throughout my PhD. I would especially like to thank Susan, Margaret-Anne, Sarah, Chris, Niki, Elspeth, Stewart and Niall for their friendship, helpful discussion and making Godfrey's lab an enjoyable place to work in. Thanks also to Anne and Aileen for their technical support.

Words cannot express how grateful I am to Godfrey for firstly giving me the opportunity to work within his group, but also his continued support, encouragement and never being too busy to help.

I would also like to thank Dr. Andrew Baker, Dr. Lorraine Work and Campbell Nicol for their help with adenovirus propagation. Also Professor Gerd Hassenfuss, Dr. Juergen Prestle and Dr. Tim Seidler, University of Goettingen for their help during my time within their group.

Finally I would like to thank my family, especially my mum Mary Reynolds and sisters Linda and Maria for helping me to keep things in perspective when times were challenging.

I would like to dedicate this thesis to the memory of my late father Walter Reynolds, whom was a remarkable person. I'm certain he would be very proud of me.

Contents

List of Figures and Tables

Chapter 1– General Introduction

Ca^{2+} has a pivotal role in the control of cell function. It is employed as an intracellular signal to regulate an array of diverse processes including fertilization, excitation-secretion coupling in secretory cells, proliferation, neuronal excitability and excitation-contraction coupling (EC-coupling) in muscle. Indeed Ca^{2+} was described as being a "Life and death" signal (Berridge MJ *et al.*, 1998).

1.1 Ca^{2+} in Cardiac EC-Coupling

Extensive research has allowed a greater understanding of the role that Ca^{2+} plays in cardiac EC-coupling. During each cardiac action potential, sarcolemmal L-type Ca^{2+} channels are activated as the result of propagation of the action potential along the T-tubule. This generates an influx of Ca^{2+} into the cytosol (see figure 1.1). In most cases this signal is amplified by additional Ca^{2+} release from the Sarcoplasmic Reticulum (SR) via the Ca^{2+} release channels or Ryanodine receptors (RyRs). There are currently 3 schools of thought as to how Ca^{2+} is released from the SR. The first of these postulated mechanisms involves electrical coupling wherein Ca^{2+} release is initiated when the SR membrane is depolarised by charge movements related to the passage of the action potential across the adjacent plasma membrane (Levi *et al.*, 1993). The second involves mechanical coupling wherein passage of the

action potential across the plasma membrane causes a shift in an intrinsic membrane protein that effectively "unplugs" a channel, allowing Ca^{2+} to flow out of the SR (Ferrier & Howlett, 2001). The third and most widely accepted mechanism is known as Ca^{2+} Induced Ca^{2+} Release (CICR). Subsequent released Ca^{2+} binds to the Ca^{2+} sensor Troponin C to activate the contractile proteins.

Extracellular [Ca^{2+}] declines to resting levels to allow relaxation by virtue of the Sarcoplasmic/Endoplasmic Reticulum Ca^{2+} ATPase (SERCA) and the Na-Ca Exchanger that allows the SR to re-sequester Ca^{2+} or extrude it from the cell (Niggli E, 1999).

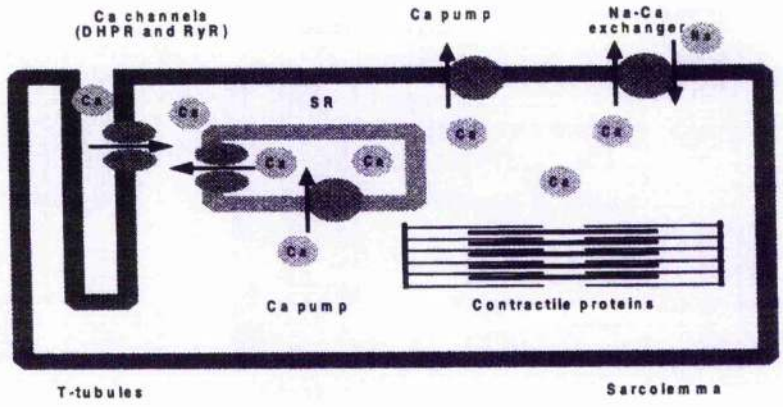

Figure 1.1. Ca^{2+} movements during E-C coupling.

T-tubule: transverse tubule, DHPR: Dihydropyridine receptor, RyR: Ryanodine receptor.

1.2 Ca^{2+} Pools, Uptake and Release

Within the cell Ca^{2+} is stored mainly in the Endoplasmic Reticulum (Sarcoplasmic Reticulum in muscle cells) and secretory granules. Mitochondria

also have the ability to accumulate Ca^{2+}, but had previously not been considered as a significant buffer of intracellular Ca^{2+}. The Endoplasmic/Sarcoplasmic Reticulum is regarded as the most important intracellular store in terms of Ca^{2+} signalling, because it contains a large amount of Ca^{2+} and is able to exchange Ca^{2+} quickly with the cytosol (Williams & Ashley, 1989).

1.3 Sarcoplasmic Reticulum

The Sarcoplasmic Reticulum (SR) of muscle is a specialized form of ER and forms an entirely intracellular membrane system that surrounds the cell's contractile apparatus. The system also forms specialized junctional regions with the sarcolemma at the cell surface and within the cell interior at the level of the transverse tubules (Williams & Ashley, 1989).

Resident in the SR is a Ca^{2+} store that is released into the sarcoplasm after electrical excitation ultimately leading to activation of the contractile machinery. Therefore it is essential that Ca^{2+} uptake and release by the SR and hence the sarcoplasmic $[Ca^{2+}]$, is tightly controlled. $[Ca^{2+}]$ inside the SR (Intraluminal Ca^{2+}), is in essence determined by 2 or possibly three factors summarised in figure 1.2; the rate of influx by SERCA, the rate of efflux via RyR and possibly a passive leak pathway.

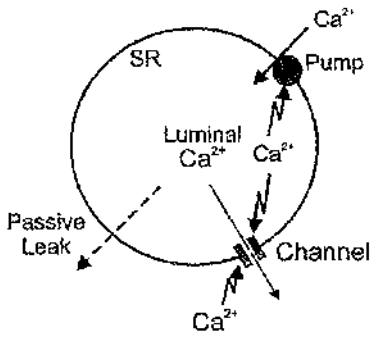

Figure 1.2. Routes of Ca^{2+} uptake and release from SR.
Channel corresponds to the ryanodine receptor, pump corresponds to SR-Ca^{2+} ATPase.

The dynamics of the storage and release of Ca^{2+} in the ER and SR have been extensively studied. As shown above, generally the results from single cells have been interpreted in terms of a global organelle containing various routes fro efflux and influx. However recent work on cultured rat astrocytes and arterial myocytes suggests that Ca^{2+} stores are organised into small, spatially distinct compartments that function as discrete units, further supporting the notion that cells can generate spatially and temporally distinct Ca^{2+} signals to control individual Ca^{2+}-dependent processes (Golovina & Blaustein, 1997).

1.3.1 SERCA

Influx of Ca^{2+} into the SR occurs through the Sarcoplasmic/Endoplasmic Reticulum Ca^{2+}-ATPase (SERCA) which translocates 2 Ca^{2+} ions driven by the hydrolysis of ATP.

At least three species of SERCA exist. SERCA 1 is expressed in fast twitch skeletal muscle, while the SERCA 2 gene encodes two alternatively spliced products, SERCA 2a and 2b. SERCA 2a is expressed in cardiac and slow-

twitch skeletal muscles; SERCA 2b in smooth muscle and non-muscle tissues (Tada & Toyofuku, 1996).

SERCA2a is a monomer of 100 kDa and is predominantly expressed in cardiac muscle (Greene *et al.*, 2000).

In recent years SERCA2a expression in relation to the incidence of disease has been the subject of intense study. For example it has been demonstrated that delayed cardiac relaxation in failing hearts has been attributed to a reduced activity of SERCA2a (He *et al.*, 1999).

SERCA2a is regulated by the concentrations of Ca^{2+} at the cytosolic face and within the SR and by the phosphorylation state of the protein Phospholamban that is integral to the SR. In the unphosphorylated state, phospholamban inhibits SERCA2a by reducing it's affinity for Ca^{2+} (Hajjar RJ *et al.*, 1997). Three sites of Serine/Threonine phosphorylation have been identified at Ser-10, Ser-16 and Thr-17. Ser-10 phoshorylation occurs via Protein Kinase C (PKC), Ser-16 by PKA, PKG or PKC, Thr-17 by CaM KII. β-Adrenergic stimulation also results in Ser-16 and Thr-17 phosphorylation. The consequence of Ser-16 and Thr-17 phosphorylation is an increase in Ca^{2+} pump activity (Colyer, 1998).

1.3.2 Ryanodine Receptor

Ryanodine receptors (RyRs) or SR Ca^{2+} release channels are ultimately responsible for the transient elevation of cytosolic Ca^{2+} following muscle cell depolarization (Conklin MW *et al.*, 1999). Several studies have suggested that

these channels have a bell-shaped sensitivity to the cytosolic [Ca^{2+}]; at low concentrations, Ca^{2+} promotes release, while higher concentrations are inhibitory (Chen *et al.*, 1993).

The receptor protein itself has been identified as a highly acidic homotetramer, with a total molecular mass of ~2.3 MDa and reacts specifically with Ryanodine, a highly toxic alkaloid (Gyorke I & Gyorke S, 1998) & (Szegedi C *et al.*, 1999).

RyR cDNA was expressed in the COS-1 cell line and it was found that the protein formed channels sensitive to adenine nucleotides and Ryanodine confirming the involvement of RyR in Ca^{2+} release from the SR (Chen *et al.*, 1993).

Three isoforms of RyR have been identified. Type 1 RyR (RyR_1) is primarily expressed in skeletal muscle, Type 2 (RyR_2) is the primary isoform in heart and is involved in the E-C coupling in cardiac muscle and Type 3 (RyR_3) is expressed predominantly in non-muscle tissues (Murayama T *et al.*, 1999).

The RyR_2 isoform predominantly in cardiac muscle exists as a homotetrameric complex. The complex itself includes accessory and other proteins. These include cAMP-dependent protein kinase (PKA), Calcineurin

(Protein phosphatase 2a) and Protein phosphatase 1. The complex is tethered to each RyR subunit via the anchor protein mAKAP. A simplified diagram of the complex is shown in figure 1.3.

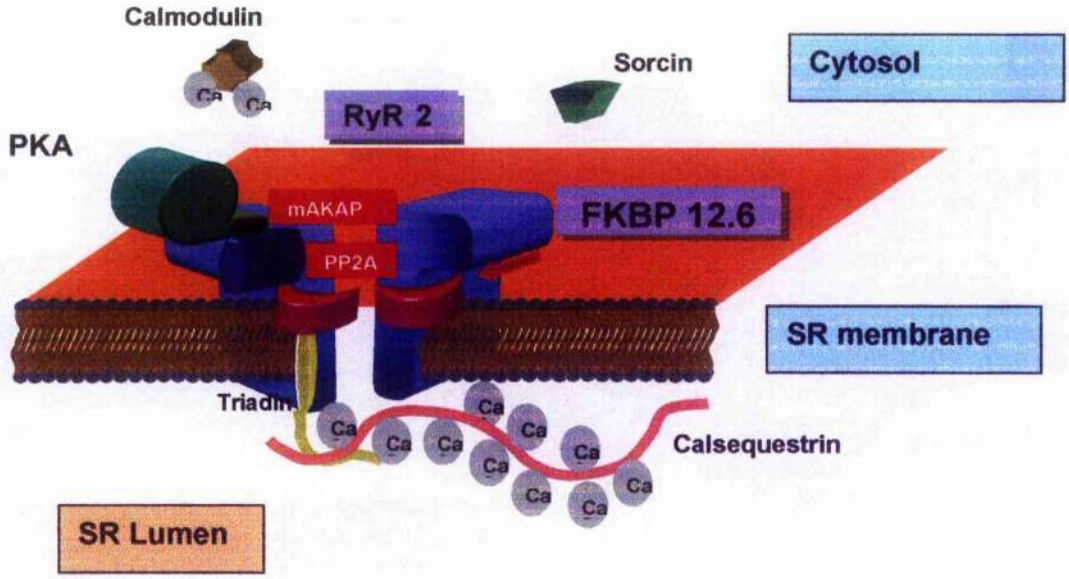

Figure 1.3 The Ryanodine receptor protein complex.

Shown is one half of the tetrameric complex Proteins are as follows: Ryanodine receptor protein (RyR2), calsequestrin, calcineurin (PP2A), cAMP-dependent protein kinase (PKA), A-kinase anchor protein (mAKAP), triadin, calmodulin and sorcin.

RyR and its properties have been studied extensively using biophysical and molecular biological techniques (Meissner, 1994). Purified skeletal and cardiac SR membrane vesicles have been incorporated into reconstituted membrane systems and the conductance studied at the single channel level under voltage clamp conditions and also radioligand binding assays using ^{3}H labelled Ryanodine. These studies have enabled researchers to relate the activity of single ryanodine receptors to global changes in the SR Ca^{2+} permeability

(Alverez J *et al.*, 1999), (Meissner *et al.*, 1988), (Lai *et al.*, 1988) & (Coronado *et al.*, 1994).

1.3.3 FK Binding Proteins

The FK binding proteins (FKBPs) are a family of low molecular weight proteins which bind to the immuno-suppressant drugs FK506 and rapamycin, the best characterized of these have been FKBP12.0 and FKBP12.6. Both proteins bind to rapamycin and the resulting complex binds to and inhibits calcineurin, the knock on effect being inhibition of the immune response (Brillantes *et al.*, 1994) Co-localization of RyR_1 and FKBP 12.0 was first demonstrated in rabbit skeletal muscle as the physiological role of these proteins was previously unclear (Jayaraman *et al.*, 1992). FKBP12.0 was found to be bound at a stoichiometry of 4 per receptor, therefore 1 molecule per RyR monomer. Binding of FKBP12.6 to RyR_2 has been shown to be regulated by phosphorylation. Phosphorylation by PKA, which is present in RyR_2 complex causes dissociation of FKBP12.6 and destabilization of the channel complex (Marx *et al.*, 2000).

Both FKBP12.0 and FKBP12.6 consist of 108 amino acids, with FKBP12.6 differing from FKBP12.0 by 18 amino acid residues. Both FKBP isoforms have been shown to associate with RyR_1. However, FKBP12.6 binds specifically to RyR_2. Studies using mutants indicated that specificity is conferred by only 3 amino acid residues (Xin *et al.*, 1999).

There is evidence that FKBP12.0 alters the kinetics of RyR activity and induces coupled gating of individual RyR_1 channels (Valdivia, 1998) & (Marx *et al.*, 1998).

The physiological role of FKBP12.6 has previously been poorly understood with conflicting evidence regarding its role. Single channel recordings using RyR_2 incorporated into planar lipid bilayers indicate that removal of FKBP12.6 using rapamycin or FK506 increases the open probability of the channel and induces long-lasting sub-conductance states (Kaftan *et al.*, 1996) & (Xiao *et al.*, 1997). Intriguingly, in parallel studies using cardiac SR preparations, removal of FKBP12.6 from the RyR_2 or addition of recombinant FKBP12.6 to preparations that had previously had FKB12.6 removed, did not alter channel behaviour (Timerman *et al.*, 1996) & (Barg *et al.*, 1997).

Adenovirus-mediated gene transfer has been used to over-express FKBP12.6 in adult rabbit cardiac myocytes and its effect on RyR_2 mediated Ca^{2+} leak from SR examined. It was shown that contractile parameters of isolated cardiac myocytes overexpressing FKBP12.6-GFP were altered. Fractional shortening, expressed as a percentage of diastolic cell length and therefore the contractility, was 21% higher than in cells overexpressing green fluorescent protein (GFP) alone, the control virus. In addition to this it was also demonstrated that FKBP12.6 overexpressing cells present a 53% reduction in leak through RyR_2. This was coupled with the result that indicates a higher SR Ca^{2+} load. These two results indicate that FKBP12.6 stabilizes the closed conformation state of RyR_2. This could provide a mechanism by which SR-

Ca^{2+} leak is reduced. The consequence of which being increased SR- Ca^{2+} release and myocyte shortening (Prestle *et al.*, 2001).

1.3.4 Calsequestrin

In addition to the proteins shown above there are others which have been found to be associated with the RyR_2 complex. One of the most important of these is the non-EF hand Ca^{2+} storage protein calsequestrin.

Calsequestrin is present in the lumen of the SR and was first identified in 1971 (MacLennan & Wong, 1971). It's major functional role is to buffer transported Ca^{2+} by serving as an intravesicular sink and thus to facilitate active transport (Ikemoto N *et al.*, 1989).

Coincidentally calsequestrin has also been shown to be present at very high levels in terminal cisternae giving rise to the hypothesis that calsequestrin sequester Ca^{2+} to sites of Ca^{2+} release. The importance of calsequestrin and it's role in regulating Ca^{2+} homeostasis within SR is further supported by the fact that when skeletal muscle SR is treated with RyR agonists, the expected decrease in lumenal $[Ca^{2+}]$ is preceded by an a transient increase in $[Ca^{2+}]$ suggesting reciprocal coupling between RyR and calsequestrin (Ikemoto N *et al.*, 1989).

The protein itself contains 109 amino acids with a large proportion of acidic residues and has an approximate molecular mass of 60 kDa (Jones LR *et al.*,

1998) & (McCleod *et al.*, 1991). Calsequestrin exists in cardiac and skeletal muscle isoforms encoded as products of separate genes (Cala & Miles, 1992). Rabbit cardiac calsequestrin was cloned and characterised from an adult rabbit cardiac cDNA library and in addition the tissue specific expression in rabbit heart was studied (Arai *et al.*, 1991). Later research investigated the regulation of Ca^{2+} signalling in a transgenic mouse model overexpressing calsequestrin. The development of a transgenic mouse overexpressing cardiac calsequestrin allowed for the first time, the probing of the role of calsequestrin at the cellular level and showed that this protein is closely and functionally linked to the Ca^{2+}-release process. In whole cell voltage-clamped transgenic myocytes, Ca^{2+} channel gated Ca^{2+} release from the SR was strongly suppressed. Intriguingly, the proteins involved in the Ca^{2+} release cascade were down-regulated, whereas Ca^{2+} uptake proteins were unchanged or slightly increased. This suggests that calsequestrin is indeed linked to SR Ca^{2+} uptake and release (Jones LR *et al.*, 1998). Further studies have suggested a role for calsequestrin in these processes.

In a different study it was demonstrated that Ca^{2+} release from SR vesicles was abolished by selective depletion of calsequestrin. The amount and rate constant of Ca^{2+} release was investigated as a function of the extent of Ca^{2+} loading. It was found that the amount of Ca^{2+} released increased monotonically in parallel to SR Ca^{2+} loading. Furthermore also the rate constant of Ca^{2+} release increased at partial SR Ca^{2+} loading and decreased on further SR loading. One can assume that most of the intravesicular Ca^{2+} is

bound to calsequestrin, therefore these results suggest that the kinetic properties of induced Ca^{2+} release show significant variation depending on the level of Ca^{2+} bound to calsequestrin at the time of induction of Ca^{2+} release (Ikemoto N *et al.*, 1989).

Calsequestrin had been shown to be a target of Casein Kinase II and recent research links the phosphorylation state of the protein to SR Ca^{2+} release. Results from this work showed that depending on the phosphorylation state, calsequestrin selectively controls the activity of RyR_2 at 1mM free lumenal [Ca^{2+}]. Calsequestrin in the dephosphorylated state enhanced the open probability of the channel implying that dephosphorylated calsequestrin regulates Ca^{2+} release from the SR. This correlates with the fact that calsequestrin has been found to exist in close proximity to RyR_2. Binding of Ca^{2+} to calsequestrin leads to conformational changes in RyR_2. As calsequestrin exists mainly in the phosphorylated state in SR (Szegedi C *et al.*, 1999), this would imply that dephoshorylation by a phosphatase of calsequestrin is a major physiological event and may be part of an as yet unidentified Ca^{2+} responsive signalling cascade within the SR.

1.3.5 Lumenal Control of Ca^{2+} uptake and release

The precise mechanism by which lumenal [Ca^{2+}] is controlled is not fully understood. The regulation of steady state filling in SR using isolated SR vesicles has been studied. This study demonstrated that lumenal [Ca^{2+}] is limited by the concentrations of ATP and ADP (Inesi G & de Meis, 1989) Later research studied the effect of changes in SR lumenal [Ca^{2+}] on Ca^{2+} release in

single cardiac Ca^{2+} release channels. Increasing Ca^{2+} on the lumenal side of the channel increased the open probability. The relative effect of lumenal [Ca^{2+}] was greater at low levels of cytoplasmic [Ca^{2+}] than at high levels of cytoplasmic [Ca^{2+}], suggesting that SR Ca^{2+} release channels are modulated by lumenal [Ca^{2+}] (Lukyanenko V *et al.*, 1996) in addition to the kinetics of the SR Ca^{2+} pump (Inesi G & de Meis, 1989).

Additional studies of the factors that determine the control of lumenal [Ca^{2+}] have produced variable and contradictory results. These include increased Ca^{2+} release channel activity by increasing lumenal [Ca^{2+}] (Ikemoto N *et al.*, 1989), decreased Ca^{2+} release channel activity with increased lumenal [Ca^{2+}] (Fill *et al.*, 1990) and a biphasic relationship (Tripathy & Meissner, 1996). Possible mechanisms have been postulated to explain the observed effects. The first mechanism involves direct action of Ca^{2+} itself on the Ca^{2+} release channel primarily on the lumenal side of the channel. The other direct mechanism suggested is action of Ca^{2+} being released from channel accessing the release channel on the cytosolic side. In addition to these two mechanisms it has also been suggested that there is somehow indirect involvement of lumenal proteins such as Calsequestrin (Kurebayashi N & Ogawa Y, 1998).

The relationship between cytoplasmic [Ca^{2+}] and lumenal [Ca^{2+}] was studied and the results indicated heterogeneous Ca^{2+} binding sites within the SR. The study concluded that lumenal [Ca^{2+}] might have a negative regulatory effect on

the Ca^{2+} release channel. This negative effect can be explained in two ways. Firstly, Ca^{2+} flowing out of the SR has access to cytoplasmic inactivation sites, or Ca^{2+} may effect the release channel indirectly via interacting proteins, the most promising candidate being Calsequestrin (Kurebayashi N & Ogawa Y, 1998).

The idea of cytoplasmic inactivation sites is supported by a different study investigating the effect of lumenal [Ca^{2+}] on single Ca^{2+} release channels. Results suggested that lumenal [Ca^{2+}] has the ability to regulate Ca^{2+} release channels by passing through the open channel and binding to cytoplasmic inactivation sites in addition to activation sites which are of low and high affinity respectively (Xu L & Meissner G, 1998).

However research by a different group provided contradictory evidence. Again the effect of lumenal [Ca^{2+}] on Cardiac Ca^{2+} release channel was investigated. At low lumenal [Ca^{2+}], increasing the cytosolic [Ca^{2+}] caused a gradual increase in the channel open probability by increasing the frequency of channel openings. Conversely, elevating the lumenal [Ca^{2+}] caused a gradual decrease in the channel open probability. The result of this work rule out the possibility that lumenal [Ca2+] acts by interacting with the cytosolic inactivation site of the channel. This is because lumenal Ca^{2+} would only have access to the cytosolic side when the pore is open, but when the channel closes, the local Ca^{2+} gradient dissipates very rapidly. Therefore rebinding of Ca^{2+} to the

channel is unlikely. Also experiments using a fast Ca^{2+} chelator such as BAPTA at the cytosolic side had no significant impact on the results.

It has been suggested that the SR Ca^{2+} release channel is an allosteric enzyme and modulation involves a lumenal regulatory site. If such a mechanism exists, then lumenal [Ca^{2+}] relieves inhibition caused by high cytosolic [Ca^{2+}] therefore allowing cells to self regulate the activity of the release channel according to SR load (Gyorke I & Gyorke S, 1998).

One of the biggest breakthroughs in understanding how lumenal [Ca^{2+}] influences total SR [Ca^{2+}] content was the result of research which led to the identification of a Protein Kinase. This so called 'state of filling' (SOF) kinase was found to be activated by depletion of SR Ca^{2+}, the principal substrate of which is the SR membrane spanning protein Phospholamban. Phosphorylation of phospholamban promotes Ca^{2+} pump activity and therefore stimulates store refilling. Intriguingly, increasing SR Ca^{2+} load was found to inhibit this protein kinase activity associated with the SR. This was demonstrated by reduced phosphorylation of phospholamban. This could possibly be due to inhibition of a protein kinase or activation of a phosphatase (Singh Bhogal M & Colyer J, 1998). This may represent an as yet unidentified signalling cascade present in the SR.

1.4 Mitochondria

Previously it was widely accepted that mitochondria did not act as a significant buffer of cellular Ca^{2+} at 'normal' cytosolic [Ca^{2+}], the exception being stressed

or damaged cells. Indeed it was believed that mitochondria were too slow to effectively compete with ER/SR. Studies in recent years have provided contradictory evidence to this. The current understanding of the identified mitochondrial influx and efflux pathways and their physiological significance is discussed. The major influx and efflux pathways are summarised in figure 1.4.

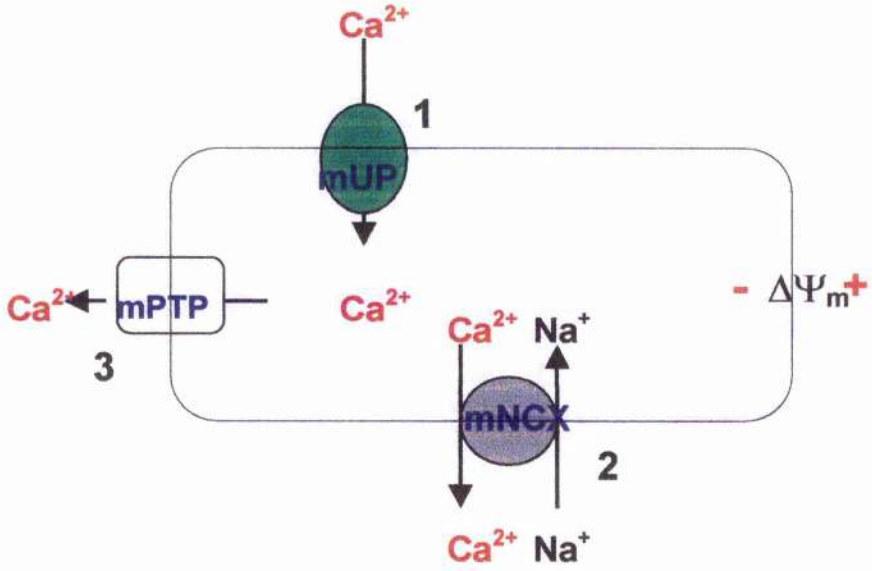

Figure 1.4 The major Ca^{2+} influx and efflux pathways.

1. Uniporter (mUP), 2. Sodium/Ca^{2+} exchanger (mNCX) & 3. Permeability transition pore (mPTP).

1.4.1 Mitochondrial Ca^{2+} influx pathways

At present two pathways of Ca^{2+} influx into mitochondria have been identified; the Ca^{2+} uniporter (CaUP) and a Rapid influx pathway (RaM). The first inkling that mitochondria may have a role, as a Ca^{2+} buffer was the result of studies carried out using agonists of G_q coupled receptors. These studies demonstrated that the subsequent IP_3 generated not only led to the expected

Ca^{2+} release from ER, but in addition led to an increase in [Ca^{2+}] within the mitochondrial matrix (Pozzan T *et al.*, 2000).

1.4.1.1 Ca^{2+} Uniporter (CaUP)

Studies of passive mitochondrial swelling found that the swelling was observed where charge and pH balance were maintained. This led to the identification of an uptake mechanism, the kinetics of which were consistent with a uniporter (Gunter *et al.*, 2000).

The influx is downhill and is driven by the large inside negative potential $\Delta\Psi_m$ (Babcock & Hille, 1998).

Characteristics of the Uniporter

The uniporter is inhibited by:

- Ruthenium Red (as a non-competitve inhibitor)
- Protonophores such as Carbonyl Cyanide *m*-Chlorophenolhydrazone (CCCP) that collapses the proton motive force.
- The novel inhibitor diaminopentane pentamine cobalt (DAPPAC) (Duchen MR, 2000)

Is activated by:

- Spermine
- Taurine

It is modulated by Adenine nucleotides. The uptake rate is near zero for external [Ca^{2+}] less than 200-300nM (Gunter *et al.*, 2000).

1.4.1.2 Rapid Uptake Mode (RaM)

Intriguingly, uptake via RaM is inhibited very soon after it has begun, after a fraction of a second when the predominant pathway becomes CaUP

Characteristics of RaM

The rate of uptake decreases dramatically when cytosolic [Ca^{2+}] is below 100-125nM.

Uptake via RaM is inhibited by:

- Uncouplers that dissipate the membrane potential, indicating like CaUP the thermodynamic driving force for uptake is the electrochemical gradient
- Ruthenium Red although the concentration required is 100 fold greater than for inhibition of CaUP (Gunter *et al.*, 2000) .

It is unknown whether or not RaM involves an alternative conformation of the uniporter and the mechanisms are one in the same, although evidence would suggest that they are related.

Possibly some of the most intriguing results in recent years came from a study offering a direct comparison of heart and liver mitochondria. It was shown that in heart mitochondria AMP, which had no effect on liver mitochondria, inhibited RaM. Results also showed a differing sensitivity to Ruthenium red (RuR) between mitochondria from the different tissues. In heart, there were two sub-populations of mitochondria: one that was stained by RuR and one that was resistant and showed no inhibition of RaM by RuR. The respiratory control

ratios of mitochondria sensitive to RuR staining were less than those resistant to RuR staining suggesting that mitochondria resistant to RuR staining include a greater proportion of damaged mitochondria.

1.4.2 Mitochondrial efflux pathways

There are two major efflux pathways for Ca^{2+} in mitochondria, Na^+ dependent and Na^+ independent. The major difference between these two mechanisms is the fact that the Na^+ independent also allows transport of Mn^{2+} whereas the Na^+ dependent mechanism does not (Gunter *et al.*, 2000). They also show very different kinetics.

1.4.2.1 Na^+ independent

This mode of efflux is dominant in tissues where ion clearance is important such as liver and kidney. Ca^{2+} is exchanged from the mitochondrial matrix for nH^+ ions against an electrochemical gradient . Studies have suggested that n=2 (Gunter *et al.*, 2000) & (Rizzuto R *et al.*, 2000).

This is an active process supported by the fact that it is inhibited by CN^- .Other inhibitors of this process are:

- Low levels of uncouplers such as CCCP
- High concentrations of Ruthenium Red

1.4.2.2 Na^+ dependent

The levels of expression of this mechanism vary in different types of tissue and correspondingly V_{max} also varies. These values are very high in heart, where rapid release of Ca^{2+} may be important. 1 Ca^{2+} is exchanged for 3 Na^+ ions.

There are many inhibitors of the process including:

- Tetraphenyl phosphonium
- Trifluoroperazine
- Diltiazem
- Verapamil
- Clonazepam

1.4.3 Permeability transition pore

In addition to the fore-mentioned efflux, there also exists a mitochondrial permeabiltiy transition pore (mPTP) the physiological significance of which remains largely unknown. The pore comprises a complex consisting of a voltage-dependent anion channel, the adenine nucleotide translocase and cyclophilin-D. Under pathological conditions associated with ischaemia and repurfusion, the complex 'deforms' into the PTP allowing free permeation of low molecular weight solutes (Buntinas *et al.*, 2001).

The pore is a voltage-dependent, non-selective channel, which is activated by:

- Matrix Ca^{2+}
- Inorganic phosphate
- Oxidants such as peroxides

and is inhibited by

- Matrix H^{+}
- Cyclosporin A that requires ADP and Mg^{2+} for inhibition (Rizzuto R *et al.*, 2000).

Studies have also suggested that Cyclosporin A is not specific for mPTP and also interferes with other signalling processes (Duchen MR, 2000).

1.4.4 Are these routes of influx/efflux of physiological significance?

Perhaps the most obvious consequence of an alteration in the Ca^{2+} content of mitochondria is the regulation in metabolism. Three key enzymes of the Krebs' cycle: pyruvate-, isocitrate- and α-keto glutarate dehydrogenases are all activated by an increase in mitochondrial matrix [Ca^{2+}]. Other loci within the metabolic pathways such as the electron transport chain are also suggested to be Ca^{2+} control points.

In recent years studies have revealed that mitochondria are key players in the induction or amplification of the processes leading to programmed cell death or apoptosis (Gunter *et al.*, 2000).

1.4.4.1 Mitochondria as amplifiers of Ca^{2+} signals?

It has been shown that IP_3 induced Ca^{2+} mobilisation also results in Ca^{2+} induced Ca^{2+} release from the mitochondria (mCICR). mCICR appears to be dependent on transitory opening of the PTP operating in a low conductance mode. This release from mitochondria therefore results in an amplification of Ca^{2+} signals from ER (Ichas F *et al.*, 1997). This is further supported by the suggestion that regions of the ER are in close proximity to mitochondria suggesting cross-talk between the two organelles (Pozzan T *et al.*, 2000) & (Pozzan & Rizzuto, 2000) .

1.5 Analysis of dynamic Ca^{2+} signals

1.5.1 Fluorescent Indicators

Measurement of [Ca^{2+}] within cells is made possible by the use of fluorescent dyes, the use of which was revolutionised by Grynkiewicz and colleagues (Grynkiewicz G *et al.*, 1985). These dyes show a spectral response upon binding Ca^{2+} and fall into two categories: single wavelength intensity modulating dyes and dual wavelength ratiometric dyes.

Single wavelength indicators exhibit changes in the intensity of their fluorescence excitation and emission spectra, whereas ratiometric indicators exhibit intensity as well as spectral changes upon binding to Ca^{2+}. Ratiometric dyes have the advantage of allowing fluorescence intensity measurements to be taken at two different wavelengths to obtain a ratio. The ratio minimises the effect of artefacts unrelated to changes in [Ca^{2+}].

It is possible to measure [Ca^{2+}] within compartments of cells using cell-permeant acetoxymethyl (AM) ester derivatives of these dyes that are loaded into cells, wherein cleavage to cell-impermeant products occurs by the action of intracellular esterases. Permeabilisation and subsequent washout of the cytosolic component renders the dye trapped within sub-cellular compartments (Meldolesi & Pozzan, 1998), (Golovina & Blaustein, 1997) & (Mogami H *et al.*, 1998).

1.5.2 Protein-Based Ca^{2+} Indicators

Another method of quantitatively measuring intracellular Ca^{2+} is using the photoprotein Aequorin that was originally isolated from the jellyfish *Aequorea Victoria*. Release of blue light occurs upon binding Ca^{2+}, the intensity of which is proportional to $[Ca^{2+}]$. This indicator's usefulness was limited by the need to microinject the protein into living cells making fluorescent dyes the method of choice for measuring intracellular $[Ca^{2+}]$. Subsequent cloning of the aequorin cDNA has expanded the possible uses of this photoprotein. Development of aequorin specifically targeted to sub-cellular locations has permitted the measurement of $[Ca^{2+}]$ within organelles (Brini M *et al.*, 1995), (Robert *et al.*, 1998) & (Brini M *et al.*, 1997). However, the major drawback of targeted aequorin is that the bioluminescent signal itself is rather weak. Therefore the signal has to be recorded from populations of cells rather than single cells.

1.5.2.1 Chameleons

The inability to effectively record Ca^{2+} signals in single cells using targeted protein based indicators has recently been somewhat overcome with the development of fluorescent indicators based on Green Fluorescent Protein (GFP). Dubbed 'Chameleons' these indicators take advantage of Fluorescence Resonance Energy Transfer (FRET) between different coloured GFP mutants (Miyawaki A *et al.*, 1997). Chameleons can be targetted to organelles in the same way as aequorin, but they exhibit much brighter fluorescence. Therefore signals can be recorded from single cells.

These indicators comprise chimaeric proteins and are tandem fusions of a blue- or cyan-emitting mutant of GFP, calmodulin, the calmodulin binding peptide M13 and an enhanced green- or yellow- emitting GFP. Binding of Ca^{2+} causes calmodulin to wrap around the M13 domain, increasing the fluorescence resonance energy transfer (FRET) between the flanking GFPs.

Different ranges of free [Ca^{2+}] can be measured by employing a range of calmodulin mutations. This indicator was used to visualise free Ca^{2+} dynamics in the cytosol, nucleus and endoplasmic reticulum in single HeLa cells (Cala & Miles, 1992) . The major advantage of using chameleons include the fact that the method is mainly non destructive to cells therefore making *in vivo* work easier, although the cytotoxicity of GFP has been under much scrutiny (Liu *et al.*, 1999). Also the detection method does not require additional cofactors, as is the case with aequorin.

1.5.2.2 Pericams

A major problem with using the described chameleon indicators and indeed the GFP variants that form the basis of these proteins, are their thermostability of folding and pH sensitivity (Tsien RY, 1998). Even small changes in pH can effect its fluorescence spectrum dramatically. Another limitation with monitoring Ca^{2+} dynamics in the cytosol is the large size of the expressed chameleon.

These problems have led to the development of another class of proteins indicators, namely pericams. These indicators are based on circularly permuted GFP variants. It was previously believed that any rearrangements or

insertions within GFP would drastically decrease the fluorescence due to the intricate post-translational modification required of GFP. However, this view was altered by the results of a subsequent study. This group discovered that when the amino and carboxy portions were interchanged and with short spacer peptides the fluorescent properties were maintained (Baird *et al.*, 1999). They also found that insertion of calmodulin in YFP had enhanced fluorescent properties that could be used to monitor cytosolic Ca^{2+} changes. Nagai and colleagues have further developed these indicators.

The basis for their indicators was circularly permuted yellow fluorescent protein (YFP) (cpYFP). cpYFP was fused to calmodulin and it's target peptide M13. Three types of pericam were obtained by mutating several amino acids adjacent to the chromophore. Of these, "flash-pericam" became brighter with Ca^{2+}, whereas "inverse-pericam" dimmed. Finally, "ratiometric-pericam" had an excitation wavelength changing in a Ca^{2+}-dependent manner. The pericams were expressed in HeLa cells and were able to monitor free Ca^{2+} dynamics, such as Ca^{2+} oscillations in the cytosol and the nucleus.

Ca^{2+} dynamics in the nucleus and mitochondria were simultaneously measured by using ratiometric-pericams having the appropriate localization signals (Nagai *et al.*, 2001)

The mitochondrially targeted ratiometric pericam has been used to monitor beat to beat oscillations in mitochondrial [Ca^{2+}] in neonatal ventricular myocytes (Robert *et al.*, 2001) In addition a ratiometric pericam has been

fused to another protein to allow specific studies of the generation of Ca^{2+} microdomains to influence cell function (Pinton *et al.*, 2002)

1.6 Aims of thesis

A considerable amount is known about cytoplasmic and sarcolemmal control of Ca^{2+} fluxes. However little is known about how $[Ca^{2+}]$ within the lumen of the SR exerts its effect on SERCA2a and RyR_2 activity. Several studies have presented indirect evidence of lumenal $[Ca^{2+}]$ effects. (Lukyanenko V *et al.*, 1996;Tripathy & Meissner, 1996)&(Xu L & Meissner G, 1998). The majority of these previous studies have used lipid bilayer preparations and the results have provided contradictory and variable results. The reason for the wide range of published results is unknown. It may be based on transport protein subtypes, or differing isolation procedures for isolation of the proteins. Although a good model system, it is not known how functional these transport proteins are in the lipid bilayers and if the correct accessory proteins are present in the complexes in the correct conformation.

The original aim of studies for this thesis was to use low sensitivity Ca^{2+} indicators to measure $[Ca^{2+}]$ within the lumen of SR in adult cardiac muscle. This approach using acetoxymethyl (AM) derivatives of these indicators has been used to study ER Ca^{2+} dynamics in non-muscle cells (Golovina & Blaustein, 1997) (Mogami H *et al.*, 1998) and SR Ca^{2+} dynamics in smooth muscle (Shmigol *et al.*, 2001)

To date, no work has been directed toward adult cardiac muscle. The main reason for this is due to lack of a specific indicator. I have shown in one of the chapters of this thesis that when adult ventricular myocytes are exposed to prolonged incubation with acetoxymethyl derivatives of FURA-based indicators almost the entire signal is attributed to mitochondria with virtually no contribution by SR. An alternative approach was used to measure lumenal SR $[Ca^{2+}]$. An adenovirus was generated to allow the expression of an indicator within the SR. This proved to be the most effective approach

The purpose of measuring the $[Ca^{2+}]_{SR}$ was to correlate SERCA2a and RyR_2 activity with lumenal Ca^{2+} and to ascertain some of the factors that limit $[Ca^{2+}]$ within the SR of cardiac muscle. Correlation of uptake or release processes with intra-SR $[Ca^{2+}]$ may reveal lumenal control over these processes. Furthermore, measurement of the free Ca^{2+} within the lumen would begin to address the debate concerning the factors that limit $[Ca^{2+}]$. This work could provide a clearer understanding of the process of excitation-contraction coupling in cardiac muscle in health and disease. Ultimately this may possibly reveal alternative routes to safely enhance cardiac SR function in disease states such as heart failure.

Chapter 2
General Methods

Chapter 2- General Methods

2.1 Preparation of Adult Cardiac Myocytes

For the investigations carried out for this thesis, adult cardiac myocytes were prepared from rabbit and rat. Experiments were performed on both freshly prepared cardiac myocytes and those that had been maintained in culture for several days. All procedures were undertaken in accordance with the United Kingdom Animals (Scientific Procedures) Act 1986.

2.1.1 Preparation of Adult Rat Cardiac Myocytes

White Wistar male rats were stunned by a blow to the head and killed by cervical dislocation. The thoracic cavity was opened, the heart quickly excised and placed into a beaker containing ice-cold Krebs' solution (120mM NaCl, 20mM HEPES, 5.4mM KCl, 0.52mM NaH_2PO_4, 3.5mM $MgCl_2.6H_2O$, 20mM Taurine, 10mM Creatine, 11.1mM Glucose, pH 7.4).

The excised heart was quickly mounted and tied via the aorta onto the cannula of a Langendorff retrograde perfusion system. Fat and connective tissues were trimmed away. 50mL of Ca^{2+} free Krebs' solution, maintained at 37°C was perfused through the heart at a rate of 13mL/min to wash out blood and Ca^{2+}. The heart was then perfused with Collagenase/Protease solution (3mg Protease and 50mg Collagenase dissolved in 25ml Ca^{2+} free, sterile Krebs' solution). The enzyme solution was collected as it passed through the heart and re-circulated after the initial volume of the solution had passed through.

Re-circulation of the enzyme solution and hence the digestion, was continued for approximately 16 minutes until the heart felt soft to the touch. The enzyme solution was washed out of the heart by perfusion with 50mL Sterile Krebs' solution containing 1mM EGTA.

The heart was excised and placed into Krebs' solution containing 1mM EGTA. The tissue was then finely chopped. The myocytes were dissociated by lightly titurating the solution using a plastic pasteur pipette. The dissociated cardiac myocytes were filtered through gauze mesh to remove undigested and other tissues. The cells were then counted using a haemocytometer and the concentration adjusted to 1 x 10^5 cells/mL. The two sub-populations of cells rod-shaped and ball shaped were deemed 'live' and 'dead' respectively. Dead cells being cells having undergone hyper-contraction.

2.1.2 Preparation of Adult Rabbit Cardiac Myocytes

White New Zealand male rabbits were subjected to deep anaesthesia with an intravenous injection of 500 U Heparin together with an overdose of Sodium Pentobarbitone (100mg/kg) via the left marginal ear vein. Animals were deemed terminally anaesthetised when both stretch and corneal reflex were absent. The thoracic cavity was opened, the heart quickly excised and placed into a sterile beaker containing sterile, ice-cold Krebs' solution (120mM NaCl, 20mM HEPES, 5.4Mm KCl, 0.52Mm NaH_2PO_4, 3.5Mm $MgCl_2.6H_2O$, 20mM Taurine, 10mM Creatine, 11.1mM Glucose, pH 7.4).

The excised heart was quickly mounted and tied via the aorta onto the cannula of a Langendorff retrograde perfusion system. Fat and connective tissues were trimmed away. 200mL of Ca^{2+} free Krebs' solution, maintained at 37°C was perfused through the heart at a rate of 25mL/min to wash out blood and Ca^{2+}. The heart was then perfused with Collagenase/Protease solution (3mg Protease and 50mg Collagenase dissolved in 75ml Ca^{2+} free, sterile Krebs' solution).

The enzyme solution was collected as it passed through the heart and re-circulated after the initial volume of the solution had passed through. Re-circulation of the enzyme solution and hence the digestion, was continued for 5-6 minutes until the right ventricular (RV) tissue felt softened to the touch. The enzyme solution was washed out of the heart by perfusion with 100mL Sterile Krebs' solution containing 1%(w/v) Bovine Serum Albumin (BSA).

The RV was excised and into Krebs' solution containing 1mM EGTA. The tissue was then finely chopped. The myocytes were dissociated by lightly titurating the solution using a plastic pasteur pipette. The dissociated cardiac myocytes were filtered through gauze mesh to remove undigested and other tissues. The cells were then counted using a haemocytometer and the concentration adjusted to 1×10^5 cells/mL.

2.2 Primary Myocyte Culture

Rabbit and rat cardiac myocytes were prepared as above under sterile conditions with some subtle changes to the methods. All solutions had previously been filtered sterilised and prepared with sterile water and autoclaved glassware. Perfused tissue was cut down and placed in a solution containing 1% BSA (w/v) in sterile glassware and the tissue finely chopped using autoclaved instruments in a laminar flow hood. The chopped tissue was then placed in tissue culture grade sterile flasks and placed on a shaker at room temperature for 1 hour.

The following steps were performed using aseptic technique in a laminar flow hood. The supernatant was removed and placed into sterile 15mL centrifuge tubes. The cells were allowed to sediment by gravity. The supernatant was removed and the pellet resuspended in Krebs' solution containing 100μM $CaCl_2$. Again the cells were allowed to sediment by gravity, the supernatant removed and the pellet resuspended in Krebs' solution containing 250μM $CaCl_2$. This step was repeated twice more and successively raised the extracellular Ca^{2+} to 500μM and then 1mM.

The cells were counted using a haemocytometer, subjected to gentle centrifugation and the pellet resuspended in M199 medium (supplemented with 312.5mg Taurine, 500mg D,L Carnitine, 327.5mg creatine, 5mL pencillin/ streptomycin per 500mL) to a concentration of 1×10^5 cells /mL.

2.2.1 The Use of Laminin as a Substrate for Cell Attachment

35mm petri dishes with coverslips (Mattek corporation, Ashland, USA) were treated with the following laminin concentrations: 1μg/mL, 3μg/mL and 5μg/mL in order to optimise cell attachment conditions. The laminin solutions were prepared by the addition of Laminin stock solution (1mg/mL) to M199 medium according to table 2.1.

Final [Laminin] (μg/mL)	Volume 1mg/mL Laminin stock solution added /mL M199 (mL)
1	1.0
3	3.0
5	5.0

Table 2.1. Volumes of Laminin required to give particular concentrations

Cells were plated at a density of 1×10^4 cells /cm^2 onto the 35mm dishes pre-treated with laminin, which corresponds to a concentration of 1×10^5 cells /mL. The dishes were then incubated in a 37°C incubator supplemented with 5% CO_2 for 4 hours to allow cell attachment.

The dishes were washed to remove unattached cells by decanting the medium using an automatic pipette, adding fresh M199 and decanting this. 2mL of fresh M199 was then added to each dish and the cells placed in a 37°C incubator.

2.3 Studying Calcium dynamics In cardiac myocytes

2.3.1 Loading of Cardiac Myocytes with Acetoxymethyl Esters of Fluorescent Calcium Indicators

Acetoxymethyl (AM) Ester derivatives of fluorescent calcium indicators are cell permeant and thus if cells are incuabted with the derivatives for a significant time, dye molecules will eventually make their way into sub-cellular compartments. The action of cellular esterases causes cleavage of the AM grouping. The cleaved product is not membrane permeant and therefore this renders the dye trapped within sub-cellular compartments and cytosol. Addition of a permeabilising agent such as β-escin or saponin removes cholesterol moieties from the sarcolemma and leaves approximately 60μ holes. These holes allow cytoplasmic component of cleaved dye to leave. Dye loaded into sub-cellular compartments remains.

Dissociated Cardiomyocytes were incubated in the above Krebs' solution containing 1mM EGTA with 10μM of Fura-2-AM, FuraFF-AM or MgFura-2-AM. Incubations were carried out for 90 minutes in 25mL Tissue culture-grade flasks in a 37°C incubator. This was followed by a 30-minute indicator free incubation at room temperature to allow dye cleavage by cellular esterases.

Cells were then permeabilised by brief exposure to either β-escin or saponin (0.1mg/mL). The cell concentration was adjusted to 0.5 x 10^6 cells/mL (previously optimised) and were then placed in a cuvette containing a mock intracellular solution of the following composition: 5mM EGTA, 25mM HEPES,

5.5mM $MgCl_2$, 100mM KCl pH 7.0. Free [Ca^{2+}] was monitored by the addition of Fluo-3 tetrapotassium salt.

2.3.2 System for studying Calcium dynamics on populations of cells

A closed cuvette system was used to study the calcium dynamics on populations of cells. A diagram of which is shown in figure 2.1.

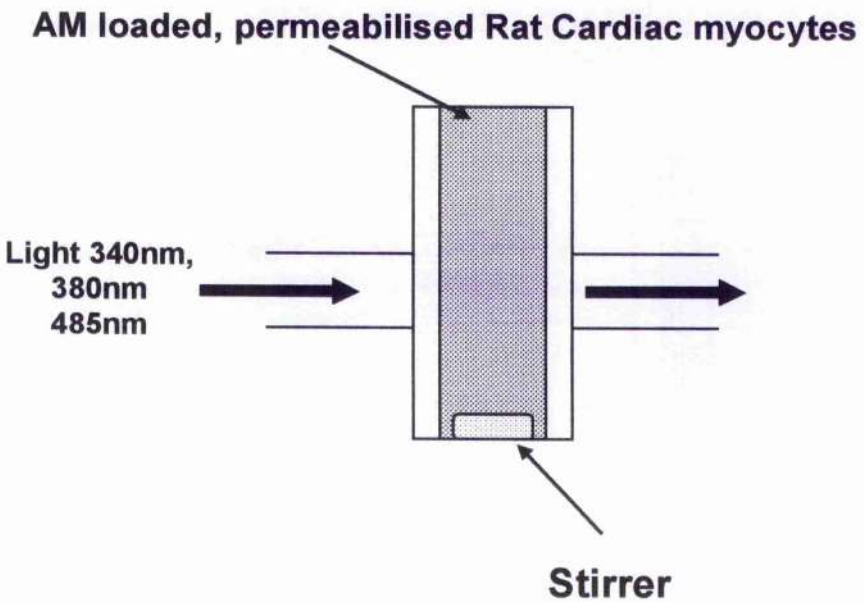

Figure 2.1. Cuvette based system for studying Ca^{2+} dynamics on populations of cells.

Measurements were made using a closed cuvette system shown in figure 2.1. Fluorescence intensity due to excitation at 488nm for fluo-3 and fluorescence ratio due to excitation at 340 and 365nm for the FURA dyes were recorded digitally. 365nm is used in preference to the conventionally used 380nm because when a fluo-3 based dye is used in conjunction with a FURA dye, there tends to be contamination of the 380nm signal by the fluorescence due

to excitation of the Fluo dye. This effect is minimised using an excitation wavelength of 365nm. This wavelength is close to the isobestic point of Fura dyes so provides little information on ion concentration, but still provides a reference signal.

2.4 Generation and Propagation of Adenovirus to allow up-regulation of Cardiac specific proteins

An adenovirus was generated to allow expression of indicator targeted to the SR. Specifics of the generation are described in detail in chapter 6.
Two methods were used to carry out large-scale preparation of adenovirus, each with subtle differences.

2.4.1 Method 1

Carried out in the laboratory of Professor Gerd Hassenfuss, Göttingen
Hamster embryonic kidney (HEK) 293 cells were cultured in IMDM (with 8% foetal calf serum (FCS)) in T-75 flasks. When cells had reached 90% confluence they were passaged by trypsin treatment and plated out onto 40 fresh 15cm tissue culture petri dishes. Medium was removed and replaced daily. 3 days later when the cells had again reached approximately 90% confluence they were infected with each of the adenoviruses with an multiplicity of infection (MOI) of 1 assuming $5x10^6$ cells per 15cm plate. Virus was added to IMDM (with 5% FCS) and this was subsequently used to infect the HEK 293 cells. The infected cells were incubated at 37°C for 2 hours. The virus-containing medium was removed, the plates washed with 1x phosphate buffered saline (PBS) and the medium replaced (IMDM, 5% FCS).

2-3 days after infection when the cells had started to detach from the surface of the plate, the medium containing the detached cells was decanted into 250mL centrifuge tubes. A 20% stock of NP-40/PBS solution was added to a final concentration of 0.1%. The tubes were then allowed to shake at room temperature for 30 minutes. After shaking, the tubes were centrifuged at 11,000rpm at 4°C for 25 minutes in a JA14 rotor. The supernatants were transferred to new 250mL centrifuge tubes and added to each tube was a half volume of 20% (w/v) PEG 8000/2.5mM NaCl solution. The tubes were then packed in ice and water and stored at 4°C for 4 hours without shaking.

The samples were centrifuged at 11,000rpm at 4°C for 25 minutes in a JA14 rotor. The pellet was resuspended in 5mL 1x PBS per 250mL tube. The resuspended viral pellets were passed through a 24G needle into 15mL falcon tubes and incubated shaking at 4°C for 1.5 hours. This was followed by centrifugation at 6,000 rpm for 10 minutes. The supernatant was then transferred to a 50mL falcon tube and CsCl added to give approximately 1.32g/mL based on the measured volume. 1mL of the solution was weighed and the CsCl concentration adjusted to 1.32-1.34 mg/mL if required either on addition of CsCl or 1x PBS. The solution was then transferred to 13mL sealable ultracentrifuge tubes. Pairs of tubes were balanced on addition of pre-made sterile 1.33mg/mL CsCl solution using a syringe and needle. The tubes were then sealed and subjected to ultracentrifugation at 40,000 rpm at 16°C overnight.

The band on the gradient corresponding to the infectious viral particles was removed using a 19G needle and placed in a sterile eppendorf tube. CsCl was removed from the prepared adenovirus by dialysing for approximately 6 hours in dialysis tubing placed in 5x PBS (pH 8.0). The PBS was removed and replaced and the preparation allowed to dialyse overnight. The prepared adenovirus was removed from the dialysis tubing.

The number of particles present was ascertained by diluting the virus 1:1000 and measuring the optical density at 260nm (OD_{260nm}) assuming that OD_{260nm} =1.0 for 1 x 10^{10} particles/mL. Glycerol was added to the prepared adenovirus to a final concentration of 10% and suitable aliquots prepared and stored at -80°C.

2.4.2 Method 2

Carried out in the laboratory of Dr. Andrew Baker, University of Glasgow.

Another method of large scale preparation was used to prepare large amounts of the adenovirus. A pure high titre stock of Ad-CSQ-Aeq was generated by the following method which is modified version of a well established method by Nicklin and Baker. In essence, the process involved co-transfection of HEK 293 cells with the viral plasmid pJM17 and a plasmid containing the cDNA encoding the SR-targeted Aequorin. Homologous recombination follows within the HEK 293 cells. This leads to cell lysis that is observed under the light microscope as a clear area on the HEK 293 monolayer. This clear area termed a plaque. There are also cell morphology changes, which is termed the cytopathic effect. Once the cytopathic effect has been observed, the cell lysate

is harvested and the resulting recombinant adenovirus extracted using a solvent. (adenovirus has no release mechanism from cells).

Culture and passage of HEK 293 cells

HEK 293 cells at a low passage number were cultured in minimal essential medium (MEM) supplemented with 10% FCS, 2mM L-glutamine, 100 international units (IU))/mL penicillin and 100μg/mL streptomycin in T-150cm^2. When cells had reached 100% confluence, in other words when the whole surface of the flask was completely covered with cells, 5mL 1x citric saline solution was added to the flask ensuring the whole surface was covered. The flask was incubated at room temperature for approximately 10 minutes. The cells were detached by gently tapping the surface. 5ml MEM (with supplements) was added to this and any resulting cell clumps re-suspended. 2mL of cell suspension was added to fresh, sterile T-150cm^2 flasks. To each flask was added approximately 25mL MEM.

Following the observed plaques cytopathic effect, the cell lysate was removed and placed in a sterile 50mL falcon tube. The flask was then washed with 5mL MEM and pooled with the cell lysate. This was then subjected to centrifugation at 250*g* for 10 minutes at room temp. The resulting pellet was resuspended in1mL sterile Phosphate buffered saline (PBS). An equal volume of the solvent ArkloneP was added to this suspension. The tube was inverted for 10s followed by shaking for 5s. This mixing step was repeated. The tube was centrifuged at 750*g* at room temperature for 15 minutes. At this point the tube contained 3 layers: the lower layer solvent, the middle layer cellular debris and the top layer aqueous solution that contains adenovirus. The top adenovirus

layer was removed using a sterile pipette and stored in sterile eppendorf tubes in 50µL aliquots at -80°C

2.4.2.1 Generation of plaque pure stocks by end point dilution

Plaques may occur as a result of multiple recombination events within the HEK 293 cells. When working with adenovirus it is vital to have "pure" stocks i.e. that have been generated by the multiplication of a single adenovirus. A simple method of plaque purification is serial dilution of the crude stock onto the HEK 293 cells.

Low passage HEK 293 cells were sub-cultured into a sterile 96 well plate that consists of 8 rows each containing 12 wells. Cells had reached 50-60% confluence by the following day. Serial dilutions of the crude adenovirus stock were made according to table 2.2.

Row on plate	Final dilution of virus	Volume of virus (µL)	Volume of media (µL)
	10^{-2}	50 stock	4950
1	10^{-4}	50 @ 10^{-2}	4950
2	10^{-6}	50 @ 10^{-4}	4950
3	10^{-7}	500 @ 10^{-6}	4500
4	10^{-8}	500 @ 10^{-7}	4500
5	10^{-9}	500 @ 10^{-8}	4500
6	10^{-10}	500 @ 10^{-9}	4500
7	10^{-11}	500 @ 10^{-10}	4500
8	control	0	5000

Table 2.2. Dilutions of Adenovirus to perform plaque assay

Starting with row 8, the media was removed using a 200μL pipette tip and replaced with 100 μL fresh media. The media in row 7 was then replaced with the correct adenoviral dilution. This was repeated for rows in ascending order. The plate was placed in a 37°C incubator. 16-18 hours post-infection the media was replaced with 200μL of complete media both removing and replacing the media with a fresh sterile pipette tip per well. The media was replaced every 2-3 days for 8 days, each time the media was changed the plate was monitored using the light microscope.

Once the cytopathic effect was apparent in a well, it was marked and replacing of the media was ceased in that well. On the seventh day of the assay another 96 well plate was prepared. On the eighth day, once the assay was completed, the cells and media was collected from three positive wells at the highest dilution for which the cytopathic effect is present. Pipetting up and down three times collected the cells. Two of the samples were then stored in sterile eppendorf tubes at -80°C. The remaining sample was extracted using an equal volume of the solvent ArkloneP as described previously. 50μL of this adenovirus stock was then used to repeat the plaque purification assay using the 96 well plate prepared on day 7. Plaques taken from the highest dilutions on this plate were considered plaque pure.

2.4.2.2 Generation of high titre stocks of adenovirus

This is achieved by large-scale multiplication of the initial pure recombinant adenovirus in HEK 293 cells.

Low passage HEK 293 cells were sub-cultured until there was 30 T-150 tissue culture flasks. Once the cell monolayer had reached 80-90% confluence they were deemed ready for infection. Infection was carried out by mixing 50μL of crude adenovirus plaque-pure stock with 750mL complete media and adding 25mL to each flask. The media was changed every 3 days until the cytopathic effect began and the cells started to detach from the flask. At this point in the procedure the cells were collected and placed in sterile 50mL falcon tubes. The cells were then centrifuged at 250*g* for 10 minutes at room temperature.

All of the resulting pellets were resuspended in a total volume of 15mL PBS. To this was added an equal volume of the solvent ArkloneP. The tube was inverted for 10 seconds followed by shaking for 5 seconds. The inversion/mixing step was repeated, this was followed by centrifugation at 750*g* for 15 minutes at room temperature. The top layer containing adenovirus was removed and transferred to a fresh tube. A further 10mL of PBS was added to the remaining solvent and cell debris and the extraction repeated.
This was followed by CsCl density gradient centrifugation as described previously in method one earlier in this chapter.

2.4.2.1 Determining the plaque forming units (pfu) value

Before using the pure recombinant adenovirus is was necessary to ascertain the infectivity. This followed the same method as that used to perform plaque purification by end point dilution described previously in this chapter. Serial dilutions were made of the purified adenovirus as described in the table earlier

in this chapter. 100μL of each dilution was added to the appropriate wells and incubated in a 37°C incubator for 16-18 hours. The media was then changed and 200 μL complete media added. The media was changed every 2-3 days. Once the cytopathic effect was evident in any well, it was marked and the replacing of the media ceased. After 8 days the number of wells containing plaques were counted and fitted to the equation below in order to calculate the adenoviral titre.

proportionate distance = $\frac{\text{\%positive above 50-50\%}}{\text{\% positive above 50\%-positive below 50\%}}$

log ID_{60} (infectivity dose) =

log dilution above 50% + (proportionate distance x -1)x dilution factor

e.g.

10^{-4} all wells positive 10/10

10^{-6} 10/10

10^{-7} 10/10

10^{-8} 9/10

10^{-9} 3/10

10^{-10} 0/10

10^{-11} 0/10

proportionate distance = $\frac{90-50}{90-30}$

$= 0.67$

$\log ID_{50} = -8 + (0.67 \times -1) = -8.67$

$ID_{50} = 10^{-8.67}$

$TCID_{50}$(tissue culture infectivity dose 50) = $\frac{1}{10^{-8.67}}$

$TCID_{50}/100\mu L = 10^{8.67}$

X dilution factor (10)

$TCID_{50}/1mL = 10^{9.67} = 4.67 \times 10^{9}$ $TCID_{50}/mL$

1 $TCID_{50} \cong 0.7$ pfu

$\therefore$ **final titre= 3.27×10^{9} pfu/mL**

2.5 Statistical Analysis

All data within the thesis are expressed as mean (± SEM) unless stated otherwise. ANOVA multi variant analysis (parametric) was used to compare multiple groups. A Tukey-Kramer multiple comparisons post test was used. A value of $p<0.05$ was considered statistically significant. A student's t test was used to compare single pairs of data.

Chapter 3
Use Of Fluorescent Indicators To Monitor Calcium Dynamics Within Cardiac Muscle

Chapter 3- Use of Fluorescent Indicators to Measure Ca^{2+}

3.1 Introduction

It is possible to monitor Ca^{2+} changes within cells using fluorescent Ca^{2+} indicators. There are two major classes of fluorescent indicator: single wavelength and dual wavelength ratiometric dyes.

A more detailed description of fluorescent Ca^{2+} indicators is given in section 1.5.1.

A number of fluorescent Ca^{2+} indicators were used to monitor the changes in intracellular free Ca^{2+}. The indicators and some of their properties ascertained experimentally are shown in table 3.1.

	Excitation λ (nm)	Emission λ_{max} (nm)	K_d (μM)	R_{min}	R_{max}
Fura-2	340,365	512	0.23	0.50	1.17
Fluo-3	488	526	0.52	1.00	16.4
FuraFF	340,365	512	10	0.43	1.30
MgFura-2	340,365	511	70	0.53	1.70
MgFluo-4	488	516	120	1.00	908.50
Fluo5N*	488	516	220	1.00	55.55

Table 3.1 Properties of the fluorescent Ca^{2+} indicators.

All were tested and some subsequently used in further studies. * fluorescence of ion-free indicator is extremely weak. K_d, R_{min} and R_{max} were ascertained experimentally. R_{min} corresponds to the fluorescence ratio or intensity in solution containing 10mM EGTA, where $[Ca^{2+}]$ is <1nM and R_{max} in a solution containing approximately 10mM Ca^{2+}

3.2 Calibration of Fluorescence

A series of calibration experiments were carried out to establish the relationship between [Ca^{2+}] and fluorescence due to excitation at 488nm or in the case of Fura-2 and MgFura-2, the fluorescence ratio due to excitation at 340 and 380nm. Solutions containing increasing free [Ca^{2+}] were used to decipher this relationship. The solutions were prepared by mixing stock solutions of 10mM EGTA and 10mM CaEGTA (10mM EGTA/CaEGTA, 100mM KCl, 1mM $MgCl_2.6H_2O$, 20mM HEPES, pH 7.0) in different ratios to give differing free [Ca^{2+}]. The ratios and free [Ca^{2+}] are shown in table 3.2.

Solution (10EGTA:10CaEGTA ratio)	Free [Ca^{2+}]
10E	0.100nM
10:1	42.170nM
3:1	0.126μM
1:1	0.380μM
1:3	1.140μM
1:10	3.428μM
10CaE	61.680μM

Table 3.2. Callbration solutions and their corresponding free [Ca^{2+}].
Values calculated using the program React version 3.

Measurements were made using a closed cuvette system described in section 2.3.2. 150μL of each of the solutions from table 3.2 was added to 1350μL

0.05R solution (0.05mM EGTA, 1mM $MgCl_2$, 10mM NaCl, 25mM HEPES, pH 7.0) with 10μM of the relevant dye. The fluorescence intensity or fluorescence ratio in the case of the ratiometric dyes was recorded digitally. These values were used to construct calibration curves using the computer software Microcal Origin. The data collected was fitted to curves using a logistic method. Curves of fluorescence or fluorescence ratio versus $[Ca^{2+}]$, whichever is applicable to each dye, were displayed on one graph and are shown in figure 3.1.

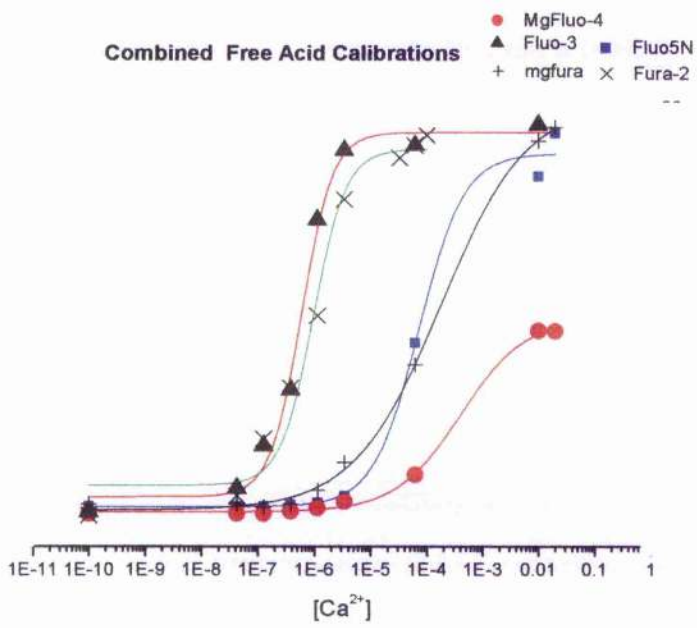

Figure 3.1. Graph showing combined calibration curves for each of the free acids.

3.3 Use of two indicators simultaneously to monitor [Ca^{2+}] changes

Since the ratiometric indicators (Fura-2 and MgFura-2) and the single wavelength indictors (Fluo-3, MgFluo-4 and Fluo5N) use different excitation wavelengths, it is possible to use single wavelength and ratiometric indicators simultaneously. Spectra were produced for each indicator by scanning between 300 and 600nm and are shown in figures 3.2A-E.. 'High Calcium' indicates use of a 10mM CaEGTA solution giving a free [Ca^{2+}] of 61.68μM and 'Low Calcium' 10mM EGTA and 0.1nM.

Figure 3.2A-3.2E.

Emission spectra of the fluorescent indicators Fura-2, MgFura-2, Fluo5N, MgFluo-4 and Fluo-3 measured at >520nm.

A

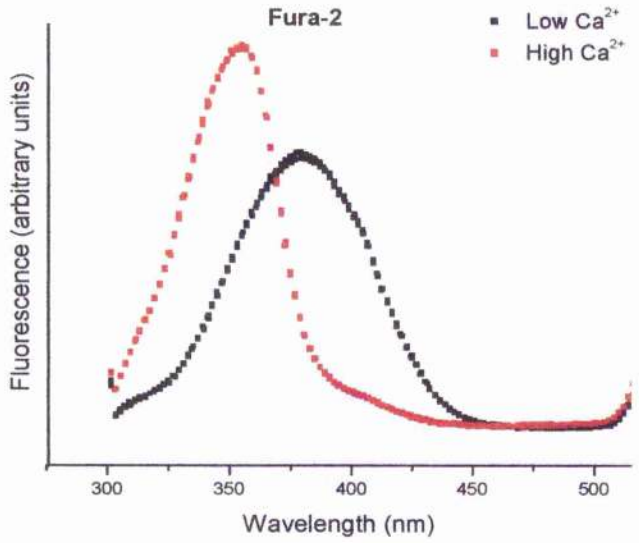

B

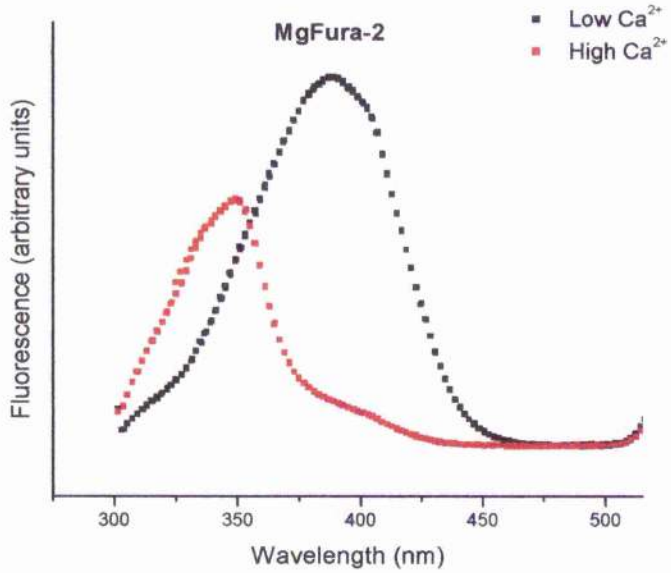

C

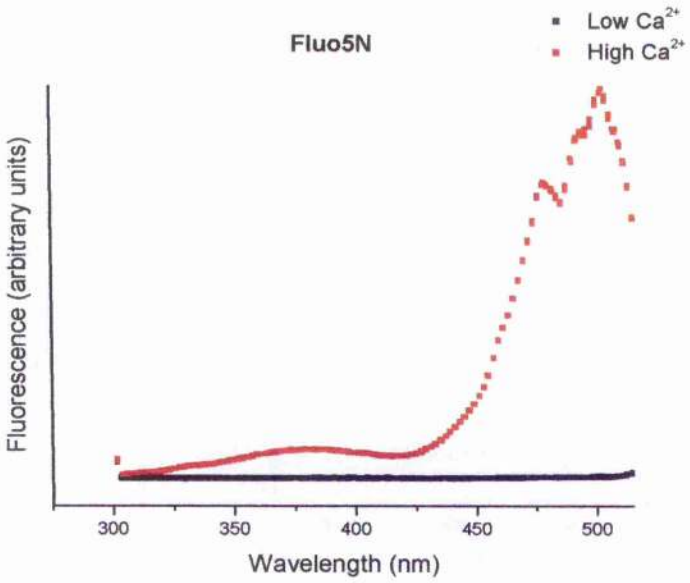
Fluo5N
Low Ca2+
High Ca2+
Fluorescence (arbitrary units)
300
350
400
450
500
Wavelength (nm)

D

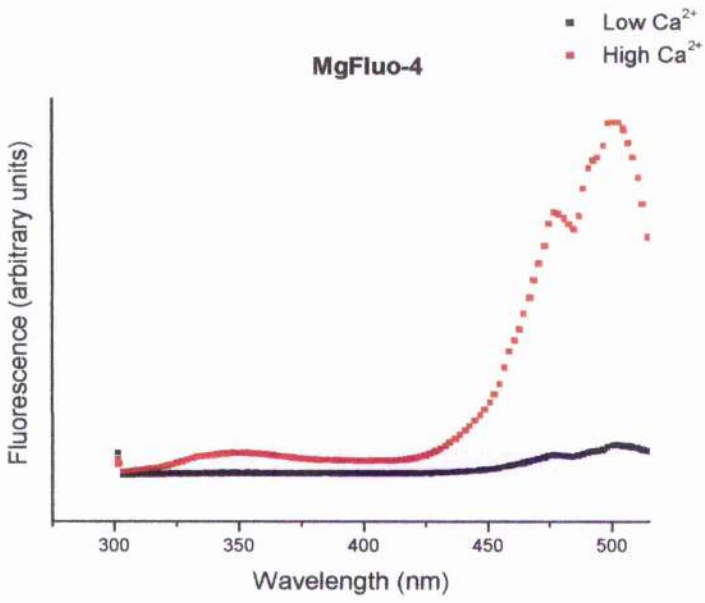
MgFluo-4
Low Ca2+
High Ca2+
Fluorescence (arbitrary units)
300
350
400
450
500
Wavelength (nm)

E

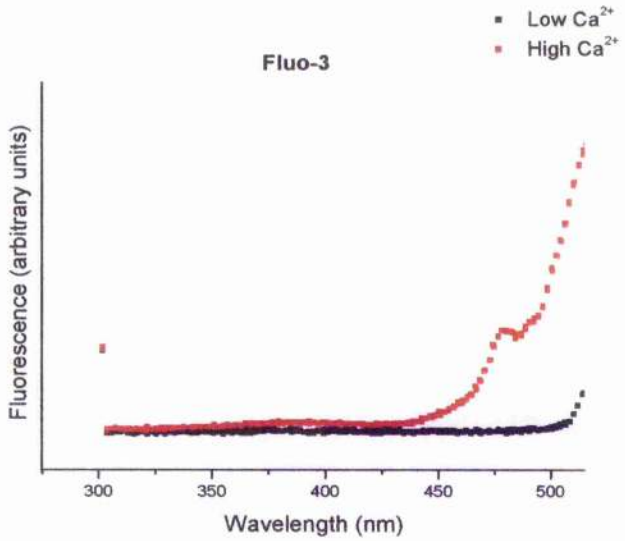
Low Ca^{2+}
High Ca^{2+}
Fluo-3
Fluorescence (arbitrary units)
300
350
400
450
500
Wavelength (nm)

Chapter 4
Use Of Fluorescent Ca^{2+} Indicators To Study Organelle Calcium Dynamics In Cardiac Muscle

Chapter 4-Use Of Fluorescent Indicators To Study Organelle Ca^{2+} Dynamics In Cardiac Muscle

4.1 Introduction

The $[Ca^{2+}]$ within sub-cellular compartments exerts an effect on diverse cellular processes such as ATP synthesis, protein processing and secretion of secretagogues from secretory cells. These processes have been subject to intense study in a variety of cell types. However the details regarding the precise regulation of organelle $[Ca^{2+}]$ within cardiac muscle remains unclear, this area is reviewed in detail in chapter 1 general introduction. Studies carried out using dissociated adult cardiac myocytes from rat investigating organelle calcium dynamics will be detailed and discussed.

The aim of this study was to examine the signals from fluorescent dyes loaded into the organelles of cardiac muscle. Insights into the types of compartments loaded with dyes were gleamed using a series of experimental interventions each using a permeabilised cell population to allow manipulation of the cytosolic $[Ca^{2+}]$ which are detailed as follows:

1. Recording of signals in response to an increased extracellular $[Ca^{2+}]$ highly buffered using EGTA
2. The effects of ionophore A23187 to dissipate any $[Ca^{2+}]$ gradients across all organelle membranes
3. Use of specific inhibitors to abolish any active organelle Ca^{2+} accumulation
   (a) Thapsigargin for SR
   (b) A cocktail of compounds to prevent mitochondrial Ca^{2+} uptake

The suitability of two main types of Ca^{2+} indicator were investigated in preliminary studies; Fluo-based and several FURA-based dyes. Fluo-based dyes have several advantages. (i) Their use to study intra-ER and intra-SR dynamics has been well documented, (Shmigol *et al.*, 2001) & (Shmigol *et al.*, 1999) (ii) Their long excitation wavelengths (approximately 490nm) reduces intrinsic fluorescence problems such as autofluorescence and (iii) The large change in fluorescence intensity over the Ca^{2+}-sensitive range of the dye should help distinguish signals from small discrete regions of the cell.

However initial experiments with the Fluo-dyes were unsuccessful primarily due to poor loading relative to the Fura-based dyes but the main problem being artefactual changes in fluorescence unrelated to changes in $[Ca^{2+}]$ but due to photobleaching or chemical quench.

Fura-based dyes appeared to load into cells/organelles more effectively and provided a ratiometric fluorescence signal that was unaffected by artefacts due to photobleaching and/or chemical quench.

The following results describe studies that were carried out in order to characterise organelle Ca^{2+} dynamics in cardiac muscle using the acetoxymethyl (AM) derivatives of Fura-2, FuraFF and MgFura-2. The dye Fluo-3 was included in the mock intracellular solution in some experiments to allow the simultaneous monitoring of the cytosolic $[Ca^{2+}]$.

4.2 Methods

Adult rat cardiac myocytes were prepared as described in the chapter 2, general methods.

4.2.1 Loading of Cardiac Myocytes with Acetoxymethyl Esters of Fluorescent Calcium Indicators

The protocol used to load cardiac myocytes with acetoxymethyl ester derivatives of fluorescent Ca^{2+} indicators is described in detail in section 2.3.1.

Figure 4.1 is a confocal fluorescence trace of a representative Fluo-3-AM loaded cardiomyocyte treated with the permeablising agent β-escin. On addition of the agent, there is a significant decline in the total cellular fluorescence. There is however, a significant level of fluorescence remaining, which can be attributed to indicator trapped within sub-cellular compartments/bound to cellular proteins or structures.

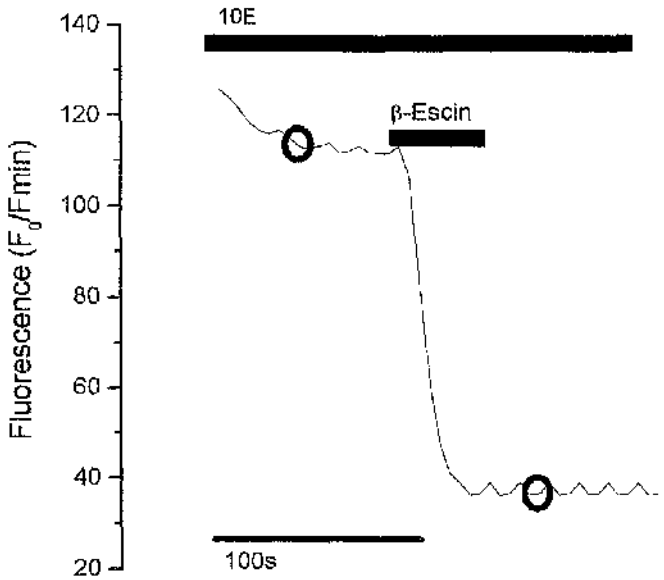

Figure 4.1 . Confocal fluorescence trace following the progression of permeabilisation

Confocal fluorescence trace monitoring the progress of permeabilisation of a representative Fluo-3-AM loaded cardiac myocyte. The cell was initially exposed to a solution containing 10mM EGTA for the period marked above the trace. At the point indicated, the cell was perfused with the same 10mM EGTA solution containing 100μg/mL β-escin. Circles on the trace denote when images shown in figure 4.2 where taken.

Figure 4.2 depicts images of representative Fluo-3-AM loaded cardiac myocytes taken before and after treatment with the permeabilising agent β-escin. The rapid decline in fluo-3 fluorescence indicates that the majority of cleaved fluo-3-AM free in the myoplasm leaves. In theory, the remaining cell fluorescence is due mainly to indicator trapped within organelles/bound to cellular structures.

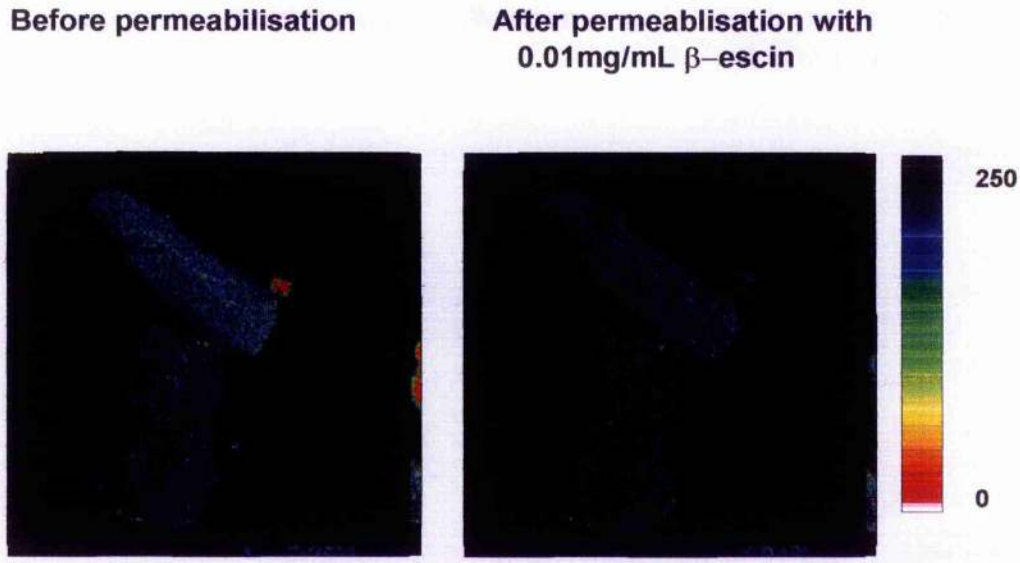

Figure 4.2. Confocal images of Fluo-3-AM loaded cardiomyocytes
Taken before and after permeablisation. The time points at which these images were acquired are shown on the graph in figure 4.1 denoted by the circles.

Dissociated Cardiomyocytes were incubated in the fore-mentioned Krebs' solution containing 1mM EGTA with 10μM of either Fura-2-AM, FuraFF-AM or MgFura-2-AM. Incubations were carried out for 90 minutes in 25mL Tissue culture-grade flasks in a 37°C incubator. This was followed by a 30-minute indicator free incubation at room temperature to allow dye cleavage by cellular esterases.

Cells were then permeabilised by brief exposure to either β-escin or saponin (0.1mg/mL). The cell concentration was adjusted to 0.5 x 10^6 cells/mL (previously optimised) and were then placed in a cuvette containing a mock intracellular solution of the following composition: 5mM EGTA, 25mM HEPES, 5.5mM $MgCl_2$, 100mM KCl pH 7.0. 4.2.2 System for studying Calcium dynamics on populations of cells

4.2.2 System for studying Calcium dynamics on populations of cells

Three different Fura based dyes were used in these studies; Fura-2, FuraFF and MgFura-2 which have different K_d values for Ca^{2+} and therefore diifferent Ca^{2+} affinities. Thus, it is possible to monitor changes within a cell in response to an identical manoeuvre, i.e. if there is a very large change in $[Ca^{2+}]$ occurring in response to the addition of a specific agent, it may be too large to be accurately measured with a high affinity indicator. Table 3.1 illustrates some of the properties of these 3 Fura dyes.

A closed cuvette system was used to study the calcium dynamics on populations of cells. This system is described in detail in section 2.3.2.

4.2.2 System for studying Calcium dynamics on populations of cells

Different compounds were used which specifically prevent active Ca^{2+} uptake by organelles of cardiac muscle.

4.2.3.1 Use of Ionophore A23187

Active accumulation of Ca^{2+} was detected by measuring the effects of the addition of the ionophore A23187. This compound binds to membrane systems and dissipates the Ca^{2+} and Mg^{2+} gradients (Erdahl *et al.*, 1996).

4.2.3.2 Use of thapsigargin

The inhibitor thapsigargin was used to selectively inhibit the SR/ER Ca^{2+} ATPase (SERCA) (Hove-Madsen L & Bers DM, 1993).

In these studies thapsigargin was used at a concentration of 25μM based on the measurements of Hove-Madsen and Bers. Using 0.5×10^5 cells this is equivalent to 0.9mg of total cell protein. This is approximately 8 times greater

than the concentration of thapsigargin required to ensure complete inhibition of active Ca^{2+} accumulation by SR via the cardiac muscle isoform SERCA2a.

4.2.3.3 Use of inhibitors of mitochondrial Ca^{2+} accumulation

Experiments were carried out in the presence of the compounds oligomycin (1μM), CCCP (3μM) and rotenone (1μM).

Oligomycin is a compound that inhibits the F_1/F_0 ATPase of mitochondria. Use of this prevents synthesis of ATP from ADP and P_i and translocation of protons from the myoplasm to the mitochondrial matrix. CCCP disconnects the electron transport chain from the formation of ATP, which in turn dissipates the membrane potential (ψ). Rotenone blocks NADH dehydrogenase (complex 1) in the respiratory chain. When used in conjunction with one another this trio of compounds should in theory completely abolish active Ca^{2+} uptake by mitochondria. The three mitochondrial inhibitors were used as a cocktail so as to ensure complete inhibition of active mitochondrial uptake (Duchen MR, 1999) & (Boitier E *et al.*, 1999).

4.2.4 Measurement of R_{min} and R_{max}

Fluorescence ratios were recorded from the cells after loading with each of the Fura-based indicators. The changes in ratio represent changes in $[Ca^{2+}]$ and is normally converted to $[Ca^{2+}]$ using the following formula (Grynkiewicz G *et al.*, 1985).

$$[Ca^{2+}] = K_{\bullet}\beta \frac{(R-R_{min})}{(R_{max}-R)}$$

Where $\beta = \frac{\text{(Fluorescence @ 365nm in low } [Ca^{2+}])}{\text{(Fluorescence @ 365nm in high } [Ca^{2+}])}$

K= Dissociation constant for Ca^{2+}

R_{min} was defined as the 340/365nm fluorescence ratio in the presence of $[Ca^{2+}]$ of <1nM in a solution containing 5mM EGTA. R_{max} was defined as the 340/365nm fluorescence ratio in the presence of saturating $[Ca^{2+}]$. For simplicity, in our measurements $K_d = (\beta \times K)$

Previous work has shown that the value of K_d is altered when the indicator is AM loaded within intracellular organelles (Poenie, 1990). We attempted to calibrate the intra-organelle indicator using a range of intracellular $[Ca^{2+}]$ in the presence of ionophore. This proved unsuccessful for high $[Ca^{2+}]$ due to changes in intrinsic cellular fluorescence. Figure 4.3 illustrates how each individual wavelength alters and it's subsequent effect on the ratio.

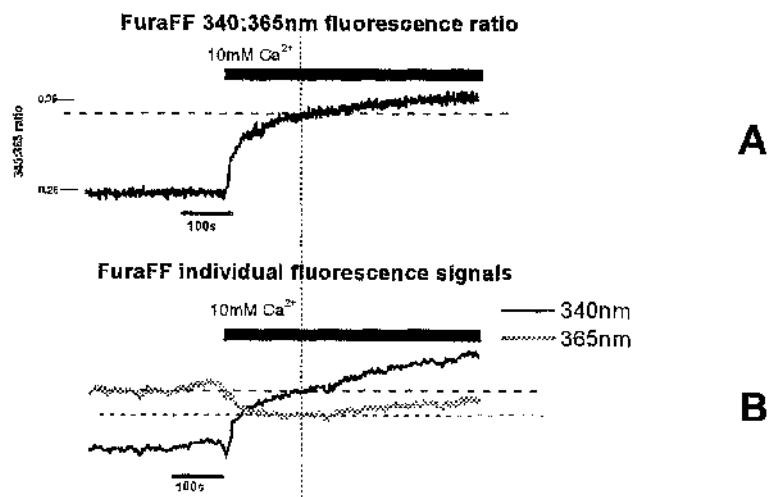

Figure 4.3 Fluorescence properties of FuraFF.

Panel A shows the 340nm:365nm fluorescence ratio. Panel B the individual wavelengths. 10mM Ca^{2+} is added in the presence of A23187

In these experiments R_{max} was measured just prior to secondary slow changes. These slow secondary changes in fluorescence were only observed at high [Ca^{2+}] and prevented calibration of low affinity dyes.

The results presented are the fluorescence ratios normalised to R_{min} and R_{max} using the following relationship:

$$\text{Normalised ratio} = \frac{(\text{Ratio}-R_{min})}{(R_{max}-R_{min})}$$

4.3 Results

4.3.1 Effects of Ca^{2+} ionophore on Fura-based organelle signal

Experiments were carried out with populations of permeablised cells loaded with Fura-2-AM, FuraFF-AM and MgFura-AM. A23187 to a final concentration of 1μM was added to the cells. Cytosolic [Ca^{2+}] was buffered using 5-15mM EGTA/CaEGTA solutions.

The three sets of studies with cells loaded with the three different dyes all followed an identical protocol; cytosolic [Ca^{2+}] was raised from <1nM using CaEGTA to give a free [Ca^{2+}] of 760nM. This was followed by addition of 25μM thapsigargin and then 1 μM A23187. The maximum fluorescence ratio (R_{max}) was achieved by addition of 10mM $CaCl_2$ to the cuvette. The experiments were repeated in the sustained presence of 1 μM A23187. Tables 4.2 and 4.3 show the mean results for each of the three dyes in the absence and presence of A23187.

4.3.1.1 Fura-2

Representative traces from experiments carried out with Fura-2-AM loaded cells in the presence and absence of A23187 are shown in figures 4.4a and 4.4b.

Raising the cytosolic [Ca^{2+}] to 760nM causes a rise in the 340:365 ratio in both cases. In the control experiments the mean 340:365 fluorescence ratio normalized to R_{min} and R_{max} is 0.281 ± 0.0067 (n=5) and the presence of ionophore 0.426 ± 0.05 (n=7). The presence of A23187 appears to speed up

the rate of Ca^{2+} uptake into a sub-cellular compartment or compartments. A significant component of this signal appears to be passive.

4.3.1.2 FuraFF

Representative traces from experiments carried out with FuraFF-AM loaded cells in the presence and absence of A23187 are shown in figures 4.5a and 4.5b. Increasing the extracellular [Ca^{2+}] to 760nM caused an increase in the FuraFF fluorescence ratio. The mean normalized ratio is 0.174± 0.01 (*n*=11) Subsequent addition of thapsigargin caused a small decrease in the fluorescence ratio in the graph shown, but the mean is 0.169± 0.01 (*n*=5). This is not significantly different from the previous level. A23187 addition caused rapid decline in ratio to almost the level of R_{min} in the control cells.

Referring to figure 5.5b, A23187 addition with an extracellular [Ca^{2+}] of <1nM did not give rise to any significant change in the fluorescence ratio. Raising the extracellular [Ca^{2+}] to 760nM caused a small increase in the fluorescence ratio. The mean ratio in this case being 0.05 ± 0.009 (*n*=10) Addition of thapsigargin and additional A23187 caused no further significant changes.

4.3.1.3 MgFura-2

Representative traces from experiments carried out with MgFura-2-AM loaded cells in the presence and absence of A23187 are shown in figures 5.6a and 5.6b.

In the control experiments, raising free $[Ca^{2+}]$ to 760nM, the mean fluorescence ratio is 0.032 ± 0.007 (n=6). In the sustained presence of A23187 this ratio is 0.015 ± 0.007 (n=5)

Addition of A23187 at the beginning of the protocol results in a decline in fluorescence ratio. The normalised ratio is represented as a negative value to R_{min}. In other words the ratio value is less than the ratio attained in <1nM Ca^{2+} Raising free $[Ca^{2+}]$ to 0.76μM, thapsigargin addition or subsequent A23187 do not alter the fluorescence ratio significantly. If a passive uptake pathway does exist, the MgFura ratio changes would not reflect this as it is a low affinity indicator.

Dye	(A) Normalized ratio in $[Ca^{2+}]_{CY}$=760nM	(B) Normalized ratio in 25μM TG	(C) Normalized ratio in 1μM A23187
Fura-2	0.281± 0.06 (n=5)	**0.352± 0.07* (n=5)**	**0.427± 0.043 * (n=6)**
FuraFF	0.174± 0.005 (n=11)	0.169± 0.01 (n=5).	**0.045± 0.005* (n=11).**
MgFura-2	0.032± 0.007 (n=6).	0.032± 0.009 (n=6).	**-0.076± 0.01 * (n=6).**

Table 4.1. Mean normalized fluorescence ratio values.

For tables 4.1, 4.2 and 4.3 values shown in bold with an asterix denote results that are significantly different from column A ($p<0.05$).

Dye	(A) Normalized ratio in $[Ca^{2+}]_{CY}$=760nM	(B) Normalized ratio in 25μM TG	(C) Normalized ratio in 1μM A23187
Fura-2	0.426± 0.03 (*n*=7)	0.471± 0.03 (*n*=6)	**0.506± 0.03* (*n*=6)**
FuraFF	0.055± 0.01 (*n*=10)	0.083± 0.01 (*n*=5).	**0.032± 0.01* (*n*=10).**
MgFura-2	0.015± 0.007 (*n*=5).	0.02± 0.009 (*n*=6).	**-0.06± 0.02* (*n*=6).**

Table 4.2. Mean normalized fluorescence ratio values for experiments in the presence of 1μM A23187.

Fura-2-AM, Fura-FF-AM, Mgfura-2-AM loaded Cardiac Myocytes in the presence and absence of 1μM A23187

Fura-2-AM loaded
Figure 4.4a

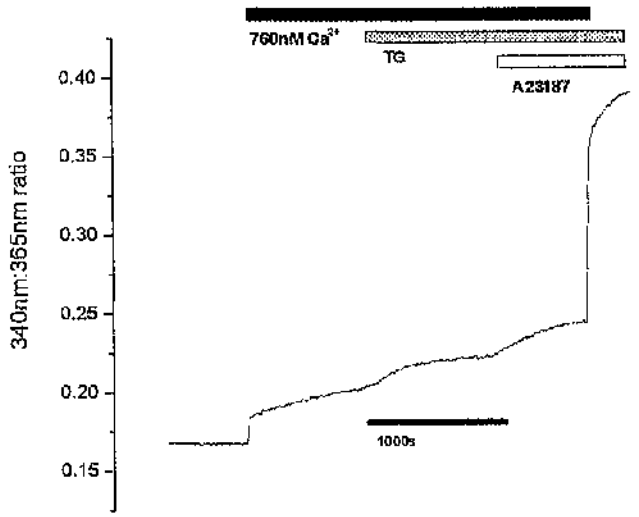

Figure 4.4b

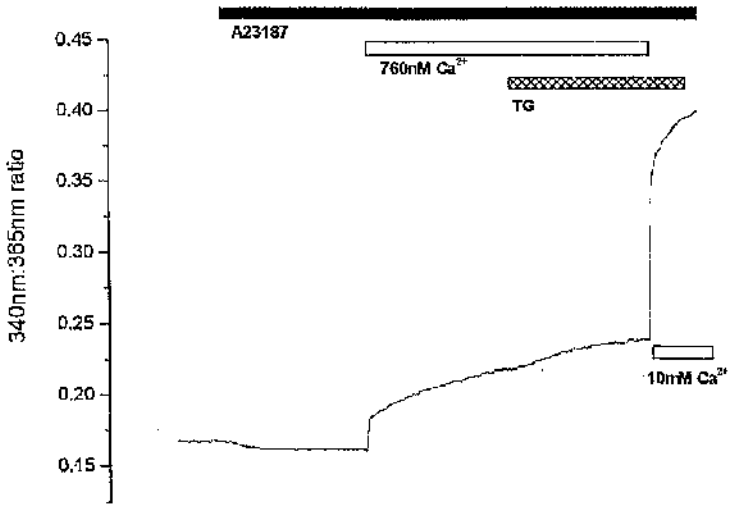

Figure 4.4. Fura-2-AM loaded Cardiomyocytes in the presence and absence of 1μM A23187. Cell populations were maintained in <1nM [Ca^{2+}] in 5mM EGTA.

FuraFF-AM loaded

Figure 4.5a

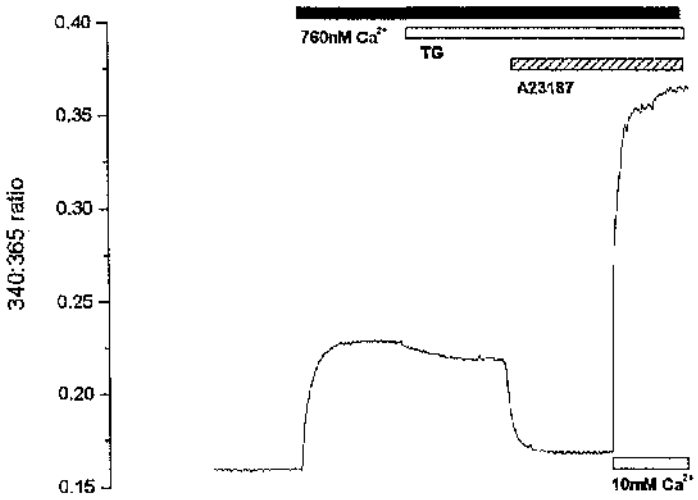

Figure 4.5b

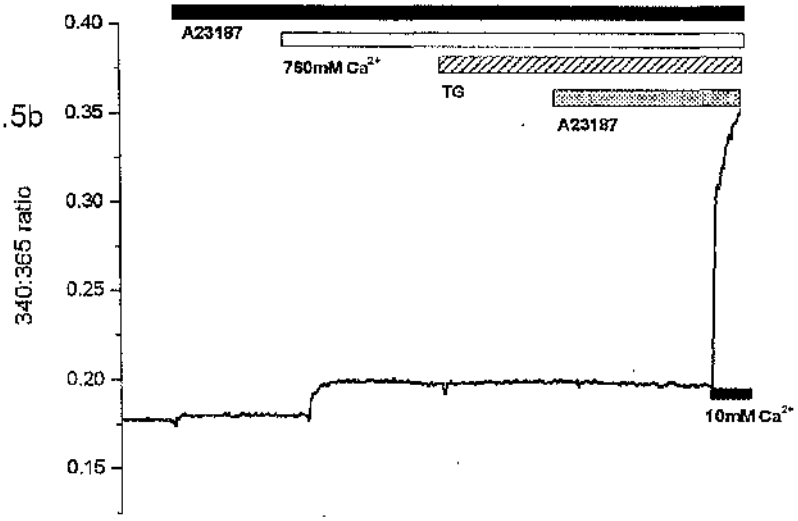

Figure 4.5. FuraFF-AM loaded Cardiomyocytes in the presence and absence of 1μM A23187. Cell populations were maintained in <1nM [Ca^{2+}] in 5mM EGTA.

MgFura-AM loaded
Figure 4.6a

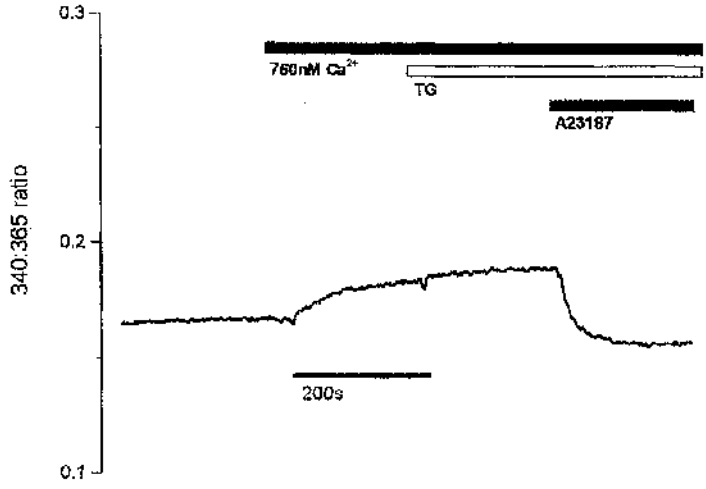

Figure 4.6b

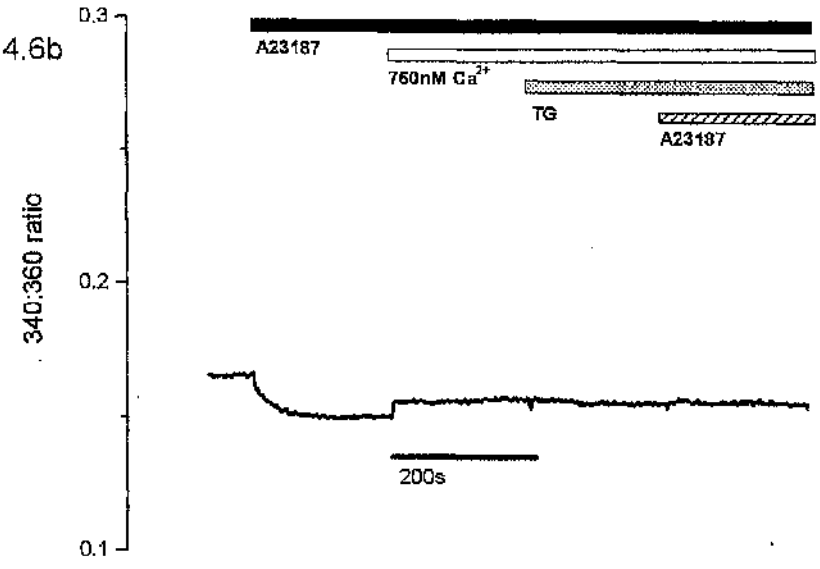

Figure 4.6. MgFura-2-AM loaded Cardiomyocytes in the presence and absence of 1μM A23187. Cell populations were maintained in <1nM [Ca^{2+}] in 5mM EGTA.

4.3.2 Experiments in the presence of mitochondrial inhibitors

Representative traces from the initial experiments carried out with these compounds and termed 'mitochondrial inhibition' with Fura-2-AM, FuraFF-AM and MgFura-2-AM loaded cardiac myocytes are shown in figures 4.7-4.9.

The protocol involved raising the free [Ca^{2+}] to 120nM, 380nM and 760nM using buffered EGTA/CaEGTA solutions. In the experiments shown for Fura-2-AM loaded cells this protocol only involved one increment in the increase of the cytosolic [Ca^{2+}] of 760nM. Table 4.4 shows the mean results for each of the three dyes in the presence of 1μM oligomycin, 3μM CCCP and 1μM rotenone.

4.3.2.1 Fura-2

Representative traces from experiments in the absence and presence of the mitochondrial inhibitor cocktail with Fura-2-AM loaded cardiomyocytes are shown in figures 4.7a and 4.7b. In the presence of the mitochondrial inhibitor cocktail (figure4.5b), raising the cytosolic [Ca^{2+}] from <1nM to 760nM causes a rise in the 340:365nm fluorescence ratio.

4.3.2.2 FuraFF

In FuraFF-AM loaded cells there is a significant difference between control experiments and those in the presence of mitochondrial inhibitors as shown in figures 4.8a and 4.8b. In the absence of mitochondrial inhibitors (Figure 4.8a), raising the cytosolic [Ca^{2+}] from <1nM in steps to 126nM, 380nM and finally 760nM each time causes a rise in the 340:365nm fluorescence ratio. In the presence of the inhibitor cocktail (Figure 6b) the same manoeuvres also

causes an increase in the fluorescence ratio but the magnitude is very much smaller. In both sets of experiments thapsigargin addition causes a small decrease in the ratio.

4.3.2.3 MgFura-2

Experiments were carried out with cells loaded with MgFura-2-AM shown in figures 4.9a and 4.9b. The same protocol was carried out as with the FuraFF-AM loaded cells. Raising the cytosolic $[Ca^{2+}]$ in the absence and presence of the mitochondrial inhibitor cocktail causes virtually no changes in the fluorescence ratio. A23187 addition in both cases a large decline in the fluorescence ratio to a value far lower than that observed at the beginning of the experiment in the presence of 5mM EGTA which conventionally was used as a measure of R_{min}.

Table 4.4 shows the mean normalized fluorescence ratio values.

Dye	(A) Normalized ratio in $[Ca^{2+}]_{CY}$=760nM	(B) Normalized ratio in 25μM TG	(C) Normalized ratio in 1μM A23187
Fura-2	0.303± 0.07 (*n*=6)	0.37± 0.08 (*n*=6)	**0.489± 0.02* (*n*=6)**
FuraFF	0.076± 0.001 (*n*=15)	**0.071± 0.014* (*n*=5).**	**0.056±0.0013* (*n*=15).**
MgFura-2	0.023± 0.001 (*n*=6).	**0.023± 0.001* (*n*=6).**	**-0.06± 0.01* (*n*=6).**

Table 4.3. Mean normalized fluorescence ratio values in the presence of oligomycin (1μM), CCCP (3μM) and rotenone (1μM).

Fura2-AM, FuraFF-AM and MgFura-AM loaded cardiomyocytes in the presence and absence of mitochondrial inhibitors

Fura-2-AM loaded

Figure 4.7a

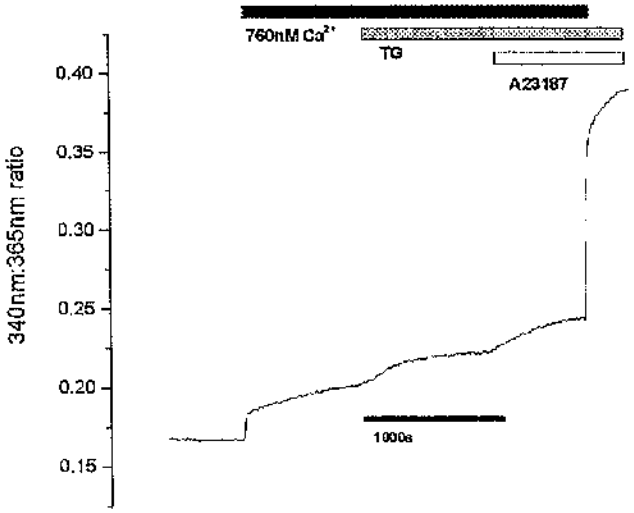

Figure 4.7b

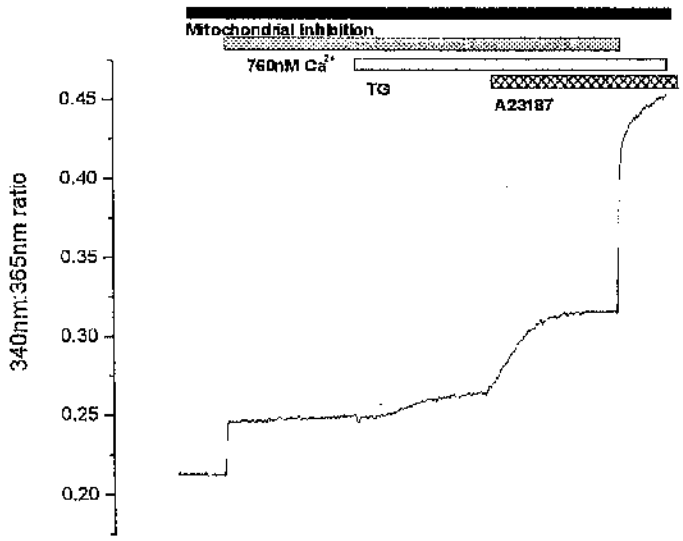

Figure 4.7. Fura-2-AM loaded Cardiomyocytes in the presence and absence of 1μM oligomycin, 3μM CCCP and 1μM rotenone. Cell populations were maintained in <1nM [Ca^{2+}] in 5mM EGTA.

FuraFF-AM loaded
Figure 4.8a

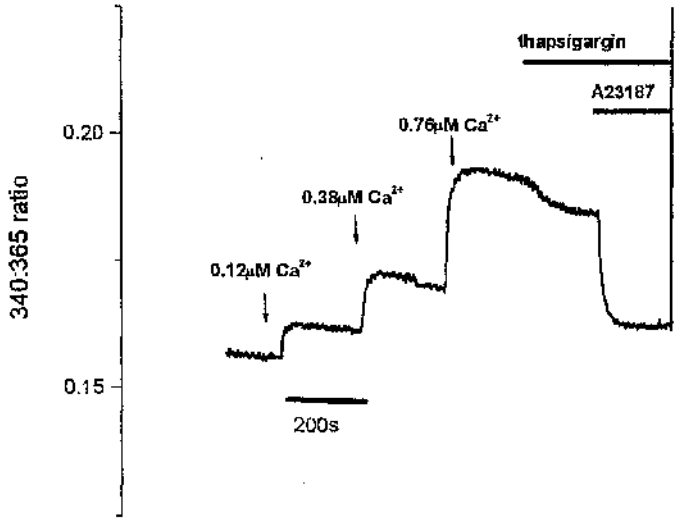

Figure 4.8b

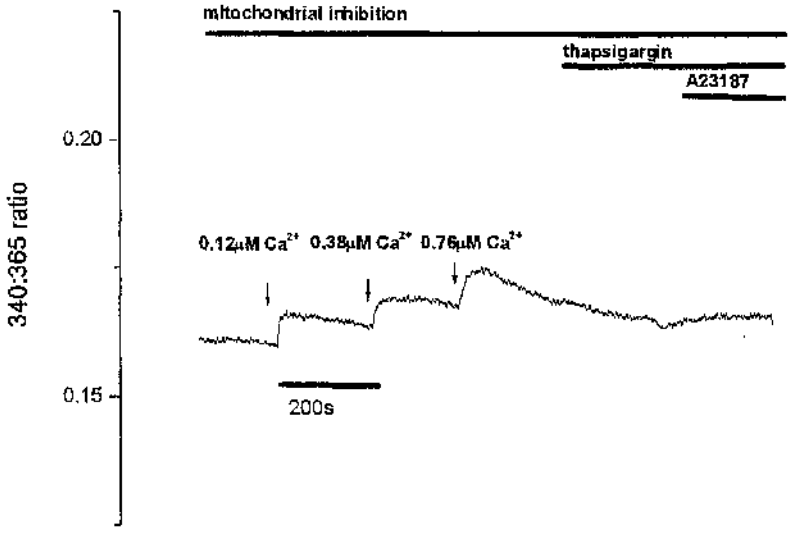

Figure 4.8. FuraFF-AM loaded Cardiomyocytes in the presence and absence of 1μM oligomycin, 3μM CCCP and 1μM rotenone. Cell populations were maintained in <1nM [Ca^{2+}] in 5mM EGTA.

MgFura-AM loaded

Figure 4.9a

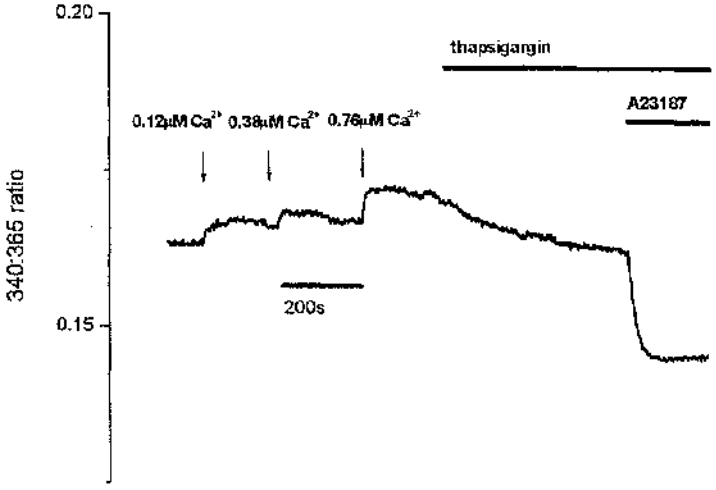

Figure 4.9b

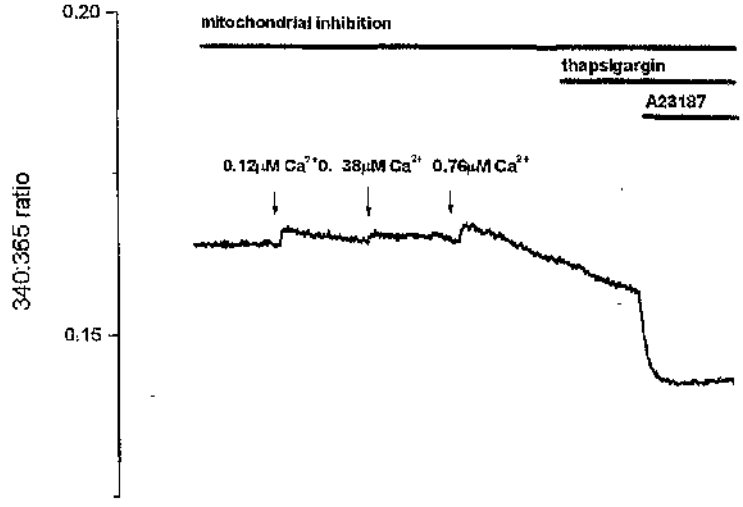

Figure 4.9. MgFura-2-AM loaded Cardiomyocytes in the presence and absence of 1μM oligomycin, 3μM CCCP and 1μM rotenone. Cell populations were maintained in <1nM [Ca^{2+}] in 5mM EGTA.

Figures 4.10a-4.10c are a summary of the experiments carried out in the presence of mitochondrial inhibitors and A23187. 340:365nm ratio shown is the mean ratio normalized to the R_{min} and R_{max} of each experiment. Figure 4.10a shows results from the Fura-2-AM loaded cardiac myocytes. The legend along horizontal axis refers to addition of either CaEGTA to increase the cytosolic $[Ca^{2+}]$to 760nM, 25μM thapsigargin and 5μM A23187. The presence of the mitochondrial inhibitor cocktail or A23187 does not appear to prevent uptake into the sub-cellular compartment(s).

Figure 4.10b shows the mean normalized ratios from experiments with FuraFF-AM loaded cardiac cells. Presence of mitochondrial inhibitors significantly reduces the increases in ratio in response to raising the cytosolic $[Ca^{2+}]$. Thapsigargin under all three conditions does not appear to have a significant effect on the ratio.

Finally, figure 4.10c depicts average, normalized 340:365nm ratios for experiments carried out with MgFura-2-AM loaded cells. Looking at the control experiments, addition of thapsigargin after raising the cytosolic $[Ca^{2+}]$ to 760nM appears to have no effect. In the experiments in the presence of mitochondrial inhibitors and A23187, thapsigargin leads to a decrease in the average normalized fluorescence ratio. Addition of A23187 under all three conditions causes a large decrease in ratio to a value below that of the initial fluorescence ratio (R_{min}).

A semi- quantitative model to help clarify these results is given in appendix I.

Figures 4.11a-411c show the normalized fluorescence ratio values obtained with varying [Ca^{2+}] are shown for each of the three indicators. Data shown are from values obtained with the pentapotassium salt (free acid, closed circles), AM loaded cardiomyocytes (open squares), AM loaded cardiomyocytes in the presence of mitochondrial inhibitors (open circles) and AM loaded cardiomyocytes in the presence of ionophore A23187 (closed diamonds).

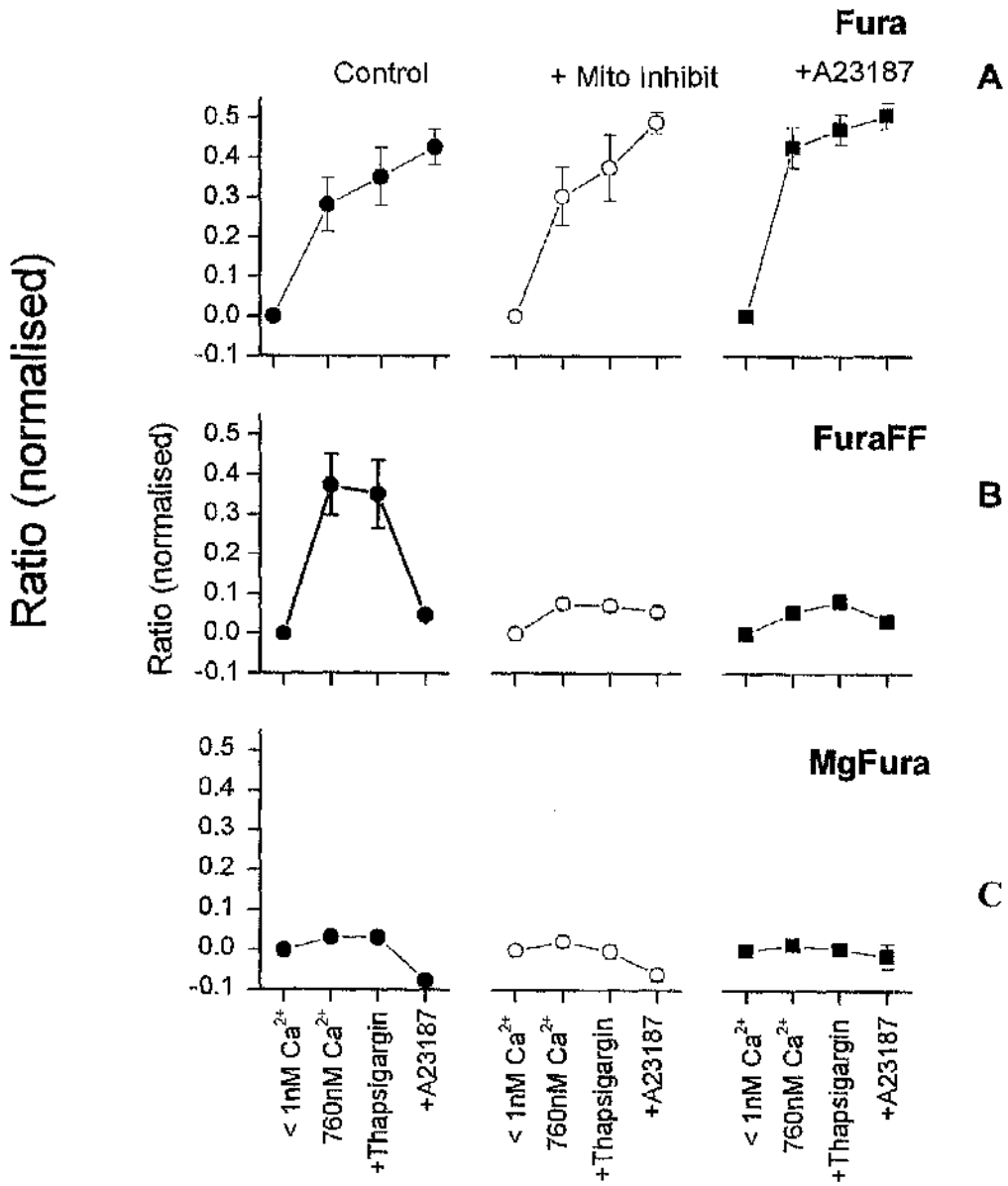

Figure 4.10. Mean normalized ratio values for each of the three sets of studies with the three different FURA indicators

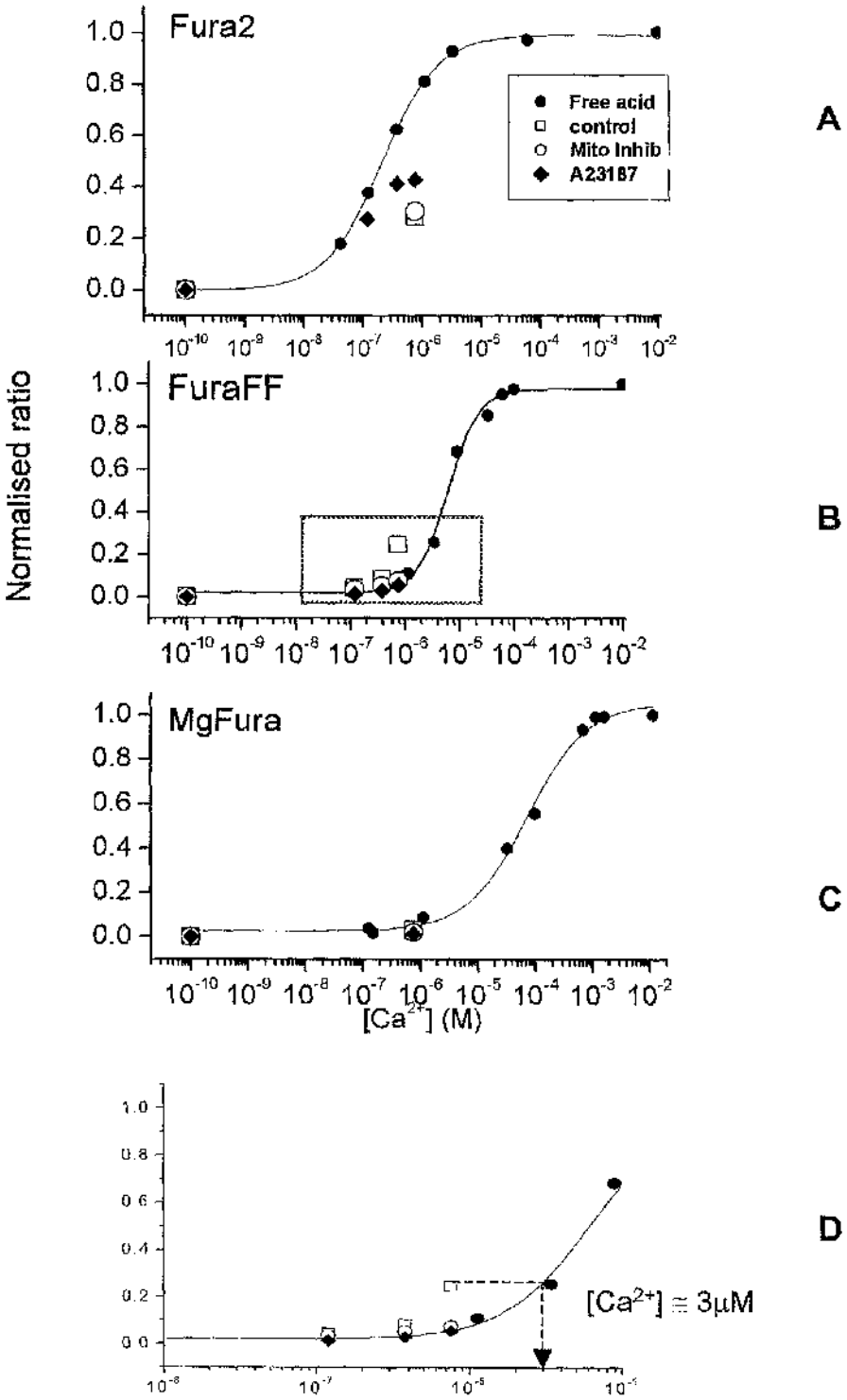

Figure 4.11. Calibration curves of the indicators. Also shown population cell data. Each of the inidicators shown in panels a-c. Panel d illustrates an expanded section of the graph in panel b for FuraFF. This illustrates the estimate of the $[Ca^{2+}]_{mito}$ due to active uptake. The section expanded is shown with a red box.

4.3.3 Investigating changes in the MgFura-2 signal

In studies with populations of cells that had been loaded with MgFura-2-AM the result obtained after addition of 1μM A23187 in the presence and absence of mitochondrial inhibitors (figures 4.9a and 4.9b) are indistinguishable. The dramatic decrease in ratio on ionophore addition cannot be easily explained by changes in $[Ca^{2+}]$. One possible explanation is changes in $[Mg^{2+}]$ interfering with the signal.

Therefore changes in $[Mg^{2+}]$ within organelles were investigated. Nigericin and the respiratory substrates Succinate with P_i are known to increase $[Mg^{2+}]$ of the mitochondrial matrix ($[Mg^{2+}]_m$) (Brierley *et al.*, 1987) & (Jung & Brierley, 1994).

These experimental manipulations were used in these studies to alter mitochondrial $[Mg^{2+}]$. Representative diagrams are shown in figures 4.12 and 4.13. As expected the MgFura ratio increases when both nigericin and succinate are added.

Representative trace from experiments carried under the same conditions but with FuraFF-AM loaded cells is shown in figures 4.15-4.17. This shows that addition of succinate with P_i causes virtually no change in ratio, as is also the case with A23187 addition. A subsequent study of the changes occurring with $[Ca^{2+}]$ using the respiratory substrate succinate with added P_i was carried out, results of which are shown in figures 4.14 and 4.16. In MgFura-2-AM and

FuraFF-AM loaded cells were studied. In both sets of experiments presence of succinate and Pi accelerates Ca^{2+} influx into mitochondria.

MgFura-AM loaded Cardiomyocytes

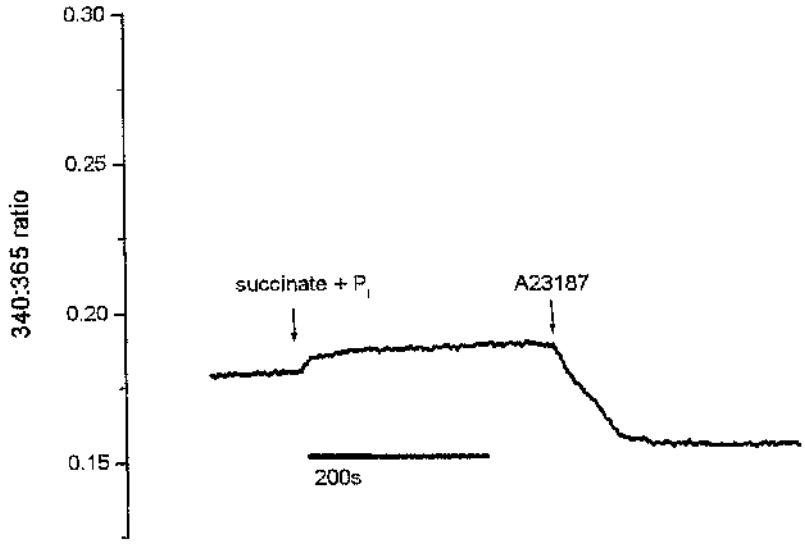

Figure 4.12. MgFura-2-AM loaded cardiomyocytes. Cells were in a mock intracellular solution containing 5mM EGTA (see methods for composition) thus clamping the [Ca^{2+}] at <1nM.

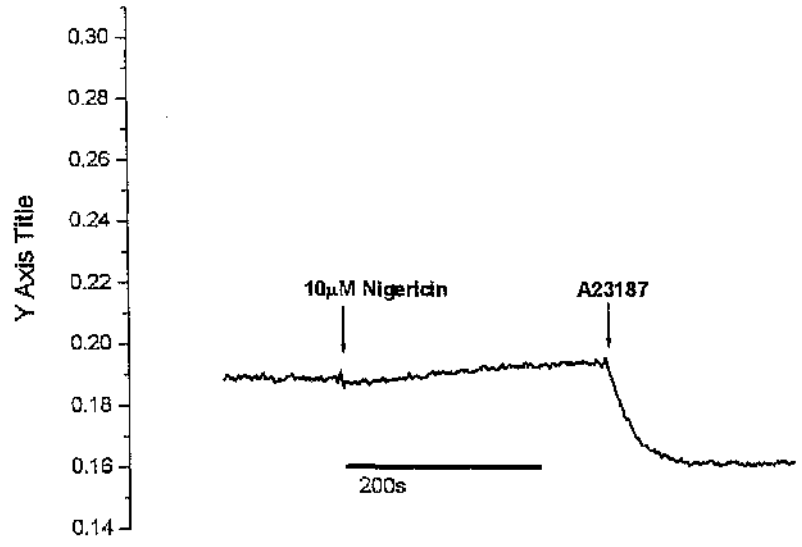

Figure 4.13. MgFura-2-AM loaded cardiomyocytes. Cells were in a mock intracellular solution containing 5mM EGTA (see methods for composition) thus clamping the [Ca^{2+}] at <1nM.

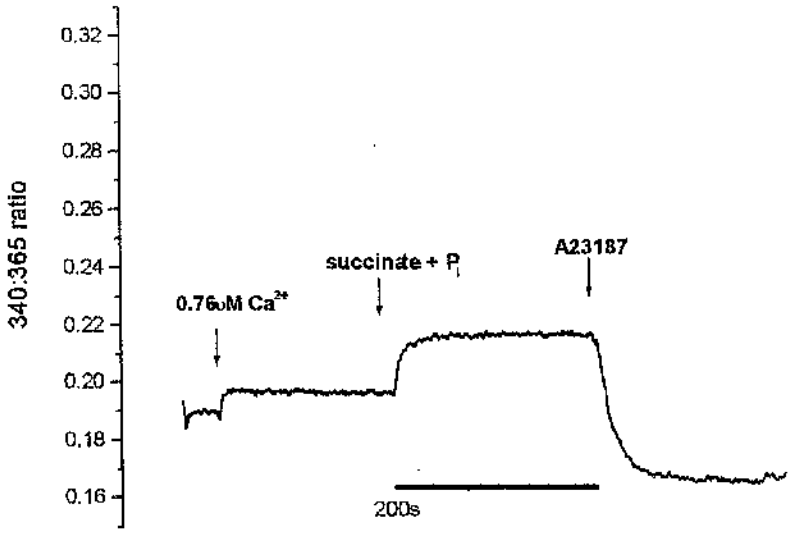

Figure 4.14. MgFura-2-AM loaded cardiomyocytes. Cells were in a mock intracellular solution containing 5mM EGTA (see methods for composition) The cytosolic [Ca^{2+}] was raised to 760nM prior to succinate addition.

FuraFF-AM loaded Cardiomyocytes

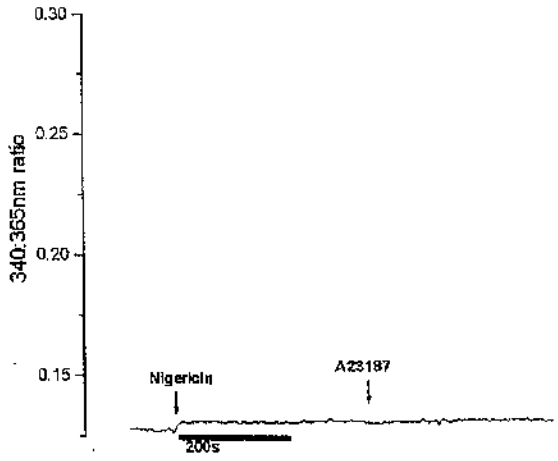

Figure 4.15. FuraFF-AM loaded cardiomyocytes. Cells were in a mock intracellular solution containing 5mM EGTA (see methods for composition) thus clamping the [Ca^{2+}] at <1nM.

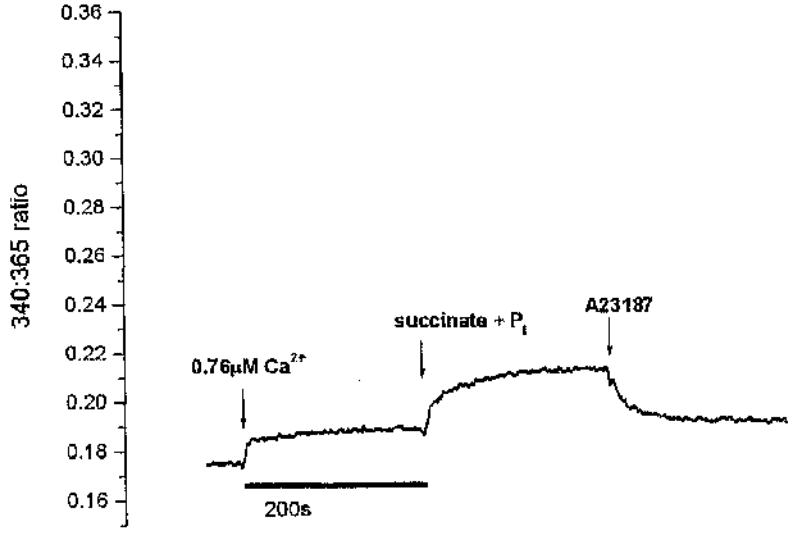

Figure 4.16. FuraFF-AM loaded cardiomyocytes. Cells were in a mock intracellular solution containing 5mM EGTA (see methods for composition) The cytosolic [Ca^{2+}] was raised to 760nM prior to succinate addition.

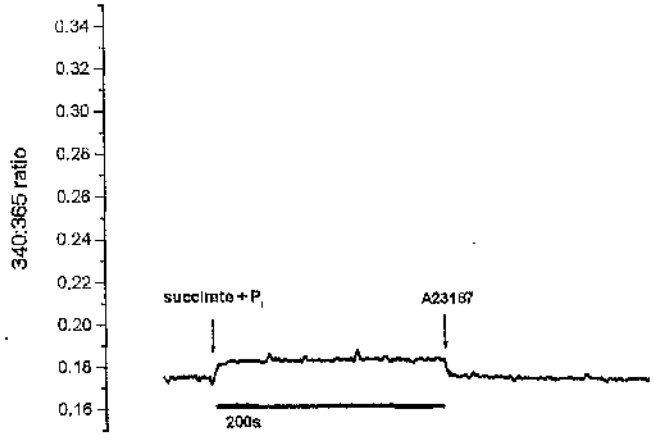

Figure 4.17. FuraFF-AM loaded cardiomyocytes. Cells were in a mock intracellular solution containing 5mM EGTA (see methods for composition) thus clamping the [Ca^{2+}] at <1nM.

4.4 Discussion

4.4.1 Studies in the presence of Ca^{2+} ionophore

Figures 4.4-4.6 illustrate the results of studies carried out with populations of permeabilised cells loaded with Fura-2-AM, FuraFF-AM and MgFura-2-AM in the presence of ionophore. 340:365 fluorescence ratio changes corresponding to the changes in $[Ca^{2+}]$ were markedly different between the populations of cells loaded with each of the dyes.

4.4.1.1 Fura-2

In control experiments with Fura-2-AM loaded cells, an example of which is shown in figure 4.4a, raising cytosolic $[Ca^{2+}]$ to 760nM causes a rapid rise in the 340:365nm fluorescence ratio which does not reach a steady state. Thapsigargin addition has no apparent effect on this signal. However in these control experiments addition of A23187 appeared to speed up the exchange of Ca^{2+} and causes a subsequent rise in the 340:365nm ratio to attain a steady state value.

Comparing the control experiments to those carried out in the presence of A23187 shown in figure 4.4b, raising the cytosolic $[Ca^{2+}]$ to 760nM causes a rise in the 340:365nm fluorescence ratio. The magnitude of this rise is greater than that observed with the control experiments. Intriguingly in the control experiments shown in figure 4.4a, A23187 addition after the 760nM step speeds up the rate of equilibration of Ca^{2+}. The ratio change attained is almost of the same magnitude of that observed in figure 4.4b after the 760nM step in

the sustained presence of A23187. Another interesting observation with these studies is that thapsigargin addition has no apparent effect on the ratio as is the case the control experiments. Previous studies have not identified a specific slow exchange compartment. A considerable amount of work has used the $^{45}Ca^{2+}$ washout technique to study the different compartments capable of Ca^{2+} exchange. In general, 3 exchangeable compartments have been identified. A rapidly exchanging compartment (half time <1s) has been attributed to the sub-sarcolemmal junctional region (Post & Langer, 1992). A second slower compartment termed "intermediate compartment" could be attributed to the SR (half time 19 s). A final third compartment with an exchange time of approximately 4 min was attributed to mitochondria (Langer *et al.*, 1990). It is conceivable that the slowly exchangeable compartment in the current study corresponds to this slow, mitochondrial compartment. Interestingly, this component was retained in the presence of mitochondrial inhibitors, suggesting that even mitochondria without an active uptake mechanism can exchange Ca^{2+}.

4.4.1.2 FuraFF

Figures 4.5a and 4.5b are representative of the results obtained from experiments with FuraFF-AM loaded cells. There is a clear difference between the ratio changes in the two sets of experiments.

In the control experiments, a representative result shown in figure 3a, increasing the extracellular [Ca^{2+}] to 760nM caused an increase in the FuraFF fluorescence ratio. Subsequent addition of thapsigargin caused a small

decrease in ratio. A23187 addition caused rapid decline in ratio almost equivalent to the R_{min} in the control cells.

Referring to figure 4.5b, A23187 addition with an extracellular $[Ca^{2+}]$ of <1nM did not give rise to any change in the fluorescence ratio. Raising the extracellular $[Ca^{2+}]$ to 760nM could only elicit a small increase in the fluorescence ratio. This rise is almost 50% of the magnitude of the rise observed in the absence of ionophore. Addition of thapsigargin and additional A23187 caused no further change in the fluorescence ratio.

These results suggest that A23187 dissipates an active $[Ca^{2+}]$ gradient between compartments and the cytosolic medium within the cardiac cell.

4.4.1.3 MgFura-2

Representative traces from experiments carried out with MgFura-2-AM loaded cells in the presence and absence of A23187 are shown in figures 4.6a and 4.6b. Cardiomyocytes loaded with this dye responded with a small increase in fluorescence ratio with increasing cytosolic $[Ca^{2+}]$

Perhaps the most intriguing observation of studies of cells loaded with this dye is the fact that thapsigargin failed to have a significant effect on the ratio but A23187 caused a rapid decline in the ratio to below the value observed in the absence of Ca^{2+}. As shown in figure 4.6b, addition of A23187 in the presence of low $[Ca^{2+}]$ caused a rapid decline the fluorescence ratio that did not change on increasing $[Ca^{2+}]$

While the results from the studies with Fura-2 and FuraFF are consistent with significant passive and active components of Ca^{2+} accumulation in cardiac cells, the response of MgFura-2 cannot be explained simply in terms of $[Ca^{2+}]$ within intracellular compartments.

4.4.2 Studies in the presence of mitochondrial inhibitors

Figures 4.7-4.9 illustrate the results of studies carried out with populations of permeabilised cells loaded with Fura-2-AM, FuraFF-AM and MgFura-2-AM in the presence of the cocktail of mitochondrial inhibitors. 340:365 fluorescence ratio changes corresponding to the changes in $[Ca^{2+}]$ were markedly different between the populations of cells loaded with each of the dyes.

4.4.2.1 Fura-2

Representative traces from experiments in the absence and presence of the mitochondrial inhibitor cocktail with Fura-2-AM loaded cardiomyocytes are shown in figures 4.7a and 4.7b. A representative graph from experiments carried out in the presence of mitochondrial inhibitors is shown in figure 4.5b.

In the presence of the mitochondrial inhibitor cocktail raising the cytosolic $[Ca^{2+}]$ from <1nM to 760nM causes a rise in the 340:365nm fluorescence ratio. The rate and magnitude of this rise is very similar to that observed in the control experiment. As is the case with the other studies carried out in the presence and absence of A23187 (Figures 4.4a and 4.4b) thapsigargin addition has no apparent effect on the signal. Another striking similarity between these and the control experiments is that ionophore addition appears to speed up the rate of equilibration of Ca^{2+}.

4.4.2.2 FuraFF

In FuraFF-AM loaded cells there is a significant difference between control experiments and those in the presence of mitochondrial inhibitors as shown in figures 4.8a and 4.8b. The most striking difference between the two sets of experiments are responses when [Ca^{2+}] is raised, particularly the 0.38 and 0.76μM additions. When mitochondrial inhibitors are present these ratio changes are very much smaller.

Comparing results obtained in the presence and absence of mitochondrial inhibitors, intriguingly, after increasing free [Ca^{2+}] to 0.76μM there is an initial rise in ratio followed by a decline, more pronounced in the control experiments. The reason for this is unclear. Possibly the Ca^{2+} influx up into sub-cellular compartment(s) is proceeded by shuttling to other parts of the organelles or binding to Ca^{2+} binding proteins.

In control experiments, but not those in the presence of mitochondrial inhibitors, thapsigargin addition causes a small decrease in the ratio. This would suggest that a small proportion of the signal can be attributed to SR Ca^{2+} dynamics, although the bulk of the FuraFF signal can be attributed to active mitochondrial Ca^{2+} uptake.

4.4.2.3 Comparing the results with known buffered [Ca^{2+}]

Figures 4.11a-4.11c shows the normalized fluorescence ratio values obtained with varying [Ca^{2+}] are shown for each of the three indicators. Data shown are from values obtained with the pentapotassium salt (free acid, closed circles), AM loaded cardiomyocytes (open squares), AM loaded cardiomyocytes in the presence of mitochondrial inhibitors (open circles) and AM loaded cardiomyocytes in the presence of ionophore A23187 (closed diamonds). Examination of the Fura-2 data (Figure 4.11a) reveals a deviation from the free acid calibration under all of the experimental conditions with the AM loaded cells. The reason for this is unclear. One possible explanation is that there is a shift in the indicator's K_d for Ca^{2+} in that the K_d increases and thus the affinity decreases shifting the curve to the right (Harkins AB *et al.*, 1993).

Based on the calibration curves constructed for this thesis, the mean free $[Ca^{2+}]_{MIT}$ was estimated at approximately 3μM at $[Ca^{2+}]_{CYT}$= 760nM. This agrees well with estimates from adult cardiac myocytes using selective mitochondrial loading of Indo-1-AM (Griffiths, 2000) and mitochondria from other cell types using mitochondrially-targeted aequorin (Montero *et al.*, 2001) and (Montero *et al.*, 2000)

4.4.2.4 MgFura-2

In addition to FuraFF, experiments were carried out with cells loaded with MgFura-2-AM shown in figures 4.9a and 4.9b. Comparing the representative traces of control and presence of mitochondrial inhibitors does not reveal a significant difference in the ratio changes. This is in direct contrast with the

experiments carried out with FuraFF-AM loaded cells where inhibition of active mitochondrial uptake significantly affects Ca^{2+} influx into sub-cellular compartments.

Perhaps the most intriguing difference between FuraFF and MgFura-2 experiments is the response to the addition of the ionophore A23187. In the presence of mitochondrial inhibitor cocktail, with FuraFF-AM loaded cells (figure 4.8b) A23187 addition apparently has no effect on the ratio, whereas with MgFura-2-AM loaded cells there is a rapid decline in the fluorescence ratio following ionophore addition. There is no significant difference in this change between control and experiments with mitochondrial inhibition. This presents somewhat of a puzzle as to why this happens as even with control experiments. The ratio decline following ionophore addition should appear to be smaller in magnitude with MgFura-2 as is the case following the Ca^{2+} additions due to the dye having lower Ca^{2+} affinity. The most probable explanation for this that the change observed with added A23187 is due to changes in $[Mg^{2+}]$ as MgFura-2 can also indicate Mg^{2+} changes and has been used in the past to monitor $[Mg^{2+}]$ within organelles (Jung *et al.*, 1996) (Jung *et al.*, 1997).

The original aim of measurements with MgFura-2 was to measure free $[Ca^{2+}]_{SR}$ within adult cardiac muscle. Previous studies using MgFura-2-AM loaded astrocytes and arterial myocytes have shown signals attributable to ER for astrocytes and SR for arterial myocytes (Golovina & Blaustein, 1997). Low affinity Fluo-based dyes have been used to estimate $[Ca^{2+}]$ within SR of

smooth muscle (Shmigol *et al.*, 2001) and skeletal muscle (Kabbara & Allen, 2001). However as shown in the results, no signal could be obtained that was clearly attributable to the SR. The modelling described in the appendix to this chapter estimates the theoretical signal had MgFura-2-AM been loaded into the SR. A later chapter discusses why the SR Ca^{2+} signal does not appear to contribute to the MgFura-2 organelle signal.

4.4.3 Effect of changing the mitochondrial [Mg^{2+}] on the MgFura signal

As described previously, a somewhat intriguing result was observed when populations of cells were studied that had been loaded with MgFura-2-AM in the presence of mitochondrial inhibitors after addition of 1μM A23187 (figure 4.8b). This is indistinguishable from the control experiment (figure 4.8a). One possible explanation for this is that the observed rapid decline is due to a decrease in [Mg^{2+}] within organelles containing MgFura-2. To investigate whether [Mg^{2+}] changes significantly within the cardiac myocyte; experiments were designed to specifically cause the free [Mg^{2+}] to rise within organelles.

Nigericin and the respiratory substrate Succinate with P_i are known to increase [Mg^{2+}] of the mitochondrial matrix ($[Mg^{2+}]_m$) (Brierly 1987, Jung & Brierly 1994). Representative diagrams are shown in figures 4.12 and 4.13. As expected the MgFura-2 ratio increases when both nigericin and succinate are added. This must be due to changes in ($[Mg^{2+}]_m$ as Ca^{2+} is heavily buffered in this system with 5mM EGTA and the solution contains 1mM Mg^{2+}. In addition to this, a representative trace from experiments carried under the same conditions but

with FuraFF-AM loaded cells is shown in figure 4.16. This shows that addition of succinate with P_i causes virtually no change in ratio as is also the case with A23187 addition.

These results coupled with the knowledge that FuraFF is not magnesium sensitive, would suggest that there are substantial active accumulation of Mg^{2+} within the cardiac myocyte. The mechanism(s) and conditions under which this may occur are not well understood or characterised (Brierly 1987). A subsequent study of the changes occurring with $[Ca^{2+}]$ using the respiratory substrate succinate with added P_i was carried out, results of which are shown in figures 4.14 and 4.15. In addition to the MgFura-2-AM loaded cells, FuraFF-AM loaded cells were also studied. Availability of respiratory substrate such as succinate + P_i accelerate and increase Ca^{2+} influx into mitochondria.

4.4.4 Explanation of the results using a model

A semi-quantitative model is provided in an appendix to this chapter in an attempt to clarify these results. The model predicts that the Ca^{2+}-sensitive signal in AM-loaded cardiomyocytes can be attributed predominantly to two compartments, one passive slowly exchanging compartment and an active compartment that is sensitive to mitochondrial inhibitors. The modelling predicts a significant thapsigargin sensitive MgFura-2 signal if significant amounts of the dye were able to load into the SR. But the absence of this component from the measurements suggests that there is no significant SR component to the signal.

Appendix to chapter 4

Semi-quantative compartmental model of permeabilised cardiac myocyte

(in collaboration with Godfrey Smith)

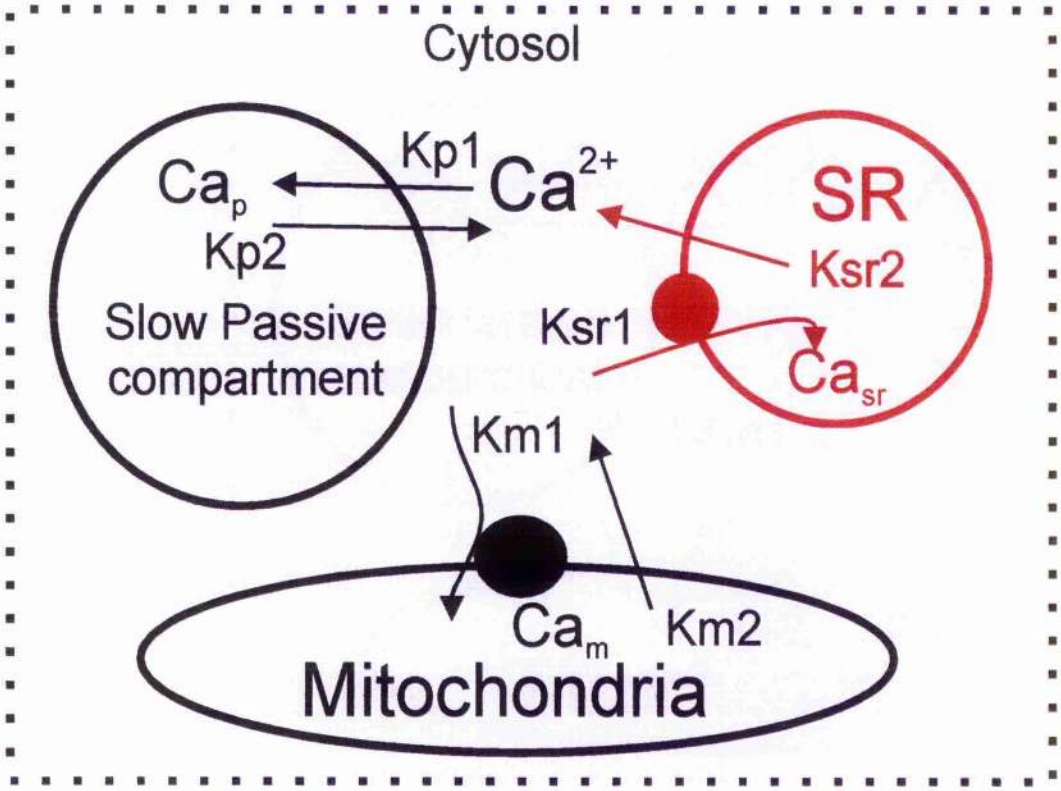

Value of rate constants:
Passive compartment: Kp1 = Kp2 = 0.01.

Mitochondrial compartment: Km1 = 10; Km2 = 1;
(+Mitochondrial inhibitors, Km1 = Km2 = 1).

SR compartment: Ksr1 = 2000; Ksr2 = 2; (+Thapsigargin, Ksr1 = Ksr2 = 2).

All rate constants increased to 5.0 to simulate ionomycin treatment.

Description of the model:
In order to aid the interpretation of the fluorescence records from –AM loaded permeabilised cardiac myocytes, a semi quantative model was constructed. Three compartments were used in the model:

(i) A passive, slowly exchanging compartment. The identity of this is unknown; exchange of Ca^{2+} is Kp1=Kp2=0.01. This exchange time is speeded up by the addition of ionomycin (Kp1=Kp2=5)

(ii) Mitochondria; this compartment accumulates Ca^{2+} to a value of 10x that within the cytosol. Addition of mitochondrial inhibitors is simulated by the reduction in the rate of uptake to the same value as leak (Km1=Km2=1). Addition of ionomycin is simulated by increasing rate constants (Km1 = Km2 = 5)

(iii) Sarcomplasmic reticulum (SR); this compartment accumulates Ca^{2+} to a value of 1000x that within the cytosol. Addition of thapsigargin is simulated by the reduction of (Ksr1 =Ksr2=2).

Included in the calculations was the conversion of the Ca^{2+} signal within the compartment to ratio for the relevant form of Fura. The respective affinity constants used in the calculations were the values measured in free solution. The possibility that the affinity constant may be lower than that measured for the free acid is discussed later. The relative contribution of passive and mitochondrial compartments were equal. The model was initially run with no contribution by the SR, this was followed by calculation assuming that the Fura signal from the SR was 10% of that from mitochondria (red trace in Figure 2).

Time course and steady state Ca^{2+} within the different compartments:
This model was used to simulate the experiments summarised in Figure 4.10. The model initially calculated the extent and time course of the changes of $[Ca^{2+}]$ within the 3 compartments in response to increasing the cytosolic $[Ca^{2+}]$ from <1nM to 760nM. The relative increase in the individual $[Ca^{2+}]$ is shown in Figure 1. The steady state values of $[Ca^{2+}]$ in mitochondria and SR were based on previously published estimates (Shannon & Bers, 1997) & (Zhou *et al.*, 1998).

Figure 1. Time-course of [Ca^{2+}] changes in different compartments

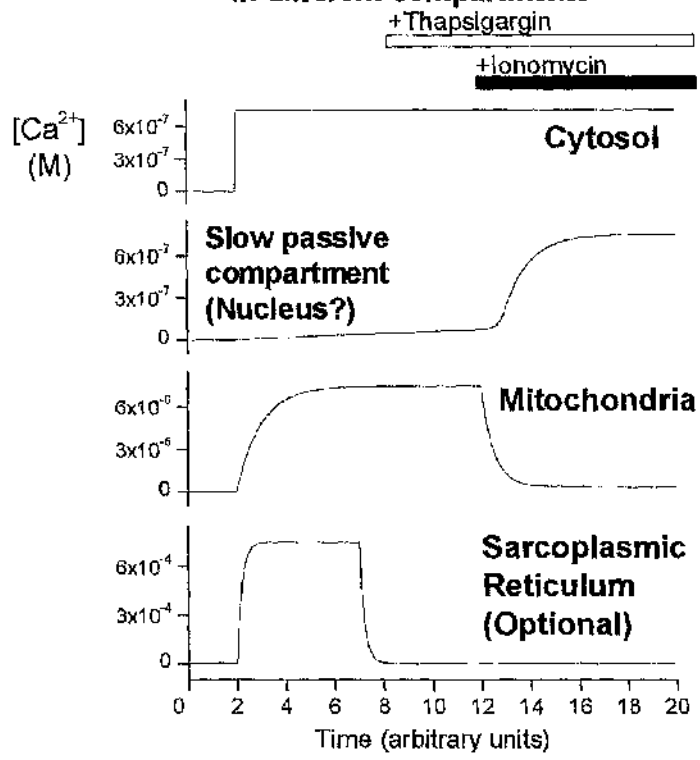

The results shown in Figure 2 indicate that the model predicts the main features of the experimental results. In particular:

(a) The initially rapid, then gradual increase in the Fura-2 ratio can be explained by the Fura-2 signal reporting Ca^{2+} from predominately two compartments; passive and mitochondrial. The rapid increase in Fura-2 ratio represents the active accumulation of Ca^{2+} in the mitochondria to values that saturate the Fura-2. The subsequent slow increase is due to the slow accumulation of Ca^{2+} in a passive compartment, this equilibration process is speeded-up by the addition of inomycin.

(b) The Fura-2 signal in the presence of mitochondrial inhibitors represents the slow accumulation of Ca^{2+} in two passive compartments namely the original compartment plus the now passive mitochondria. Hence the very large increase in ratio on addition of ionomycin. Note that the contribution from an SR component is predicted to be small.

(c) The Fura-FF signal is as observed in the experimental results. Note that the the addition of an SR compartment (grey line) mimics the small decrease in Fura-FF ratio seen in some preparation on addition of thapsigargin. However, the change in FuraFF ratio would be expected to be large when measured in the presence of mitochondrial inhibitors.

(d) The smallest changes in ratio were observed when simulating the use of MgFura. Note, modelling the SR contribution suggests that this indicator would be the best to discriminate the higher Ca^{2+} within this

compartment (grey trace). The fact that no significant effect of thapsigargin was measured in practise indicates that the contribution of the SR to the MgFura signal is small.

This simple modelling supports the conclusion that –AM loaded cardiomyocytes contain predominately from two compartments, one passive slowly exchanging compartment and a second, active compartment, sensitive to mitochondrial inhibitors. There is no evidence of a significant signal from cardiac SR.

Figure 2, Model Data

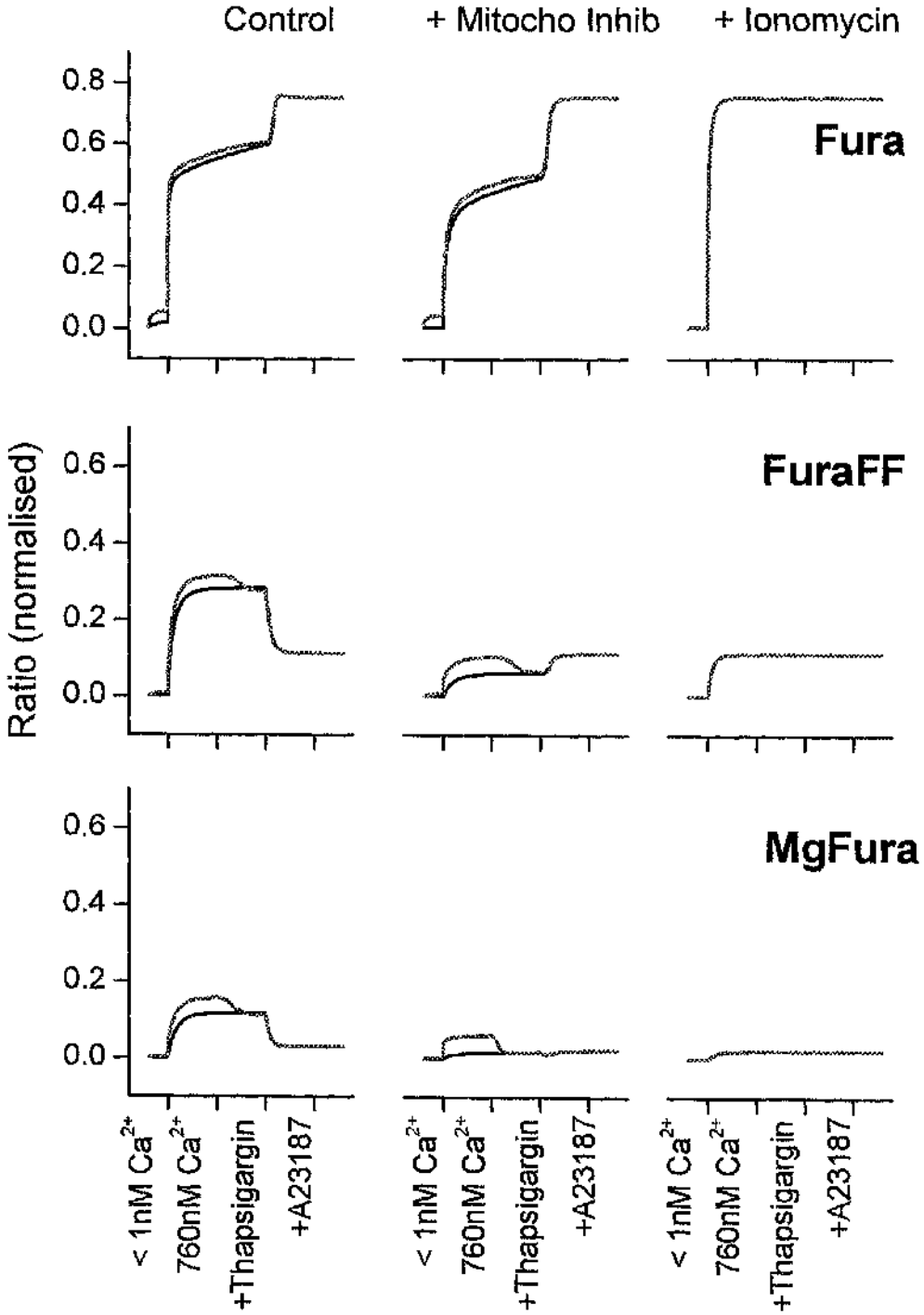

Characteristics of the passive compartment.

As described previously, the physical identity of the passive compartment is unknown. The main evidence for its existence comes from the results recorded from Fura-2 loaded cardiomyocytes. The model described earlier can be used to illustrate the differences in the predicted results if, instead of a compartment, calculations modelled simple Fura-2 binding (i.e. not rate constants affected by ionomycin). As shown in figure 3, the model would predict a decrease in Fura-2 ratio on addition of ionomycin. This results from a decrease in $[Ca^{2+}]$ within an active compartment (mitochondria). This decrease was not observed experimentally, instead the Fura-2 ratio increased, suggesting an increase in Fura-2 ratio due to rapid passive equilibration of Ca^{2+} . As discussed previously, options for this compartment include nucleus and/or non-functional mitochondria.

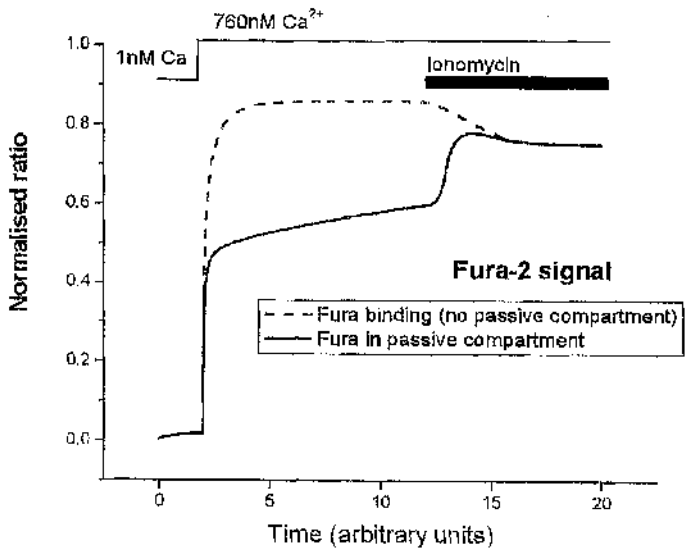

Figure 3. Passive compartment vs Fura binding

Chapter 5
Further studies of organelle calcium dynamics in cardiac muscle

C hapter 5-Further Studies Of Organelle Calcium Dynamics In Cardiac Muscle

5.1 Introduction

Results from chapter 4 suggest that the majority of the Fura-2 sensitive organelle signal arises from a passive exchange with organelles, while the majority of the FuraFF sensitive component is due to mitochondrial Ca^{2+} accumulation. This chapter describes experiments designed to address (i) the contribution of the SR Ca^{2+} signal to the total organelle signal and (ii) The ability of isolated SR and mitochondria to cleave AM derivatives of FURA dyes and prove a Ca^{2+} sensitive indicator.

5.2 Methods

5.2.1 Oxalate driven SR Ca^{2+} accumulation

Rabbit cardiac myocytes were enzymatically isolated as described in chapter 2 general methods. Isolated cardiomyocytes were loaded with FuraFF-AM as described in methods section, chapter 4. Cells were permeabilised by brief exposure to 0.01mg/ml saponin and resuspended in a mock intracellular solution of the following composition: 50μM EGTA, 100mM KCl, 1mM $MgCl_2$, 10mM NaCl, 25mM HEPES, pH 7.0. Permeabilised ventricular myocytes were placed in a closed cuvette system, a description of which is given in the methods section of chapter 4. Measurements of the FuraFF fluorescence ratio (organelle) were made. The cytosolic (cuvette) [Ca^{2+}] was simultaneously monitored with 1.3μM Fluo-3 pentapotassium salt. It is possible to use these indicators simultaneously as their excitation wavelengths are sufficiently

different. A more detailed description of these indicators and their spectra is given in chapter 3.

Experiments were carried out in the presence of 10mM Oxalate to act as an agent to precipitate Ca^{2+} and to lower the intra-lumenal [Ca^{2+}] so as to drive active Ca^{2+} uptake. The protocol involved addition of 2x 50nmol boluses of Ca^{2+} followed by thapsigargin. Following this was another 50nmol bolus then the EGTA concentration was raised to 5mM to give a measure of R_{min}. The cytosolic [Ca^{2+}] was raised to 380nM by adding 5mM CaEGTA. R_{max} was obtained on addition of 10mM $CaCl_2$. The experiments were carried out in the presence and absence of thapsigargin.

5.2.2 Studies of passive Ca^{2+} dynamics in cardiac muscle

In addition to the studies previously described in this chapter, experiments were carried out both in the absence and presence of ATP in order to study the characteristics of passive uptake.

Adult rabbit cardiac myocytes were prepared as described in the general methods section. Cells were loaded with 10μM Fura-2-AM under the conditions described in chapter 4.

Aliquots of 2x 10^6 cells were then permeabilised by brief exposure to the agent saponin and the cells placed in a mock intracellular solution containing 50μM EGTA, 100mM KCl, 1mM $MgCl_2$,10mM NaCl & 25mM HEPES to mimic the cells' intracellular environment. Experiments were carried out with and without

the addition of 5mM ATP and 15mM CrP to the mock intracellular solution. Cytosolic free [Ca^{2+}] was monitored with the addition of 1.3μM Fluo-3.

For these studies the same closed cuvette system described in this chapter was used. The protocol involved the addition of 3x 50nmol aliquots of $CaCl_2$ at equally spaced time intervals. This was followed by the addition of 25μM thapsigargin, 50nmol $CaCl_2$, 5mM EGTA to obtain a value of the minimum fluorescence ratio value and finally 5μM A23187 4-Bromo.

5.2.2.1 Studying Calcium Dynamics using confocal microscopy

Freshly isolated rat cardiac myocytes as described in general methods, were loaded with 20μM Fluo-3-AM in a 37°C incubator supplemented with 5% CO_2 on coverslips (thickness 1.5) pre-treated with 4μg/mL laminin for 1 hour. Calcium dynamics were studied in the cells using Biorad Radience 2000 MP confocal microscopy system. Cells were perfused with the following buffered solutions at pH 7.0: (1) 10mM EGTA, (2) 10mM EGTA + 0.01mg/mL β-Escin, (3) 0.12μM $CaCl_2$ & (4) 0.38μM $CaCl_2$.

Parallel experiments were run using unloaded cells and solutions 1-4 above with added 10μM Fluo-3 pentapotassium salt. Cells were visualized using 60x water objective lens and excited at 488nm with an Argon/Krypton laser (peak emission 488nm (5mW)) and the fluorescence detected using a 515±30nm band pass filter. Fluorescence and transmission images were captured. Sets of time series (each cycle 2s) were recorded using the Biorad software Laser

sharp 2000 and the images obtained analysed using the Biorad software LaserPix.

5.2.3 Studies of Ca^{2+} dynamics in organelles isolated from cardiac muscle

In order to understand the observed results from studies of calcium dynamics of populations of cells, it was necessary to isolate organelles from cardiac tissue and to study the calcium dynamics in each individual fraction.

Mitochondria and SR were isolated from rabbit heart and the resulting organelles used for subsequent study.

5.2.3.1 Preparation of Mitochondria from Cardiac tissue

White New Zealand male rabbits were subjected to deep anaesthesia with an intravenous injection of 500 U Heparin together with an overdose of Sodium Pentobarbitone (100mg/kg). The thoracic cavity was opened, the heart quickly excised and placed into a sterile beaker containing sterile, ice-cold Krebs' solution (120mM NaCl, 20mM HEPES, 5.4Mm KCl, 0.52Mm NaH_2PO_4, 3.5Mm $MgCl_2.6H_2O$, 20mM Taurine, 10mM Creatine, 11.1mM Glucose, pH 7.4).

Atrial and fatty tissue were removed. The remaining tissue was transferred to 3 volumes/g tissue of solution containing 0.3M Sucrose, 25mM HEPES pH 7.4 and cut up into small pieces using scissors. The preparation was homogenized at 1,000 rpm keeping it as cold as possible. The homogenate was centrifuged at 500 x *g* at 4°C for 10 minutes.

The nuclear pellet and supernatant were both retained. The supernatant was placed on ice. The pellet was re-suspended in 0.3M Sucrose, 25mM HEPES pH 7.4 and re-homogenized for 1 minute. This was centrifuged again at 500 x *g* at 4°C for 10 minutes. After this step the pellet was discarded. Supernatant from both the 500 x *g* spins were pooled and placed on ice. The aim of pooling the supernatants is to increase the yield of mitochondria in the subsequent step. The pooled supernatants were centrifuged at 10,000 x *g* at 4°C for 15 minutes.

The mitochondrial pellet was re-suspended in a solution containing 0.4M sucrose and 4.2mM HEPES pH 7.2. Mitochondria were either used for studies immediately prior to preparation or stored at -80°C until use. Prior to use, a small aliquot of the preparation was retained and placed on ice in order to ascertain the protein concentration present.

5.2.3.2 Preparation of SR vesicles from Cardiac tissue

Rabbit heart ventricular tissue was obtained in the same manner as described for preparation of the mitochondria. Tissue was placed in 3 volumes/g tissue of solution containing 0.3M Sucrose, 25mM HEPES pH 7.4 and cut up into small pieces using scissors. The preparation was homogenized at 1,000 rpm keeping it as cold as possible. The homogenate was then centrifuged at 6,500*g* for 20 minutes at 4°C. The supernatants from this step were transferred to fresh centrifuge tubes and centrifuged at 100,000*g* for 35 minutes at 4°C. During this 35 minute period discontinuous sucrose gradients were poured by

carefully layering 2ml of 10%, 20%, 30% and 40% sucrose solutions in ascending order of the sucrose concentration, so therefore the solution with the greatest density first. Sucrose solutions were prepared by addition of the appropriate mass of sucrose in a solution containing 2M KCl, 0.5M EGTA, 30mM HEPES, 0.5mM $MgCl_2$ and 0.5mM $CaCl_2$. The pellets from the 100,000*g* spin were resuspended in 10% sucrose solution and 1ml of homogenate carefully layered onto each sucrose gradient. The purpose of this step is to further purify the crude SR prep into the heavy SR vesicle (HSR) fraction. This is obtained at a higher density containing terminal cisternae, the ryanodine receptors and the Ca pumps (SERCA).

The band corresponding to the HSR on the 30%/40% interface of the gradient was removed and the sucrose concentration lowered on addition of 0.4M KCl. The HSR was then centrifuged at 100,000*g* for 35 minutes at 4°C. The resulting pellet was resuspended in a solution containing 0.4M Sucrose and 5mM HEPES. A small aliquot of the preparation was retained and placed on ice in order to ascertain the protein concentration present. The remaining preparation was flash frozen in liquid Nitrogen and stored at -80°C.

5.2.4 Determination of total protein concentration present

The method is a modification of the Bradford protein assay. Protein content (mg ml^{-1}) was determined using the Coomassie Plus protein reagent (Pierce). Protein standards were prepared using MilliQ grade water and Bovine serum albumin (BSA) at concentrations of 0.1-1mg ml^{-1}.

Prepared mitochondria and HSR samples were diluted in MilliQ grade water 1in 10, 1in 20 and 1 in 50. Both the standards and the diluted samples were assayed in triplicate on a 96 well plate. 10μL of each sample or standard was placed in each well. To each well was added 200μL of Coomassie reagent. Protein content was determined by measuring the absorbance of the samples at 595nm. The BSA standards were used to construct a calibration curve and from this the protein content of the preparations ascertained. A typical calibration fitted to a sigmoidal curve is shown in figure 5.1.

Figure 5.1. Protein calibration curve using BSA standards and coomassie plus reagent.

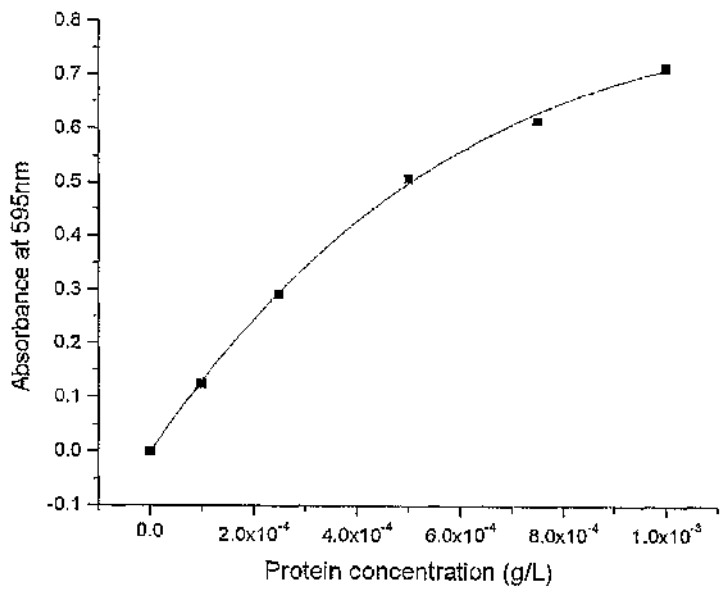

5.2.5 Studying the calcium dynamics in isolated HSR & Mitochondria

It was necessary to first optimise the concentration of HSR and mitochondria used in each experiment so as to demonstrate that there was measurable Ca^{2+} uptake activity. Varying concentrations of HSR were used to demonstrate oxalate-driven Ca^{2+}. The appropriate volume of HSR was placed in a cuvette containing 10μM Fura-2 pentapotassium salt and a mock intracellular solution of the following composition: 50μM EGTA, 100mM KCl, 1mM $MgCl_2$,10mM NaCl, 25mM HEPES, 5mM ATP and 10mM CrP. The studies were performed using the cuvette system described in the methods section earlier in this chapter using excitation wavelengths for Fura-2 of 340 and 365nm.

Experiments were carried out in the presence of 10mM oxalate and involved the addition of 2x 50nmol Ca^{2+} boluses, thapsigargin addition and finally an additional 50nmol Ca^{2+} bolus. An estimation of Fura-2 R_{min} was obtained by raising the EGTA concentration to 5mM and R_{max} estimated on addition of 15μL 1M $CaCl_2$ solution.

The optimum concentration of HSR and mitochondria (500μg) was used and an attempt was made to load the organelles with FuraFF-AM. HSR were placed in the above mock intracellular solution containing 1mM EGTA with 10μM FuraFF-AM. The samples were placed at 4°C for 1 hour and a duplicate aliquot placed at room temperature. The aim of these experiments was to simulate experiments carried out within the whole cell populations. The protocol involved using 500μg of HSR/mitochondria per preparation in a mock

intracellular solution of the following composition: 5mM EGTA, 25mM HEPES, 5.5mM $MgCl_2$, 10mM KCl, 5mM ATP and 10mM CrP. The cuvette free $[Ca^{2+}]$ representative of the cytosolic free $[Ca^{2+}]$ in the cell populations described earlier in this chapter, was raised to 760nM using CaEGTA solution. This was followed by addition of 25μM thapsigargin and then 1μM of A23187-4-bromo.

5.3 Results

5.3.1 Oxalate driven SR Ca^{2+} accumulation

Representative traces showing the simultaneous measurement of the FuraFF (organelle) and Fluo-3 (cytosolic) signals is shown in figure 5.2.

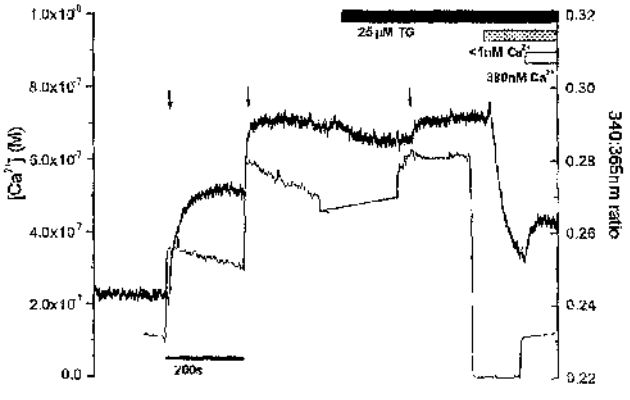

Figure 5.2. Oxalate driven Ca^{2+} uptake with FuraFF-AM loaded cardiomyocytes.

The grey trace depicts the FuraFF ratio and the black trace the cytosolic [Ca^{2+}] ascertained using Fluo-3 pentapotassium salt. Arrows indicate addition of 50nmol Ca^{2+}. [Ca^{2+}] decreased to <1nM on addition of 5mM EGTA and increased to 380nM on addition of 5mM CaEGTA.

Addition of the initial 50nmol bolus of Ca^{2+} causes an increase in the FuraFF ratio (grey trace) implying an increase in the [Ca^{2+}] within a sub-cellular compartment or compartments. A subsequent 50nmol addition causes a further increase in the FuraFF ratio. In parallel, the cytosolic [Ca^{2+}] indicated by

the Fluo-3 signal (black trace) initially rises and then declines. Addition of 25μM thapsigargin causes a small decrease in 340:365nm ratio and a small increase in the fluo-3 signal. An additional 50nmol bolus does not cause an increase in the FuraFF ratio and the cytosolic [Ca^{2+}] increases and does not change.

Figure 5.3 shows representative traces from experiments carried out in the presence of 25μM thapsigargin. Addition of 2x 50nmol Ca^{2+} boluses causes an increase in the FuraFF ratio. The Fluo-3 signal also increases but does not

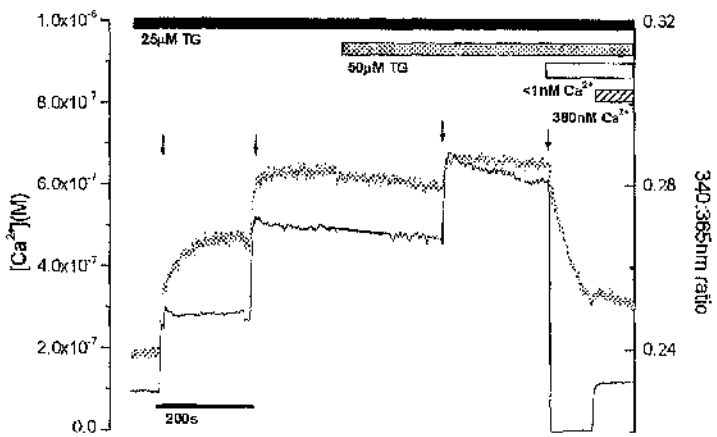

decline.

Figure 5.3. Oxalate driven Ca^{2+} uptake with FuraFF-AM loaded cardiomyocytes in the presence of 25μM thapsigargin.

The grey trace depicts the FuraFF ratio and the black trace the cytosolic [Ca^{2+}] ascertained using Fluo-3 pentapotassium salt. Arrows indicate addition of 50nmol Ca^{2+}.

Table 5.1 shows the mean changes in FuraFF ratio per second (ΔFuraFF) and the mean rate of Ca^{2+} uptake. Measurements made in the presence and absence of 25μM thapsigargin.

	ΔFuraFF ratio	**Rate of Ca^{2+} uptake nM s^{-1}**
Control	0.567 ± 0.031 *n*=3	22.3 ± 5.1 *n*=7
25μM thapsigargin	0.568 ± 0.033 *n*=3	0.032 ± 0.02 *n*=6

Table 5.1. Mean Ca^{2+} transport rates of subcellular compartments and cytoplasm in the presence and absence of 25μM thapsigargin.
Change in FuraFF ratio per second and rate of Ca^{2+} uptake in FuraFF-AM loaded cardiac myocytes in a mock intracellular solution containing 50μM EGTA.

5.3.2 Calcium dynamics with low buffering

Experiments were carried out both in the presence and absence of 5mM ATP/15mM CrP.

In the absence of ATP, shown in figure 5.4, on addition of 50nmol aliquots of Ca^{2+} there is a decline in fluo-3 fluorescence and rise in Fura-2 ratio. However the rate of the apparent Ca^{2+} influx into a sub-cellular compartment is slow.

Thapsigargin addition caused an increase in the Fura-2 ratio, accompanied by a decline in Fluo-3 fluorescence.

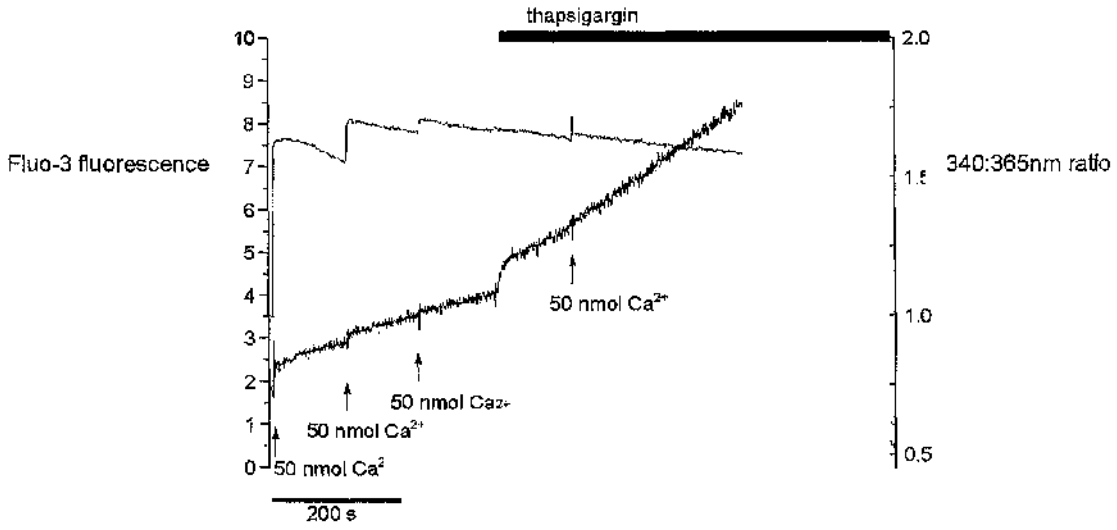

Figure 5.4. Fura-2-AM loaded cardiomyocytes.

Shows the changes in fluo-3 fluorescence and fura-2 ratio in response to the addition of 50nmol Ca^{2+} before and after the addition of a compound to block active uptake of Ca^{2+} into an intracellular store. Fluo-3 fluorescence is shown in black and indicates the external [Ca^{2+}]. Fura-2 ratio is shown in grey indicates [Ca^{2+}] within sub-cellular compartments.

The mean change in [Ca^{2+}] under these conditions is 5.3±1.15 nM s^{-1} (n=13) that corresponds to approximately 300nM min^{-1}

5.3.3 Single cell studies

A number of Fluo-3-AM loaded cells were perfused with different solutions and studied using confocal microscopy. Fluorescence changes due to excitation at 488nm of a representative cell are shown in figure 5.5. Addition of the permeabilising agent β-escin caused a rapid decline in fluo-3 fluorescence

indicating that the majority of cleaved fluo-3-AM free in the myoplasm is leaving. In theory, the remaining cell fluorescence is due mainly to indicator trapped within organelles/bound to cellular structures.

Addition of 0.38μM free Ca^{2+} caused a rise in fluorescence with 2 components; an initial rapid rise followed by a secondary slower rise. Subsequent addition of 10mM EGTA caused a decline in fluorescence.

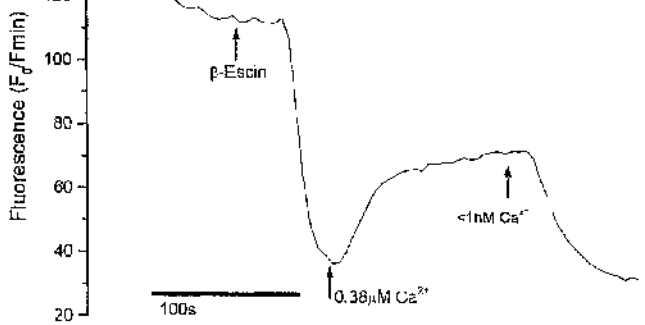

Figure 5.5. Representative Fluo-3-AM loaded cell.

Shows the changes in fluorescence after permeabilisation with 0.1mg/mL β-escin followed by an increase in the free [Ca^{2+}] to 0.38μM and then decreasing the free [Ca^{2+}] to <1nM.

Parallel experiments were carried out using unloaded cells. A representative fluorescence trace is shown in figure 5.6.

After permeabilisation with 0.1mg/mL β-escin, the cells were perfused with the same perfusates as used with the fluo-3-AM loaded cells with added Fluo-3 acid. Higher fluorescence within the cell indicates significant fluo-3 binding.

Increasing Ca^{2+} to 0.38μM causes an increase in fluo-3 fluorescence without a subsequent secondary slow rise.

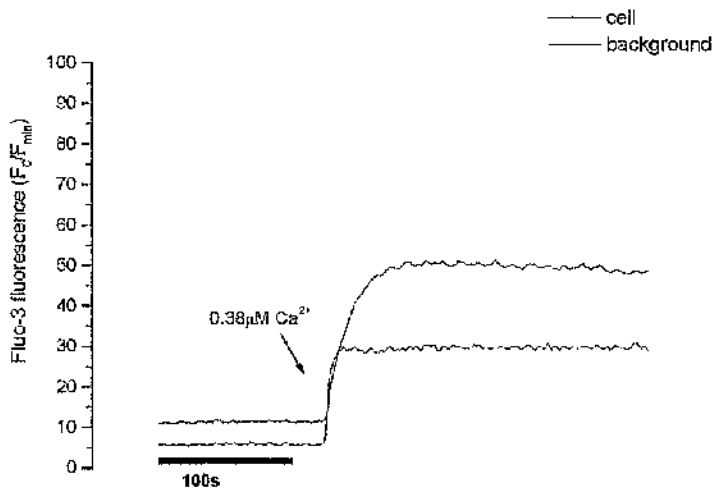

Figure 5.6. Fluo-3 acid loaded single cell study.

Representative unloaded cell permeabilised with β-escin with 10μM Fluo-3 acid in the extracellular solution. Fluorescence monitored from the cell and the background (extra-cellular solution)

5.3.4 Calcium dynamics in isolated organelles

Mitochondria and SR were isolated from rabbit heart and the resulting organelles used for subsequent study.

5.3.4.1 Studies with isolated SR

The concentration of prepared HSR was determined using the modified version of the Bradford protein assay. The optimum amount of HSR used per experiment was ascertained as being 500μg. Figure 5.7 demonstrates a typical

trace from an experiment following the oxalate driven Ca^{2+} uptake characteristics of HSR.

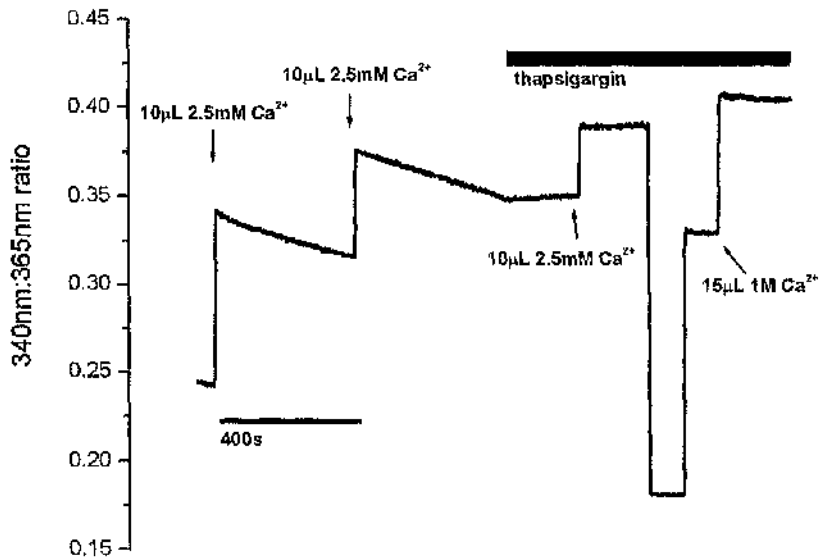

Figure 5.7. Ca^{2+} dynamics of HSR.
HSR in solution containing 50µM EGTA, 10mM oxalate and 10µM Fura-2 pentapotassium salt. Ca^{2+} additions indicated on the diagram by arrows.

Addition of the first two 50nmol Ca^{2+} boluses causes an increase in the Fura-2 340nm:365nm fluorescence ratio followed by a decline. The fluorescence ratio increased by a small amount following thapsigargin addition. A final 50nmol Ca^{2+} bolus caused a sustained rise in the Fura-2 fluorescence ratio. Figure 5.8 shows a representative trace from experiments carried out with HSR incubated with 10µM FuraFF-AM. The graph shown is representative of experiments carried out in a mock intracellular solution containing 5mM EGTA. The protocol

shown here simply involved raising the cuvette free [Ca^{2+}] to 760nM and addition of 15µL 1M $CaCl_2$ solution in order to obtain an estimate of R_{max}.

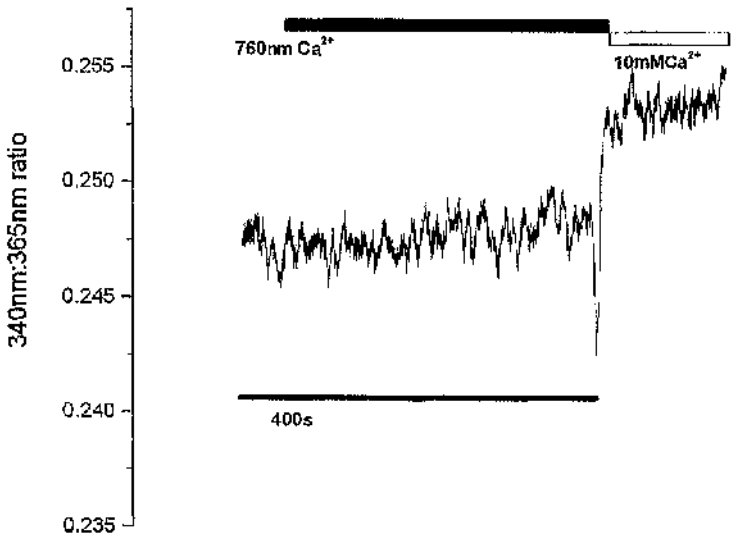

Figure 5.8. FuraFF fluorescence ratio recorded from 500µg HSR incubated with FuraFF-AM.

Extra-SR [Ca^{2+}] increased to 760nM followed by an increase to 10mM Ca^{2+}.

Raising the extra- SR [Ca^{2+}] from <1nM to 760nM does not cause any change in the FuraFF fluorescence ratio. A similar study was carried out with a modified protocol to that above. A representative graph is shown in figure 5.9.

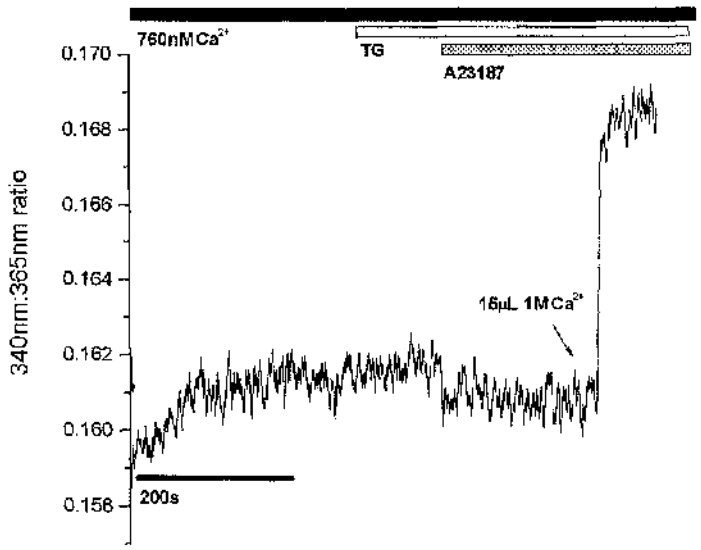

Figure 5.9. A study in the presence of 5-15mM EGTA. HSR incubated with FuraFF-AM.

In this subsequent study, a representative trace shown in figure 5.9, again the cuvette free [Ca^{2+}] was raised from <1nM to 760nM. This causes a very small hardly detectable rise in the 340:365nm fluorescence ratio. Following thapsigargin and ionophore additions, again there appears to be virtually no change in the ratio.

5.3.4.2 Studies with isolated mitochondria

Figures 5.10-12 show representative graphs from experiments carried out with isolated mitochondria loaded with Fura-2-AM in the absence and presence of A23187 and a cocktail of mitochondrial inhibitors. The protocol was a repeat of

that used for the cell population experiments. The concentration of mitochondria required to give a measurable fluorescence signal was optimised and found to be 250μg. Mitochondria were suspended in the same mock intracellular solution as used for the cell experiments containing 5mM EGTA. The study involved raising the extra-mitochondrial [Ca^{2+}] from <1nM to 760nM. This was followed by thapsigargin addition, then ionophore. R_{max} was ascertained by raising the [Ca^{2+}] to 10mM. Under all 3 experimental conditions, raising extra-mitochondrial [Ca^{2+}] to 760nM causes an increase in the 340:365nm fluorescence ratio. Subsequent thapsigargin and ionophore addition has no effect on the ratio.

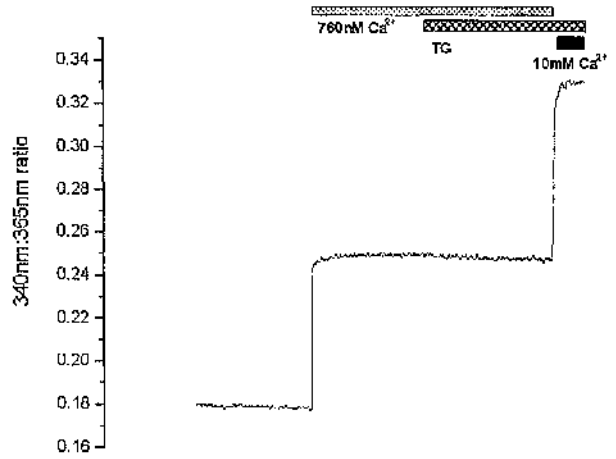

Figure 5.10. 500μg Fura-2-AM loaded mitochondria in the presence of 5-15mM EGTA.

Extra-mitochondrial [Ca^{2+}] was raised to 760nM followed by thapsigargin addition and finally increasing the [Ca^{2+}] to 10mM.

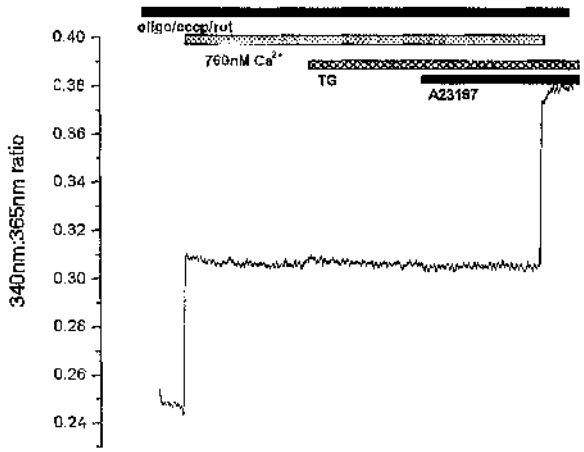

Figure 5.11. 500μg Fura-2-AM loaded mitochondria in the presence of 5-15mM EGTA and 1μM Oligomycin, 2μM CCCP and 1μM rotenone.

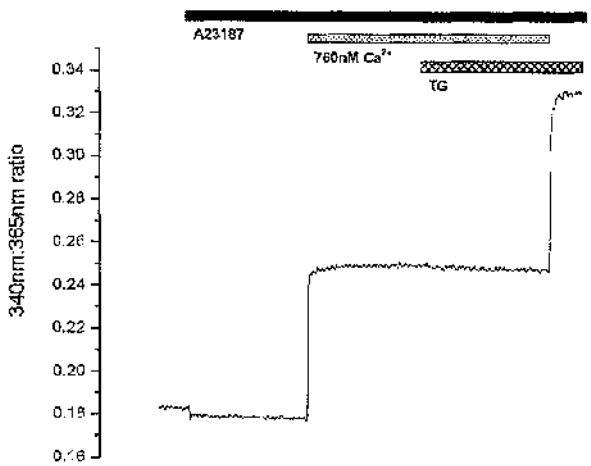

Figure 5.12.. 500μg Fura-2-AM loaded mitochondria in the presence of 5-15mM EGTA and 1μM A23187.

Figures 5.13-15 are representative graphs from studies with isolated mitochondria loaded with FuraFF-AM. Mitochondrial Ca^{2+} dynamics was studied in the absence and presence of mitochondrial inhibitors and ionophore using the same protocol as that used for the Fura-2-AM experiments. In the control experiments, raising extra-mitochondrial [Ca^{2+}] to 760nM causes a small rise in the 340:365nm fluorescence ratio. Thapsigargin addition also causes a very small increase in the ratio. A23187 addition causes a small decrease in the fluorescence ratio. In the presence of the mitochondrial inhibitor cocktail, again increasing the [Ca^{2+}] to 760nM causes a small increase in the 340:365nm fluorescence ratio. In the studies in the presence of A23187, initial ionophore addition causes a decrease in the ratio. Raising the extra-mitochondrial [Ca^{2+}] from <1nM to 760nM causes an increase in the 340:365nm fluorescence ratio. Thapsigargin addition causes no change in the fluorescence ratio.

FuraFF-AM loaded mitochondria

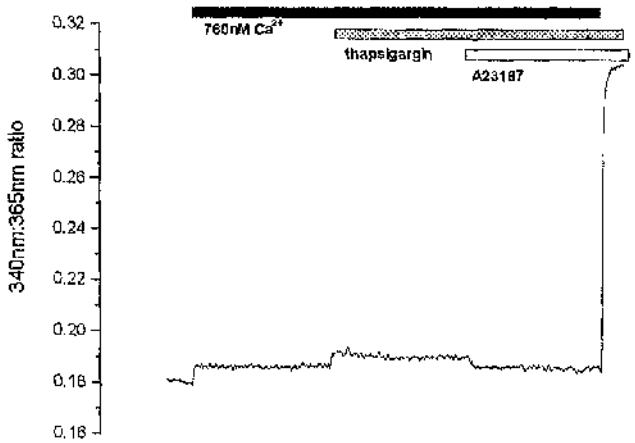

Figure 5.13. 500μg FuraFF-AM loaded mitochondria in the presence of 5-15mM EGTA.

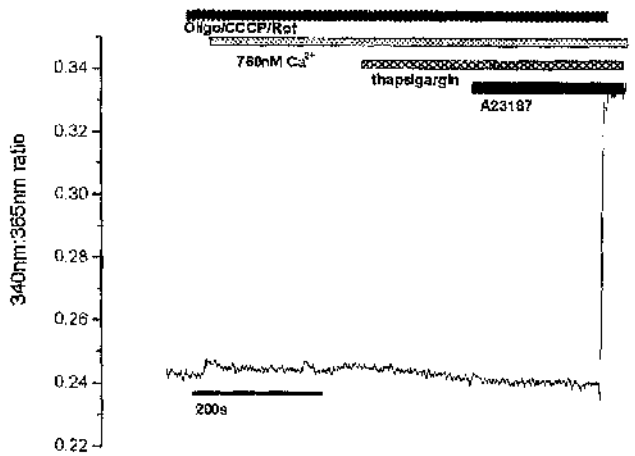

Figure 5.14 500μg FuraFF-AM loaded mitochondria in the presence of 5-15mM EGTA and 1μM Oligomycin, 2μM CCCP and 1μM rotenone.

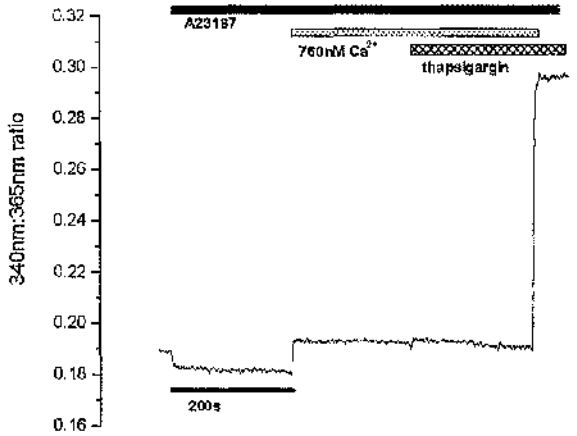

Figure 5.15. 500μg FuraFF-AM loaded mitochondria in the presence of 5-15mM EGTA and 1μM A23187

5.3.4.3 Comparing the responses of isolated cardiac myocytes and isolated mitochondria

Figure 5.16 shows the mean normalized ratio for isolated cardiac myocytes and mitochondria loaded with Fura-2-AM and FuraFF-AM in the presence and absence of the mitochondrial inhibitor cocktail (1μM oligomycin, 3μM CCCP and 1μM rotenone)

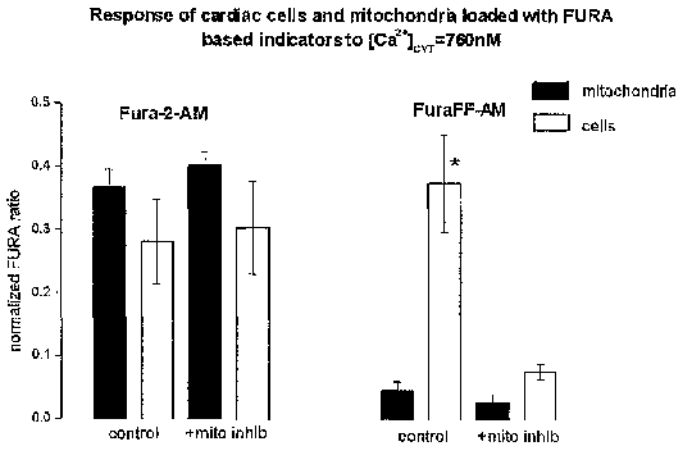

Figure 5.16. Comparison of response of mitochondria and cardiomyocytes loaded with Fura-2-AM & FuraFF-AM to $[Ca^{2+}]_{CYT}$=760nM

* Indicates that this data is significantly different ($p<0.01$)

The ratio is normalized to R_{min} and R_{max} and measured at $[Ca^{2+}]_{CYT}$=760nM. For Fura-2-AM loaded preparations, for both cells and mitochondria the presence of mitochondrial inhibitors does not significantly alter the mean normalized ratio. This is the case for both the mitochondria and cell preparations. However, with FuraFF-AM loaded cell preparations the mean normalized FURA ratio is substantially smaller in the presence of mitochondrial inhibitors compared to the control. The response of the mitochondria loaded with FuraFF-AM to the 760nM Ca^{2+} challenge is a great deal smaller than of the FuraFF-AM loaded cells.

5.3.4.4 Comparing efficiency of loading of FuraFF-AM into isolated cells, mitochondria and HSR

The efficiency of loading of FuraFF-AM was compared for cells, mitochondria and HSR. Data is expressed as R_{max}-R_{min}. The mean values for cells, mitochondria and HSR are shown in figure 5.17. The highest R_{max}-R_{min} mean value is for the cells, followed by mitochondria and the lowest is for HSR.

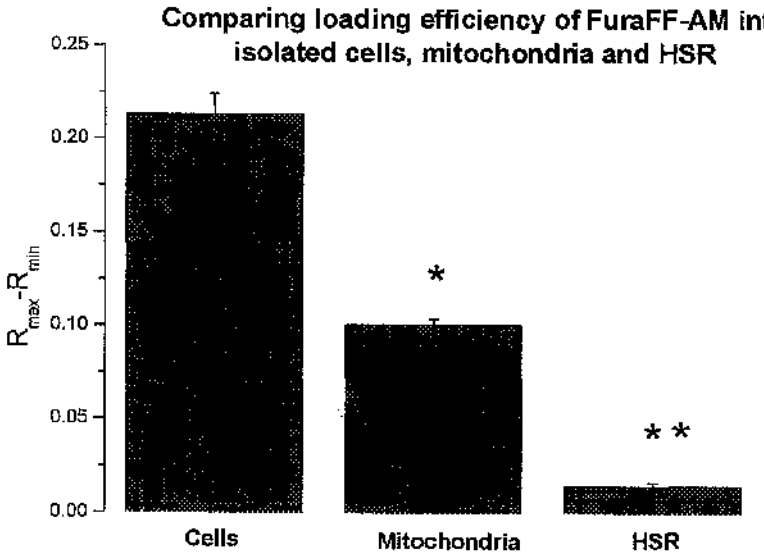

Figure 5.17. Comparison of the loading efficiency of FuraFF-AM

* denotes $p<0.05$, ** $p<0.001$.

5.4 Discussion

5.4.1 Is there a thapsigargin sensitive component to the FuraFF signal?

The mean data for the change in FuraFF ratio (ΔFuraFF) shown in table 5.1 indicate that within our cell preparations there is an active SR indicated by the changes in the Fluo-3 signal. Comparing the FuraFF traces from studies in the presence and absence of thapsigargin, there does not appear to be a significant difference between them further suggesting that SR does not contribute significantly to the organelle based FuraFF signal. This is consistent with the results from chapter 4. The reason for the absence of significant FuraFF-AM loading of the SR is unknown. Previous work on other muscle preparations have demonstrated a signal from low affinity indicators that was thought to originate from the SR (Golovina & Blaustein, 1997) and (Shmigol *et al.*, 2001)

5.4.2 Studying passive Ca^{2+} equllibration

5.4.2.1 Ca^{2+} accumulation in low buffering

Following the results of chapter 4 where a passive equilibration of Ca^{2+} was revealed, it was decided to study this further. Experiments were carried out in the absence of. A representative trace from such experiments with Fura-2-AM loaded cardiomyocytes using Fluo-3 as an indicator of the cytosolic [Ca^{2+}] and 50μM EGTA, is shown in figure 5.4. Addition of 3 x 50nmol Ca^{2+} boluses in each instance causes a rise in the fluo-3 fluorescence followed by a decline, however the rate of decline following the second and third additions is slower. The mean rate of rise corresponds to 5.3± 1.15nM s^{-1} (*n*=13) in the absence of

ATP. Interestingly, thapsigargin addition appears to speed up the rate of equilibration of Ca^{2+} in the intracellular shown by the red Fura-2 ratio, albeit a small effect. This is also apparent in studies using Fura-2-AM cardiomyocytes in the presence and absence of ionophore A23187. Representative diagrams from these experiments are shown in chapter 4, figures 4.4a and 4.4b. The reason for this result is undear. One possibility is a non-specific effect on cellular membranes of the substance DMSO used as a solvent for thapsigargin.

The cellular origin of the slow-exchanging compartment is unknown. As discussed in chapter 4, one possibility is passive exchange across the mitochondrial membrane. Previous studies of Ca^{2+} exchanging compartments have identified this as the slowest exchanging compartment (Langer *et al.*, 1990)

5.4.2.2 Single cell studies

Parallel experiments were carried out with Fluo3-AM loaded cells using confocal microscopy. A representative graph is shown in figure 5.5. Addition of the permeablising agent β-escin causes a rapid decline in the cellular fluorescence although a significant level of fluorescence remains. Raising the cytosolic $[Ca^{2+}]$ to 380nM results in a rise in the fluo-3 fluorescence. This rise consists of 2 components: an initial rapid rise followed by a secondary slower rise. Lowering the cytosolic $[Ca^{2+}]$ to <1nM by perfusing the cell with a solution containing 10mM EGTA causes a decline in the fluo-3 fluorescence. This is due to buffering of the Ca^{2+} within the system and could be attributed to apparent passive unloading of sub-cellular compartment(s) as the $[Ca^{2+}]$

becomes altered when the cytosolic [Ca^{2+}] becomes heavily buffered and very much lower.

In addition to these studies, experiments were carried out using unloaded cells. A representative fluorescence trace is shown in figure 5.6.
After permeabilisation with β-escin, the cells were perfused with the same perfusates as used with the fluo-3-AM loaded cells with added 10μM Fluo-3 acid. The background and cellular fluorescence are shown. The higher fluorescence within the cell indicates significant fluo-3 binding. Increasing Ca^{2+} to 0.38μM causes an increase in fluo-3 fluorescence without a subsequent secondary slow rise. The rise in the fluorescence does not show a biphasic response, as is the case with the Fluo-3-AM loaded cardiomyocytes.

These results from the single cell confirm that the results observed with the multi-cellular preparations are valid. Thus it is unlikely that the slow components of Ca^{2+} exchange seen in the multi-cellular preparations are the result of a fraction of the cell population remaining unpermeabilised after saponin exposure.

5.4.3 Ca^{2+} dynamics in isolated organelles

5.4.3.1 Ca^{2+} dynamics in HSR

The viability of the HSR fraction was determined by measuring the rate of Ca^{2+} uptake. On addition of a bolus of Ca^{2+} using 500μg HSR protein, thapsigargin sensitive Ca^{2+} uptake was easily measured. Using this concentration of HSR, attempts were made to load fluorescent indicator (FuraFF) via incubation with the AM derivative. The extent of FuraFF-AM loading was assessed by examining the change in fluorescence ratio in switching from low to high Ca^{2+}. As shown for the mean values (figure 5.17), there appeared to be negligible loading of the indicator compared to cells or isolated mitochondria. Previous researchers have obtained signals from SR vesicles by incorporating free acid derivatives of the Ca^{2+} indicators during the differential centrifugation steps (Saiki & Ikemoto, 1997) and (Shannon & Bers, 1997)

It is clear from this result that either there is no Ca^{2+} sensitivity of the AM loaded FuraFF or there is no uptake of Ca^{2+} by the preparation. It is most likely to be the former rather than the latter as examination of figure 5.7 shows the preparation to be viable, demonstrated by the ability to actively sequester Ca^{2+}. A similar study was carried out with a modified protocol. In this subsequent study, a representative trace shown in figure 5.9, again the cuvette free [Ca^{2+}] was raised from <1nM to 760nM. This causes a very small hardly detectable rise in the 340:365nm fluorescence ratio. Following thapsigargin and ionophore additions, again there appears to be virtually no change in the

ratio. Addition of 15µL 1M $CaCl_2$ does result in a significant increase in the fluorescence ratio, albeit a great deal smaller than one would expect.

Taking all of the results from figures 5.7-9, I conclude that this method of preparation of HSR generates a preparation that is viable and behaves as a representation of the native SR present in the whole cell. It does not appear to be possible to use FuraFF-AM as an indicator to monitor the intra-lumenal $[Ca^{2+}]$ within the HSR of cardiac muscle. One possible explanation is that the esterases present with SR are for some reason relatively inactive or possibly not present in the same proportion as in other sub cellular compartments. Another possibility is that the efficiency of loading of FuraFF-AM is poor as indicated in figure 5.17, where the loading efficiency of cells, isolated mitochondria and HSR is compared. Since HSR has the lowest R_{max}-R_{min} value, this would indicate that HSR have the lowest FuraFF-AM loading efficiency and could provide an explanation for the results observed.

This technique was tried several times during this study, but no significant dye loading was obtained. The conclusion from this work is that SR vesicles do not contain significant amounts of active esterase. This would suggest that previous studies obtain fluorescence indicator loading because (1) Intact SR contains active esterase and (2) Cleaving of the indicator occurs elsewhere in intact cells and the active indicator is shuttled to the SR. This latter explanation may be compatible with the observations in non-muscle cells (Mogami H *et al.*, 1998) (Mogami H *et al.*, 1999)

Here ER-loading with fluorescent dyes is routine, therefore in some muscle cells ER and SR may be linked and allow equilibration of the dye.

5.4.3.2 Studies with isolated mitochondria

The results from these FuraFF studies again show a small component of the signal being attributed to passive equilibration. However the magnitude of this is far smaller than that observed with the mitochondria loaded with Fura-2-AM. However the active component of this signal is smaller than that observed with the whole cell. This is demonstrated in figure 5.16 where the responses of Fura-2-AM and FuraFF-AM loaded mitochondria and cells to 760nM Ca^{2+} challenge are compared in the presence and absence of mitochondrial inhibitors. The magnitude of the response of FuraFF-AM loaded mitochondria to the challenge is substantially smaller shown by the reduction in the FuraFF ratio. Indeed statistical analysis using the student's t-test indicates that the difference is significant. One possible explanation for this is the fact that we may be dealing with a large proportion of damaged mitochondria within the preparation. This could render the mitochondria apparently less sensitive to Ca^{2+} due to damaged mitochondrial membrane proteins involved in sequestering Ca^{2+} such as the uniporter. The susceptibility of cardiac mitochondria to damage has been previously reported in terms of a variable activity of the uniporter (Buntinas *et al.*, 2001).

Chapter 6
Calcium Dynamics Within The SR Of Cardiac Muscle Using A Targeted Probe

Chapter 6- Specific Studies Of SR Calcium Dynamics Using An Aequorin Based Probe

6.1 Introduction

Previously I have demonstrated that it is not possible to monitor Ca^{2+} dynamics specifically within SR in cardiac muscle using the commercially available FURA-based Ca^{2+} indicators. The majority of the signal from –AM loaded cells could be attributed to mitochondria with no clear contribution from SR.

For this reason I considered the generation of a Ca^{2+} indicator specifically targeted to the SR, namely Aequorin. Aequorin is a photo-protein and was originally isolated from the jellyfish *Aequorea Victoria*. The aequorin complex comprises a 22,000-dalton apoaequorin protein, molecular oxygen and the luminophore coelenterazine. When three Ca^{2+} ions bind to this complex, coelenterazine is oxidized to coelenteramide, which results in release of carbon dioxide and blue light, the intensity of which is proportional to $[Ca^{2+}]$.

This indicator's usefulness was limited by the need to microinject the protein into living cells making fluorescent dyes the method of choice for measuring intracellular $[Ca^{2+}]$. The complete aequorin cDNA has cloned and sequenced (Inouye *et al.*, 1985). This has expanded the possible uses of this photoprotein.

Development of aequorin specifically targeted to sub-cellular locations has permitted the measurement of $[Ca^{2+}]$ within organelles (Brini M *et al.*, 1995), (Robert *et al.*, 1998) & (Brini M *et al.*, 1997).

Targeting of a protein-based indicator molecule is achieved by fusing the cDNA of the indicator to the cDNA of a protein native to the particular sub-cellular compartment or a targeting sequence that causes its localisation to the compartment. The resulting is then endowed with a defined intracellular location. A simplified scheme of this targeting within the cell is shown in figure 6.1.

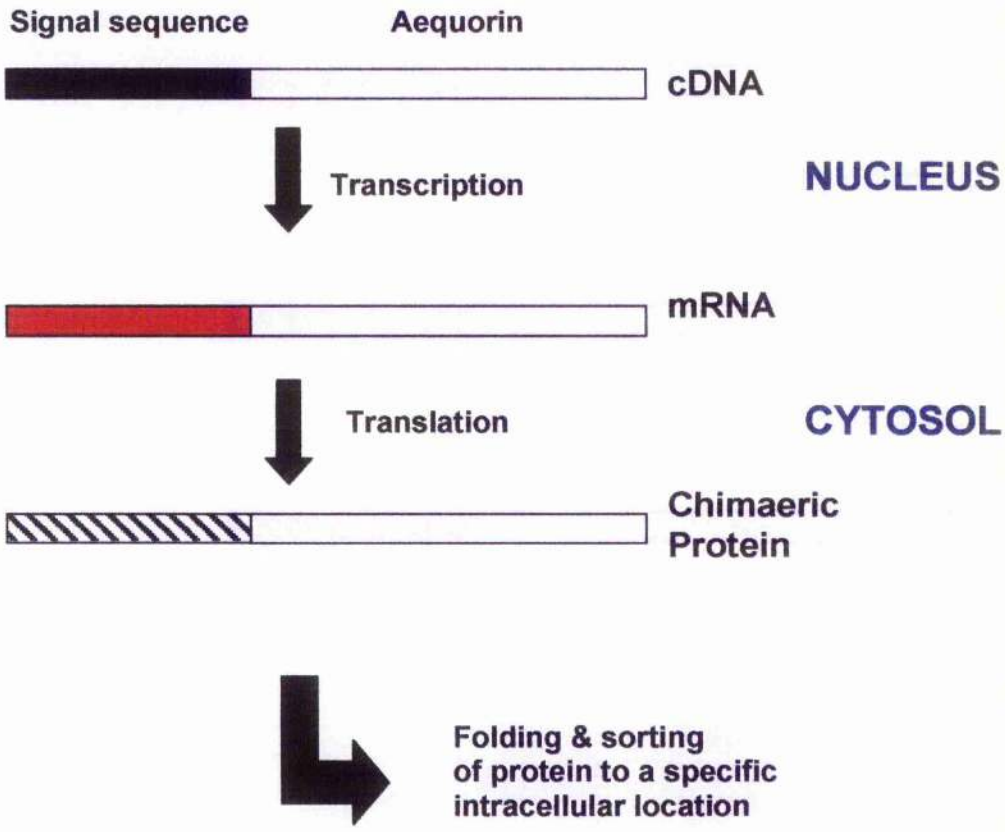

Figure 6.1 Simplified scheme for targeting of aequorin to a specific intracellular location.

However, the major drawback of targeted aequorin is that the bioluminescent signal is rather weak. Therefore the signal has to be recorded from populations of cells rather than single cells.

In order to monitor Ca^{2+} dynamics within cells that have been transfected with apoaequorin cDNA, it is first necessary to reconstitute the bioluminescent aequorin complex with coelenterazine. Several synthetic analogues of coelenterazine exist that confer different Ca^{2+} affinities and spectral properties on the aequorin complex. The coelenterazine analogue we used in our studies was coelenterazine *n* as it decreases the Ca^{2+} sensitivity of the reconstituted complex to values appropriate for measurement of $[Ca^{2+}]_{SR}$.

6.1.1 SR targeted Aequorin

A mutated aequorin chimera has been previously used to measure free SR $[Ca^{2+}]$ in cultured myotubes. The Ca^{2+} affinity was reduced in this aequorin mutant by an amino acid change of Aspartate-119 to Alanine (Asp-119→Ala) in the Ca^{2+} binding sites. The Ca^{2+} affinity was further reduced using a modified prosthetic group, Coelenterazine *n*.

Targeting of the photoprotein was achieved by generation of a construct that consisted of cDNA encoding the SR resident protein calsequestrin fused to the aequorin cDNA (p srAEQ) (Brini M *et al.*, 1997). The construct also contains a HA1 tag containing 9 amino acids, which is derived from Haemagglutinin A. The purpose of this tag is to enable immunocytochemical localisation of the

expressed protein. Aequorin itself is a poor immunogen and thus effective antibodies are not available (Chiesa *et al.*, 2001). A simplified diagram of the construct is shown in figure 6

Figure 6.2. CSQ-AEQ chimera.
An adenovirus was generated from the aequorin-calsequestrin plasmid (Ad srAEQ).

6.1.2 Adenovirus mediated gene transfer

Classic transfection methods such as the use of commercially available transfection reagents, electroporation or Calcium Phosphate assisted transfection are limited by their poor efficiency in terminally differentiated cells such as cardiac myocytes. The method of choice when working with such cells is adenoviral mediated gene transfer. Recombinant Adenoviruses have been used to over-express particular proteins both *in vivo* and *in vitro both* in cells in culture and whole organs (Kohout *et al.*, 1996), (Villarreal *et al.*, 1996), (Baudet *et al.*, 2001), (Westfall *et al.*, 1997), (Miyamoto *et al.*, 2000) & (Donahue *et al.*, 1997)

Adenoviruses are a group of double-stranded DNA viruses that infect a variety of vertebrate hosts (Horwitz, M.S., 1996). More than 40 serotypes and 93 different varieties of adenovirus have been identified to date. Serotype 5 has

been the most widely used in the quest to produce viral expression vectors as they have been extensively characterised and the genome sequenced.

6.1.2.1 Structure of Adenovirus

Adenovirus consists of an icosahedral protein capsid 70-100 nm in diameter. Inside the capsid resides the double stranded DNA genome. The main features of Serotype 5 are shown in figure 6.1.

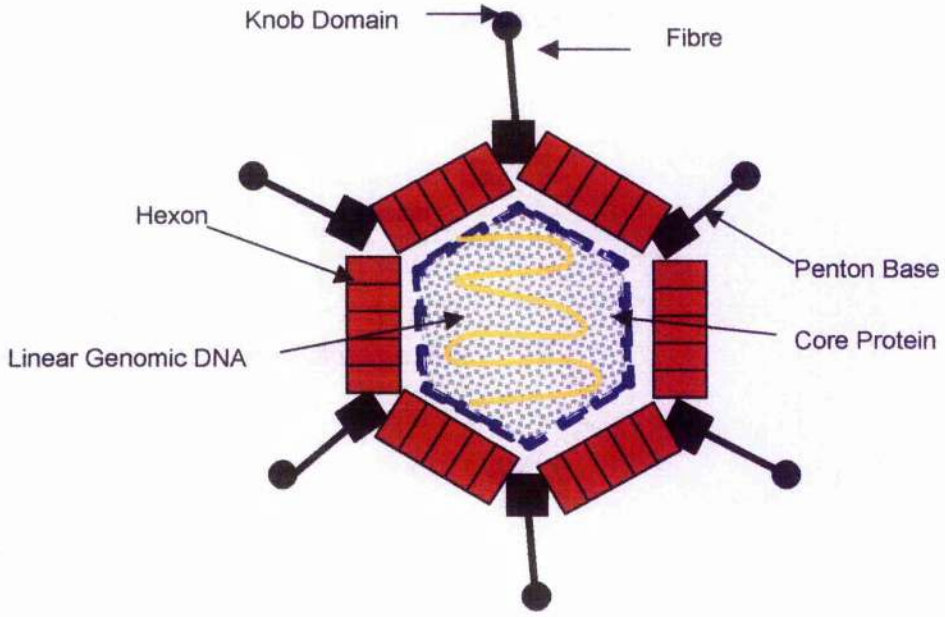

Figure 6.3. Adenovirus type 5.
Main structural and molecular features.

Conveniently, the complete 35,935 bp sequence of type 5 has been elucidated.

The genome is divided up into 100 equally spaced map units. There are nine major transcription units divided into early (E1-E4) and late (L1-L5).
Upon initial infection of the cell, the E1A protein is produced from transcripts in the E1 region. E1A is required for transcription of all of the other early transcripts. In replication deficient viral vectors the E1 region is deleted.

The first step in the development of adenoviral vectors occurred with the generation of transformed Hamster Embryonic Kidney cells (Graham *et al.*, 1977).
The cells were transformed by exposing them to sheared fragments of adenovirus type 5 DNA. This transformation gave rise to the HEK 293 cell line. HEK 293 cells contain the left 14% of the 5' end of the adenovirus genome integrated into cellular DNA including the E1 region (Becker *et al.*, 1994).

Adenoviral mediated gene transfer offers many advantages when used with cells such as cardiac myocytes. These include:

1. **Broad host Range**: Adenoviruses can infect a broad range of mammalian cells and permit expression of recombinant proteins in most mammalian cell lines and tissues.
2. **High expression levels**: High levels of exogenous protein expression even in terminally differentiated cells.

3. **Cell viability**: Cells tolerate infection and remain viable to perform functional studies (Graham *et al.*, 1977).
4. **High infectivity:** Cells in culture are infected with almost 100% efficiency.
5. **Ease of production**: It is relatively easy to propagate virus in high titres.

Although there seem to be a great deal of advantages in using this system, there are however several drawbacks. It has indeed been demonstrated that using adenoviral transfer vectors can achieve high expression of the transgene in many target organs. *In vivo* expression of the transgene is limited in time due to a complex combination of innate and adaptive immune host defences against the virus (Hackett, 2000).

6.2 Methods

6.2.1 Generation of AdCSQ-Aeq

This follows the method of Becker *et al.* (1994).

6.2.1.1 Subcloning of CSQ-Aeq into the vector pACCMV.pLpA

The construct containing the aequorin chimera (pCSQ-Aeq) was a kind gift from Dr. Rosario Rizzuto (Ferrara, Italy). pCSQ-Aeq and the vector pACCMV.pLpA were subjected to restriction digestion with *EcoR*I and *Hind*III. The plasmid pACCMV.pLpA is a shuttle vector. The plasmid contains a Cytomegalovirus (CMV) early promoter to drive transcription of the cDNA of interest with a cloning cassette downstream. In addition there are fragments of adenovirus type-5 genome that allows the subsequent generation of the infectious adenovirus. The presence of these sequences does not affect construct function.

Linearisation of the pACCMV.pLpA vector was confirmed by subjecting a small aliquot to agarose gel electrophoresis (1% agarose, TBE, ethidium bromide) and visualising using UV light. A ligation reaction was set up using Fast-Link™ DNA ligation kit (Epicentre technologies). Manufacturer's instructions were followed.

After this, the ligated construct (pACCMV.pLpACSQAeq) DNA was extracted by ethanol precipitation. Sodium acetate solution (NaOAc) was added to a final volume of 0.3M. This was followed by addition of 2.5 volumes of ice-cold

absolute ethanol and thorough mixing. The tube was then placed at -20°C for 15 minutes to allow precipitation of DNA. The sample was centrifuged at top speed in a bench top centrifuge at room temperature. The pellet was then washed with 70% ethanol and the tube placed on ice for 20 minutes, followed by centrifugation at top speed at 4°C. The supernatant was removed and the pellet allowed to air dry and was resuspended in 2μL of sterile de-ionised water.

This was followed by transformation of *E. Coli* DH5α by electroporation. The transformed bacteria were spread on LB-Agar plates with 50μg/mL ampicillin to allow selection. This is possible because pACCMV.pLpA contains an ampicillin resistance gene and therefore only bacteria transformed with the plasmid will survive the selection process. Ampicillin resistant colonies that contained the plasmid were picked and used to inoculate 5mL LB broth. This mixture with 50μg/mL ampicillin was allowed to shake overnight at 37°C. Small scale DNA preparation was carried out using Qiagen™ Qiaprep spin miniprep kit. Restriction analysis confirmed identity of the constructs and two of the cultures were selected and sub-cultured into 250mL LB broth with added 50μg/mL ampicillin and large scale DNA preparation carried out using Qiagen™ Qiafilter maxi prep kit. Prepared plasmid was quantified and purity ascertained by measuring the optical density (OD) at 260 and 280nm.

1μg of each pACCMV.pLpACSQAeq and pJM17 plasmids were used to transfect HEK 293 cells seeded in 6 well plates using Qiagen™ superfect tranfection reagent. HEK cells were cultured in IDM Media (Gibco BRL) supplemented with 8% FCS, penicillin/streptomycin and L-glutamine and passaged using standard cell culture technique.

Plasmid pJM17 is derived from adenovirus type-5 genome with deletion of the E1 region of the genome. The absence of this region facilitates allow site-specific recombination and subsequent insertion of cDNAs. This contrasts with the pAdenovator vectors in which the E3 region is deleted in addition to the E1. pJM17 contains insertions and deletions in the E3 gene rendering it non-functional. The E1 region of the genome is required for replication. Thus the resulting adenoviruses are fully infectious but unable to replicate. The HEK 293 cell line was generated by transformation by a type 5 adenovirus and hence the HEK genome contains adenovirus type 5 genome. It is possible to propagate adenovirus within HEK 293 cells as the E1 function is complemented allowing the adenoviruses to replicate (Becker *et al.*, 1994).

Co-transfection of pACCMV.pLpACSQAeq and pJM17 is followed by homologous recombination to generate a functional adenovirus with the CSQ-Aeq cDNA incorporated. The cloning and transfection procedure is summarised in figure 6.3.

Figure 6.3. Simplified scheme for cloning and generation of recombinant adenovirus

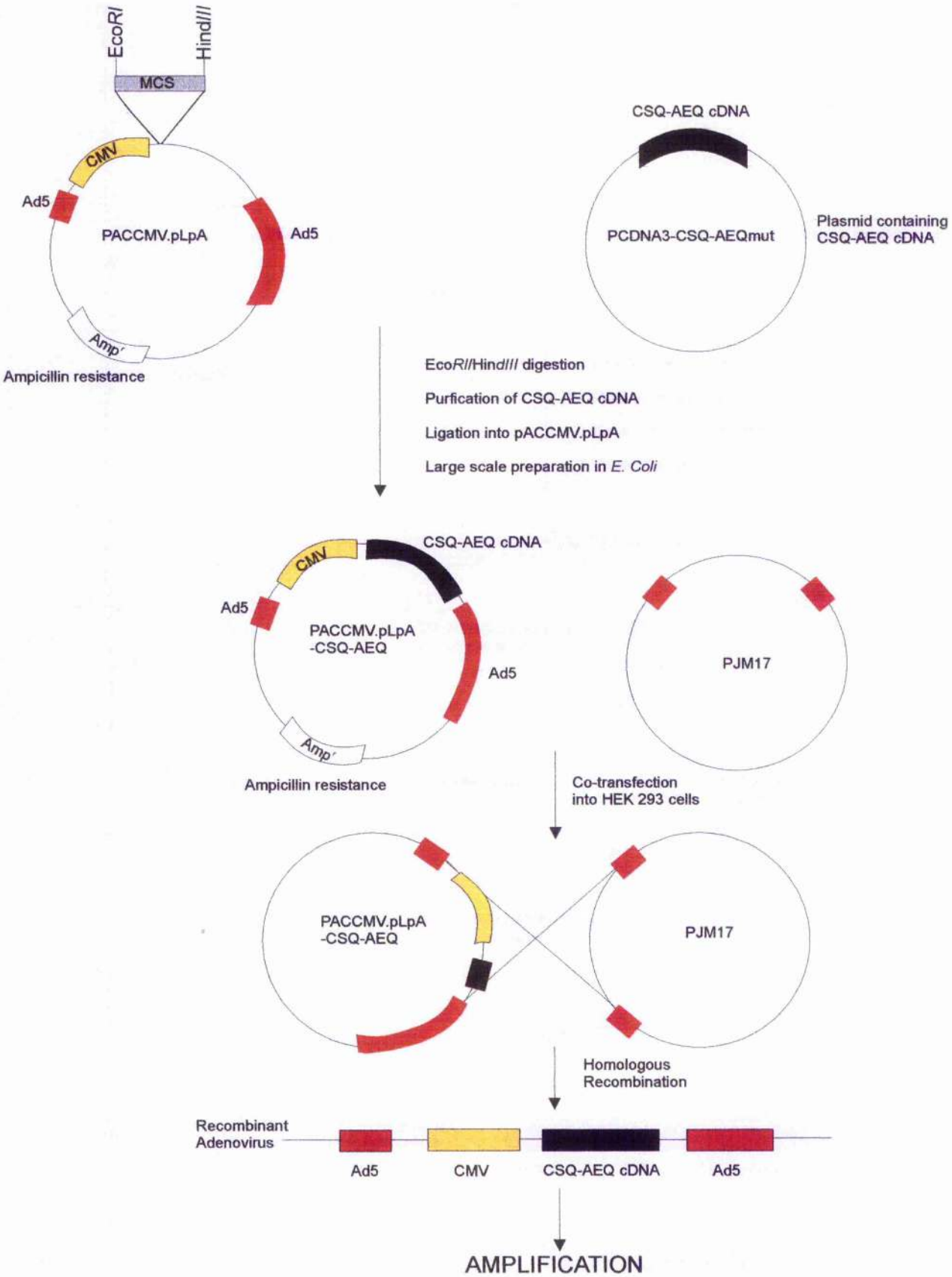

6.2.2 Studying AdSRAeq expression

To ascertain whether the chimaeric protein was being expressed in the cardiac myocytes it was necessary to perform several expression studies.

Sterile ventricular myocytes were prepared and cultured in M199 as described in chapter 2. Cells were infected with Ad-CSQ-Aeq with a MOI of 100. Infected cells were used 24 hours post-infection for the described expression studies.

6.2.2.1 Western blot analysis of CSQ-Aeq expression

Lysates from Ad-CSQ-Aeq infected myocytes were prepared. Equal amounts of total protein from untransfected cells and cells infected with Ad-CSQ-Aeq were loaded onto a 10 well mini gel (Invitrogen). CSQ-Aeq protein was resolved using a 4-12% Bis-Tris gel and subjecting to SDS-PAGE. This was followed by blotting onto a nitrocellulose membrane. After blocking in Swiss buffer with 1% BSA (see general methods chapter for solution composition) overnight at 4°C, the protein was detected using a rabbit antiserum to calsequestrin (SWant). The antiserum was diluted 1 in 40,000 in Swiss buffer and incubated at room temperature on a bench-top shaker for 2 hours.

After several washing steps, the membrane was probed with an anti-rabbit secondary antibody conjugated to horseradish peroxidase (Transduction laboratories) diluted 1 in 5,000 in Swiss buffer, for 1 hour at room temperature. The membrane was incubated for 1 minute in ECL reagent (Amersham) and exposed to photographic film.

6.2.2.2 Immunofluorescence labelling of CSQ-Aeq

To verify the effectiveness of the adenovirus-mediated over-expression and its ability to target the SR of cardiomyocytes, Immunofluorescence labelling and fluorescence imaging was used to determine the distribution of the expressed protein.

As described previously, the Calsequestrin-Aequorin fusion also contains a 9 amino acid HA1 epitope tag. This property was exploited in the immunofluorescent labelling protocol.

Infected ventricular myocytes were allowed to settle on pre-flamed slides. Cells were fixed for 30 minutes at room temperature in NaCl/Pi solution (140mM NaCl, 2.7mM KCl, 10mM Na_2PO_4, 1.8mM KH_2PO_4, pH 7.3) containing 2% paraformaldehyde. Slides were then washed 3 times with NaCl/Pi solution. The fixed cells were then permeabilised for 30 minutes at room temperature with 0.1% Triton X-100 prepared in NaCl/Pi solution. The cells were blocked for 2 hours at room temperature in NaCl/Pi solution with 10% Horse serum added. The slides were incubated overnight at 4°C with a rabbit polyclonal anti-HA1 antibody (abcam) diluted 1 in 200 in Swiss buffer. Following this the slides were washed 3 times in NaCl/Pi solution. The samples were then incubated with Donkey FITC conjugated anti-rabbit antibody (abcam) diluted 1 in 100 in Swiss buffer for 1 hour at room temperature. After incubation the slides were washed 3 times in NaCl/Pi solution. Coverslips (thickness 1.5) were mounted using the mounting medium VectaShield ™ (Vector laboratories)

that also maintains the fluorescent properties of the FITC and prevents photobleaching when excited.

6.2.2.3 Visualisation of fluorescent labelled cardiomyocytes

The location of the FITC conjugated antibody was visualised using Biorad™ Radience 200 MP confocal microscopy system. Cells were visualised using a 60x water objective lens and excited at 488nm with an Argon/Krypton laser (peak emission 488nm (5mW)) and the fluorescence detected using a 515±30nm band pass filter. Fluorescence through the Z-plane of the cells was recorded using the Biorad software Laser sharp 2000 and the images analysed using the Biorad software LaserPix.

Controls containing no antibodies, no primary antibody and no secondary antibody were carried out in parallel.

6.2.2.4 Calibration of the photoprotein

This particular aequorin mutant had previously been calibrated (Montero *et al.*, 1995). However it was not clear from the publication whether purified recombinant protein or an in situ calibration was used. Calibration of the intra-SR probe within permeabilised cells was carried out using buffered Ca^{2+} solutions in the presence of high concentrations of Ca^{2+} ionophore.

Ventricular myocytes were isolated and cultured in Medium 199 as described previously. The cultured myocytes were infected with Ad-CSQ-Aeq with an

MOI of 100. 24 hours post infection the myocytes were washed in the mock intracellular solution described above but containing 1mM EGTA. Ca^{2+} buffer solutions were prepared as follows using nitrilo-triacetic acid (NTA) and CaNTA.

5N solution

5mM K_3NTA
100mM KCl
4.16mM $MgCl_2$
25mM HEPES
30mM NaCl
pH 7.0

100CaN solution
100mM Ca K_3NTA
25mM HEPES
pH 7.0

5 x 10^5 cardiomyocytes were permeabilised by brief exposure to 0.01mg/ml β-escin and bathed in 1mL 5N solution. 1μM A23187 was added. 100CaN solution was added in order to give the following N:CaN ratios and free [Ca^{2+}] according to table 6.1. Free [Ca^{2+}] values were calculated using the programme React version 3.1

NTA:CaNTA ratio	Volume 100mM CaN added to give ratio (μL)	Free [Ca^{2+}]
5NTA	**N/A**	**250nM**
3N:1CaN	**25**	**100μM**
1N:1CaN	**25**	**282μM**
1N:3CaN	**25**	**680μM**

Table 6.1. Solutions used for in situ calibration of Aequorin and corresponding free [Ca^{2+}].

The protocol was terminated by assaying the total amount of aequorin remaining on addition of 100μL of 100mM $CaCl_2$. The calibration procedure was repeated several times with different batches of cells.

6.2.3 Studying SR Ca^{2+} dynamics

Calcium dynamics were studied on populations of cells 24 hours post infection. An outline of the experimental procedure used to study SR Ca^{2+} dynamics and the cuvette based system used for the luminometer measurements are shown in figure 6.4.

Infected cardiomyocytes were incubated with 1μM coelenterazine *n* and the cells permeabilised by brief exposure to 0.01mg/ml β-escin and bathed in a mock intracellular solution of the following composition: 5mM EGTA, 25mM HEPES, 5.5mM $MgCl_2$, 100mM KCl pH 7.0. Bioluminescence was monitored using a luminometer. Compounds, which alter the Ca^{2+} uptake and release properties of SR, were used in studying SR Ca^{2+} dynamics. These included thapsigargin, a description of which is given in chapter 4 and ruthenium red.

Ruthenium red is a polycationic compound which has been shown to inhibit the mitochondrial Ca^{2+} uniporter and the Ca^{2+} release channels of the SR or Ryanodine receptors ((Kargacin *et al.*, 1998)). Ruthenium red was used at a concentration of 5μM.

A

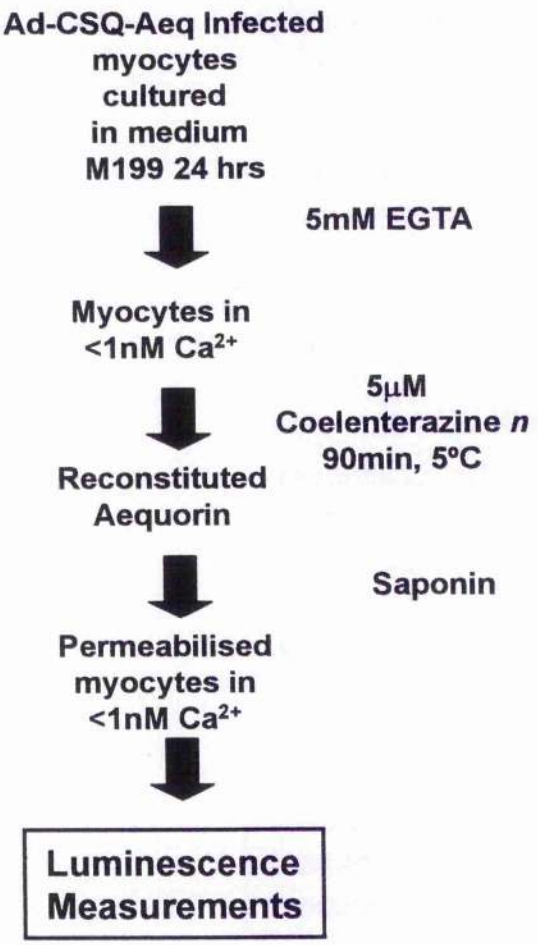

B

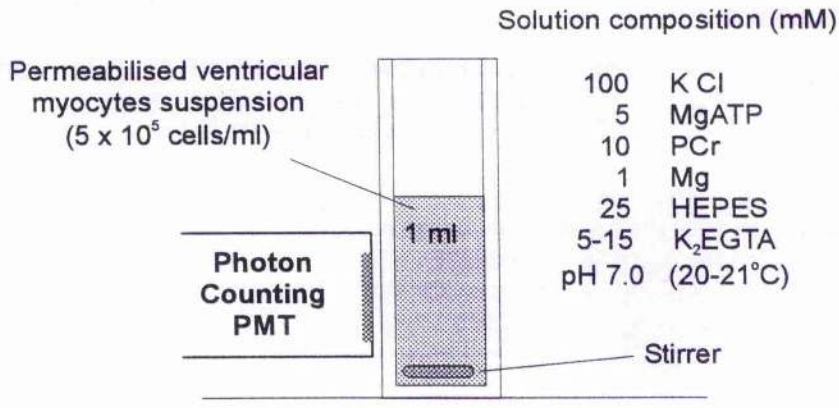

Figure 6.4. A. Outline of the experimental protocol used to study SR Ca^{2+} dynamics. 6.4 B. Cuvette based luminometer system used to capture light emitted from aequorin

6.3 Results

6.3.1 Western blot analysis of CSQ-Aeq expression

Cell lysates were prepared and the equivalent of 1 $x10^4$ cells were run per lane of 4-12% Bis-Tris gels. Samples from infected cells and uninfected cells were run in addition to 5μg SR preparation to aid identification of the calsequestrin. Following transfer to a nitrocellulose membrane and probing with a primary antibody to calsequestrin and a Horseradish peroxidase conjugated secondary antibody, the membrane was incubated with ECL reagent and an autoradiograph produced. A section of the autoradiograph is shown in figure 6.5.

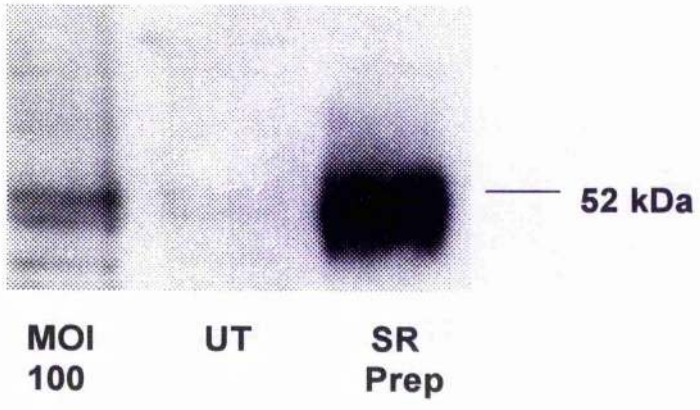

Figure 6.5. Western blot using an antibody to calsequestrin.

Comparing the samples from MOI 100 and the uninfected (UT) cardiomyocytes, it is clear that there is over-expression of the calsequestrin and since the protein is expressed as a chimera, also the aequorin. However it is somewhat puzzling that the protein does not appear to migrate according to

the expected molecular weight of approximately 75kDa. One possible explanation is degradation of the expressed protein.

6.3.2 Immunofluorescence labelling of CSQ-Aeq

A primary antibody to the HA1 tag was used to label to CSQ-Aeq fusion protein. The labelling pattern was detected using a secondary antibody conjugated to the fluorescent molecule FITC to aid visualisation by confocal microscopy. A confocal fluorescence image and the corresponding transmission image of a representative cell are shown in figure 6.6.

Confocal Fluorescence Image

Transmission Image

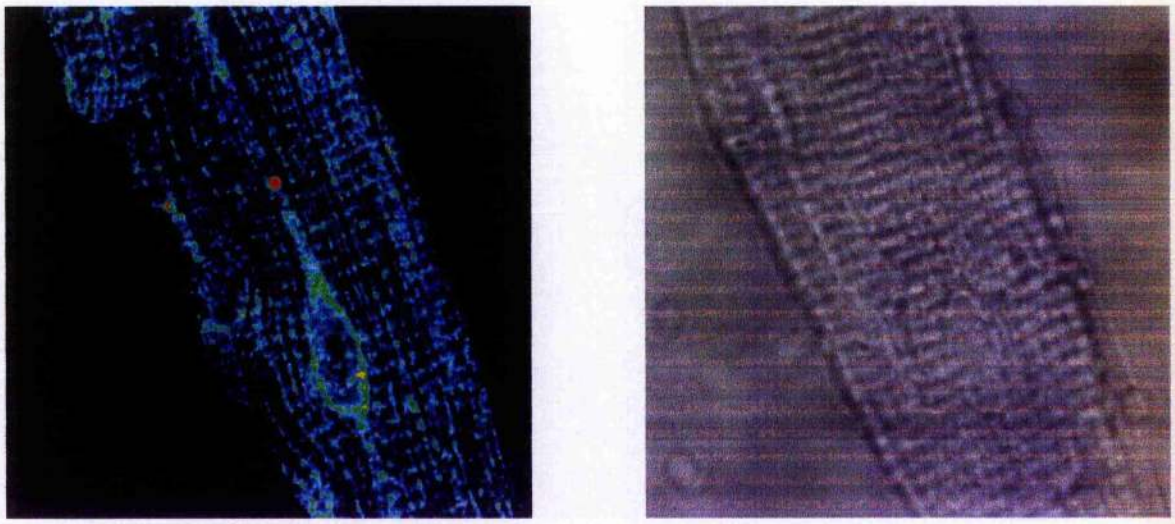

Figure 6.6. Immunofluorescent labelled section of a cardiac myocyte infected with Ad-CSQ-Aeq.

These images reveal the pattern of expression of CSQ-Aeq in two major regions: perinuclear and in discrete bands in synchrony with the striation pattern.

6.3.3 Studying SR Ca^{2+} dynamics in Ad-CSQ-Aeq infected cells

As described in the methods section, cardiac myocytes expressing the aequorin chimaera were used to study SR Ca^{2+} dynamics. Figure 6.7 shows a representative trace from an experiment carried out in the presence of 5μM Ruthenium red. The protocol involved raising the $[Ca2+]_{CYT}$ from <1nM to 380nM followed by thapsigargin addition. The protocol is terminated by addition of 1% Triton X-100 and raising the $[Ca^{2+}]$ to 10mM which assays the remaining unconsumed aequorin and thus allows calculation of the total counts present.

Panel A shows the raw count data at each time point. The raw counts curve is integrated to the total counts at each time point. This is shown by the grey curve on panel B. This data is then used to calculate the fractional luminescence (FL) values at each time point, which is shown by the black trace on panel B.

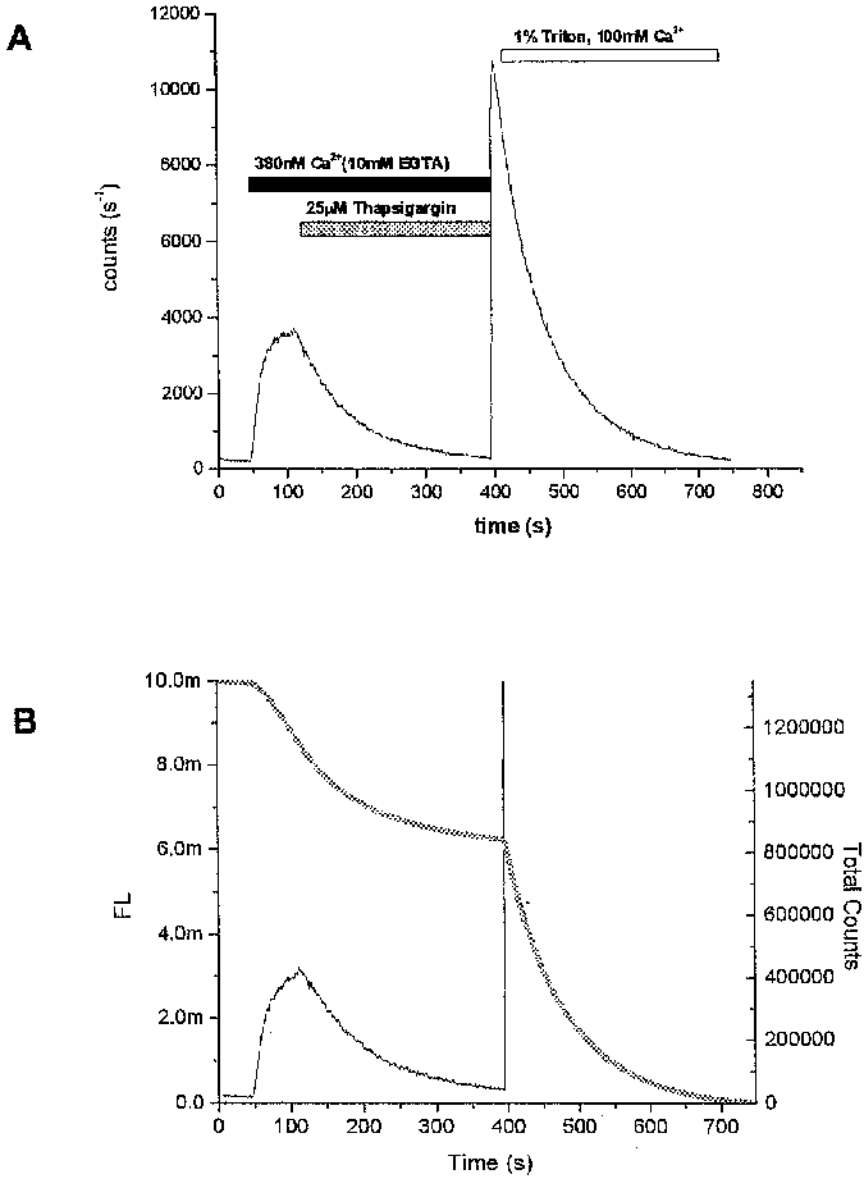

Figure 6.7. Conversion of raw counts to fractional luminescence.
A. Raw count data for a typical experiment where the $[Ca^{2+}]_{CYT}$ was raised from <1nM to 380nM followed by thapsigargin addition. This is followed by addition of 1% Triton X-100 and raising the $[Ca^{2+}]$ to 10mM.
B. The grey trace shows the total counts at each time point. The black trace shows the fractional luminescence (FL) values at each time point.

6.3.3.1 Conversion of fractional luminescence to $[Ca^{2+}]_{SR}$

As discussed earlier in this chapter, the expressed protein within the SR was calibrated in the presence of Ca^{2+} ionophore using buffered Ca^{2+} solutions. Figure 6.8A shows the fractional luminescence values obtained when the $[Ca^{2+}]$ is raised using buffered NTA and CaNTA solutions. Fractional luminescence value increases as the $[Ca^{2+}]$ increases as expected. Figure 6.8B shows the calibration curve constructed from mean FL values obtained, this is shown in black. The grey trace is derived from the published calibration curve for this aequorin mutant (Montero *et al.* 1995). Whether this was constructed from purified recombinant protein is unclear. This may provide an explanation as to why the curve obtained using ionophore and cell populations is shifted to the right indicating an apparent lower Ca^{2+} sensitivity. The protein within the sub-cellular compartment may provide a different reaction environment, for example the pH may differ or other ions may vary. Subtle differences such as these could alter the Ca^{2+} affinity.

Figure 6.8C is the equation used to fit the data to the logistic curve with the following parameters obtained from the curve; A1 is the minimum FL value, A2 the maximum FL value, X_0 is the affinity of the indicator for Ca^{2+} and p is the slope of the curve. In the subsequent studies these values were used in an algorithm that converts FL obtained into $[Ca^{2+}]_{SR}$.

A

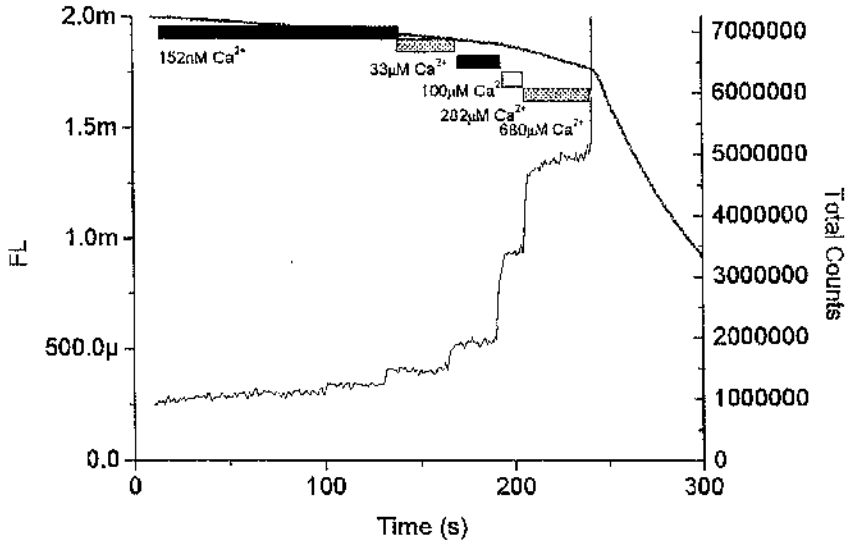

B

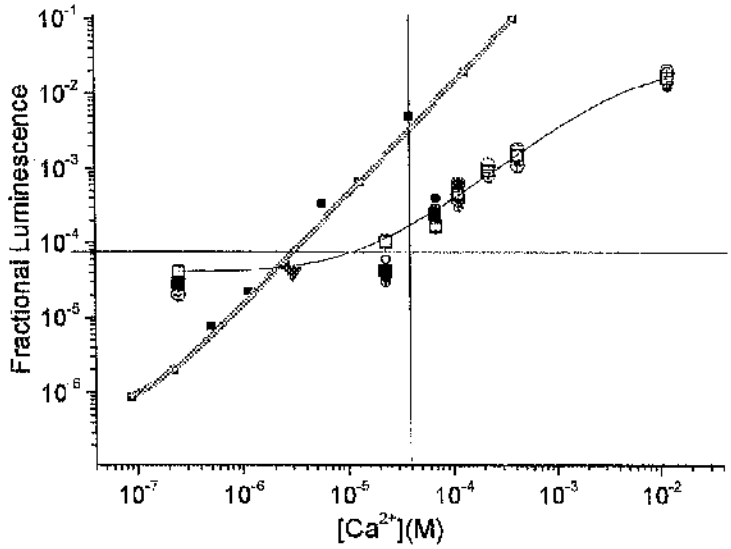

C

$$FL = \frac{A1-A2}{(1+(Ca^{2+}/X_0)^P)}$$

$A1 = 5 \times 10^{-7}$
$A2 = 100$
$X_0 = 0.041$
$P = 1.48$

Figure 6.8. Calibration of Aequorin.
A. Fractional luminescence and total counts data with buffered Ca^{2+} solutions in the Presence of 1µM A23187. B. $[Ca^{2+}]$ plotted against fractional luminescence. C. Logistic curve Equation used to relate fractional luminescence to $[Ca^{2+}]$

6.3.3.2 Identification as a Ca^{2+} signal from SR

In initial studies, experiments were carried out in the presence and absence of 25μM thapsigargin to ensure that all of the Ca^{2+} sensitive signal was due to SR activity. Figure 7.9 depicts results from experiments carried out in the presence and absence of thapsigargin. The traces are shown in grey and black respectively.

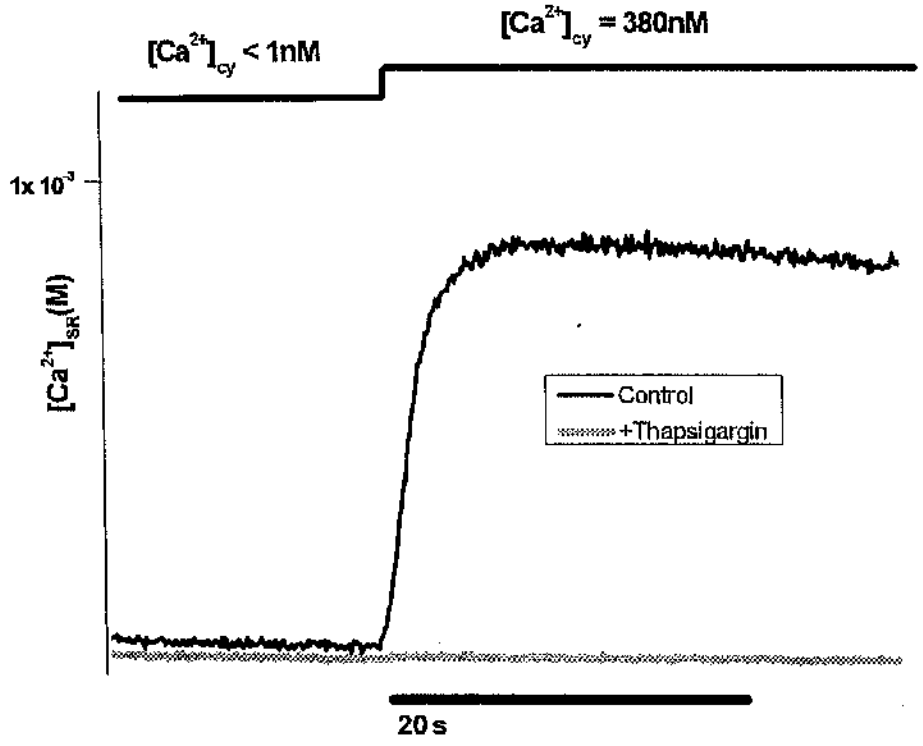

Figure 6.9. Studies in the presence and absence of 25μM thapsigargin

6.3.3.3 Studies of $[Ca^{2+}]_{SR}$ in the presence of Ruthenium Red

It was decided to initially study SR Ca^{2+} dynamics in cardiac muscle in the presence and absence of ryanodine receptor activity. Inhibition of RyR_2 activity was achieved by inclusion of Ruthenium Red.

Using a protocol similar to that shown in figures 6.7 and 6.9, the peak $[Ca^{2+}]_{SR}$ was measured using two fixed values of $[Ca^{2+}]_{CYT}$ at 162nM and 380nM in mock intracellular solutions in the presence and absence of ruthenium red. The mean values of $[Ca^{2+}]_{SR}$ under these conditions are shown in figure 6.10 and table 6.2.

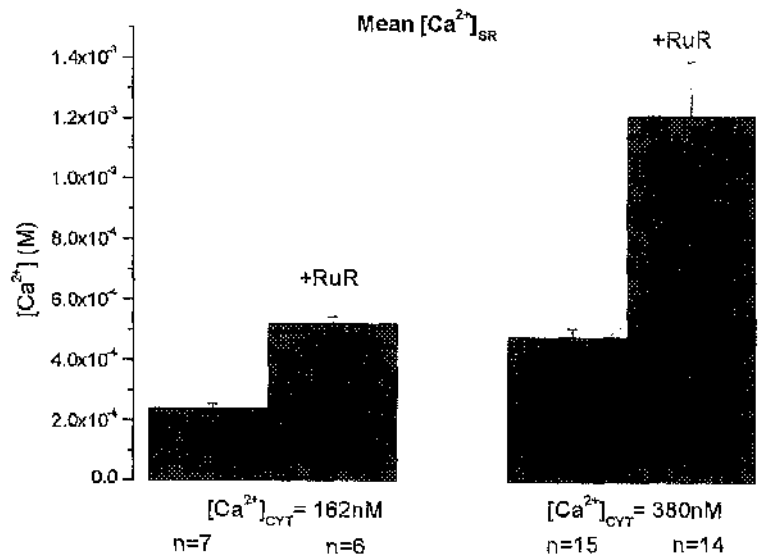

Figure 6.10. Mean $[Ca^{2+}]_{SR}$ in the presence and absence of 5μM ruthenium red.

Cytosolic $[Ca^{2+}]$ ($[Ca^{2+}]_{CYT}$) was clamped at 162nM and 380nM.

	$[Ca^{2+}]_{CYT}$=162nM		$[Ca^{2+}]_{CYT}$=380nM	
	$[Ca^{2+}]_{SR}$	n	$[Ca^{2+}]_{SR}$	n
-RuR	$2.40 \pm 0.140 \times 10^{-4}$	7	$4.78 \pm 0.289 \times 10^{-4}$	15
+RuR	$5.20 \pm 0.230 \times 10^{-4}$	6	$1.21 \pm 0.180 \times 10^{-3}$	14

Table 6.2. Mean $[Ca^{2+}]_{SR}$ in the presence and absence of ruthenium red.

ANOVA analysis indicated that addition of ruthenium red significantly increased the $[Ca^{2+}]_{SR}$ at both 160nM and 380nM. Furthermore, increasing $[Ca^{2+}]_{CYT}$ resulted in a significantly higher $[Ca^{2+}]_{SR}$ both in the presence and absence of ruthenium red.

However, an interesting result is obtained in the prolonged presence of ruthenium red as illustrated in figure 6.11.

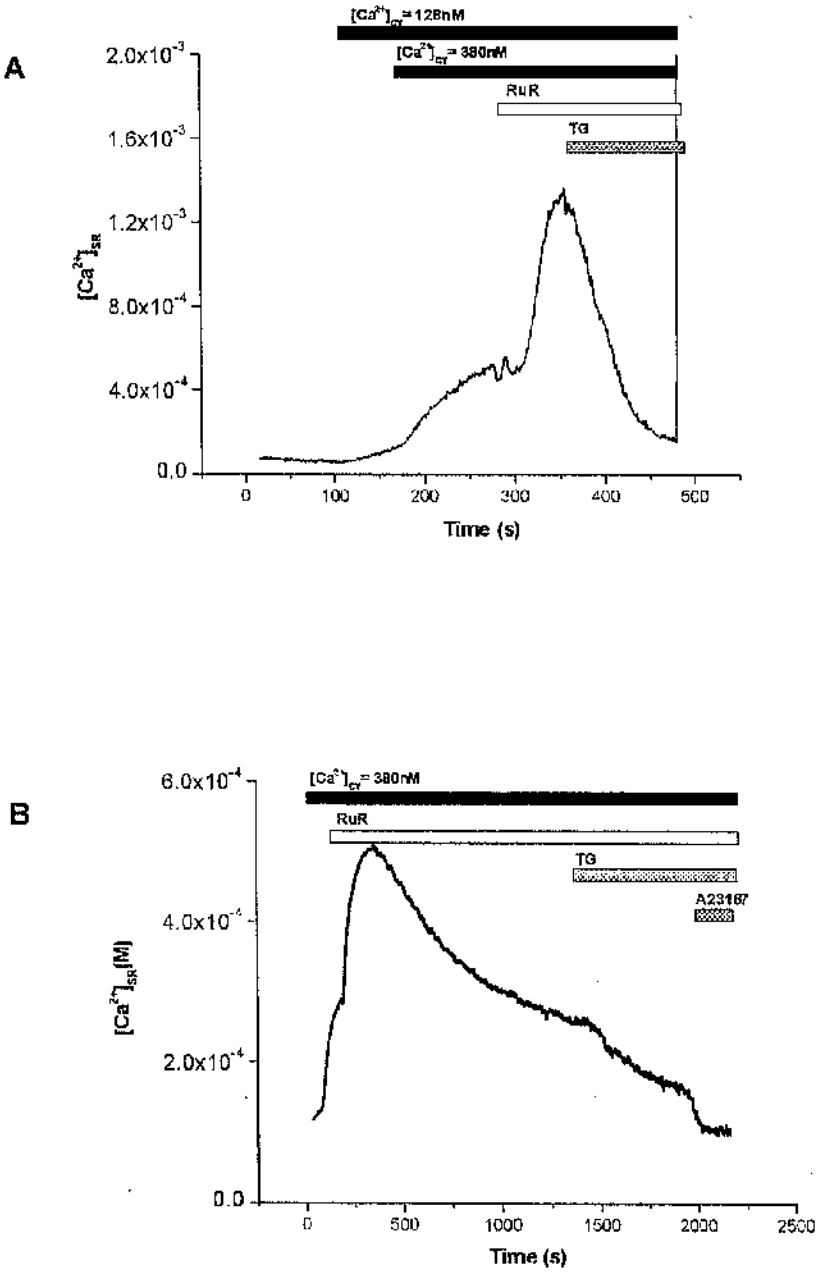

Figure 6.11. Effects of ruthenium red

Figure 6.11A depicts the primary effect of ruthenium red addition. In the graph shown there is an increase in $[Ca^{2+}]_{SR}$ when the $[Ca^{2+}]_{CYT}$ is increased to 128nM and then 380nM. Ruthenium red addition causes a more than 2 fold increase in $[Ca^{2+}]_{SR}$ at a $[Ca^{2+}]_{CYT}$ of 380nM. In the record shown, the $[Ca^{2+}]_{SR}$ increases from approximately 520μM to approximately 1.3mM. As discussed later, this can be accounted for by inhibition of Ca^{2+} release via RyR thus allowing SR to attain a higher steady state value of $[Ca^{2+}]_{SR}$.

6.3.4 Analysis of Ca^{2+} leak and uptake in the absence of RyR_2 activity

The leak and uptake profiles were examined in the presence of 5μM ruthenium red to inhibit RyR_2 -mediated Ca^{2+} leak. Figure 6.12A shows the raw leak and uptake phases of a representative experiment. Figure 6.12B shows in detail the individual uptake and leak phases of the curve.

Each phase of the curve was taken in turn and differentiated to obtain the rate of change of $[Ca^{2+}]_{SR}$ with respect to time. This differential was then plotted against the $[Ca^{2+}]_{SR}$ to give the relationship between $[Ca^{2+}]_{SR}$ and the rate of leak/uptake. The leak and uptake curves for the experiment shown in figure 6.12A are shown in figure 6.12C.

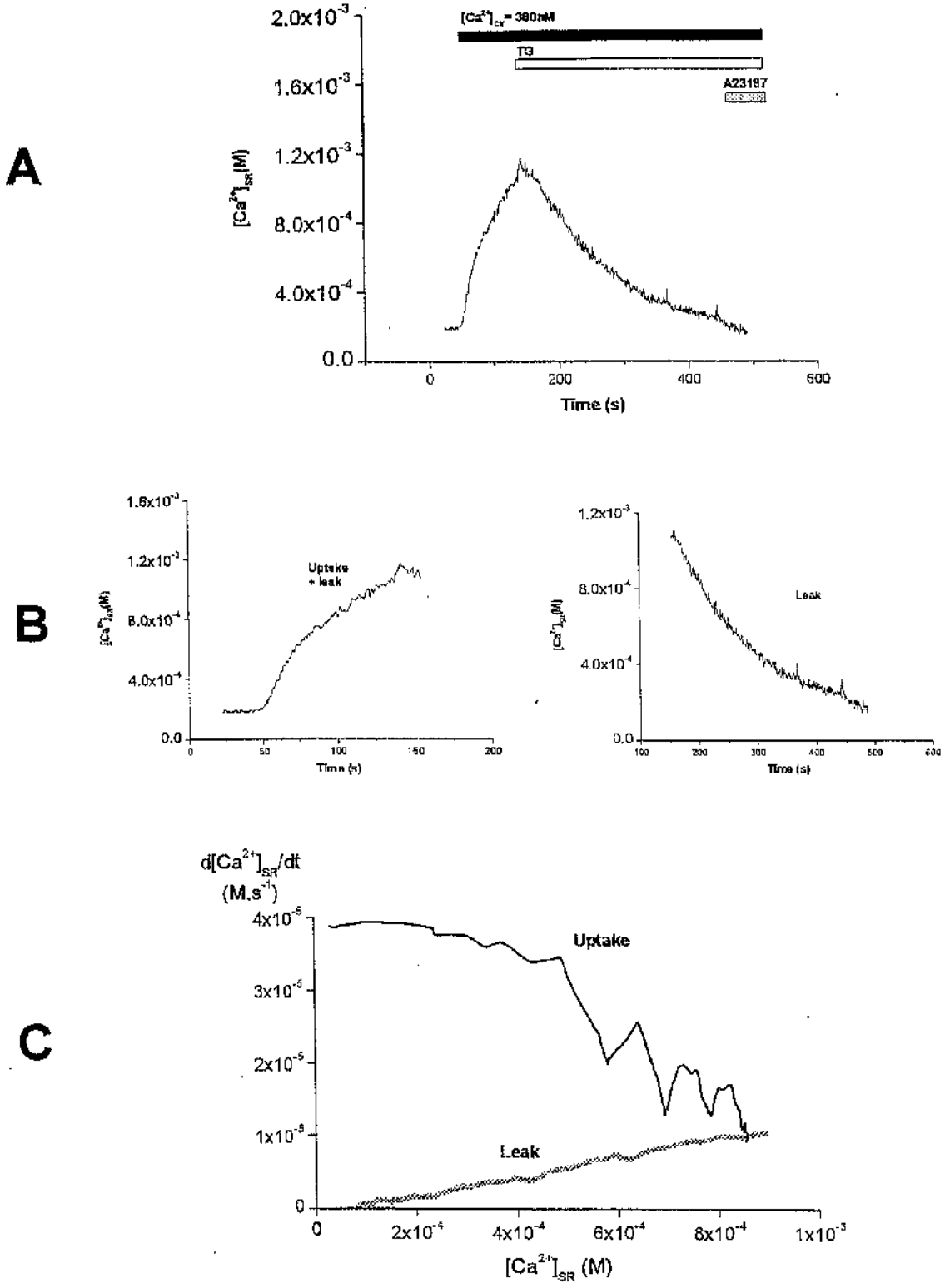

Figure 6.12. Analysis of leak and uptake data.
Raw leak and uptake data shown in panel A. The individual uptake and leak phases shown in panel B. Differential of each uptake and leak plotted against $[Ca^{2+}]_{SR}$ shown in panel C.

6.3.4.1 Analysis of data to give a general curve for mean uptake and leak in the absence of RyR_2 activity

All data obtained in the studies were analysed as described below.

Leak data

Leak was measured in the presence of 5μM ruthenium red and 25μM thapsigargin that allows unopposed leakage from SR.

For each study, the rate of change of $[Ca^{2+}]_{SR}$ was obtained by differentiation of the leak phase of each data set and with respect to $[Ca^{2+}]_{SR}$ was plotted against $[Ca^{2+}]_{SR}$. The resulting curves were fitted to a linear regression of the form y=a + bx. Values of a and b were noted for each study and mean values for these constants were calculated. A record from one of these studies and its corresponding linear fit is shown in figure 6.13.

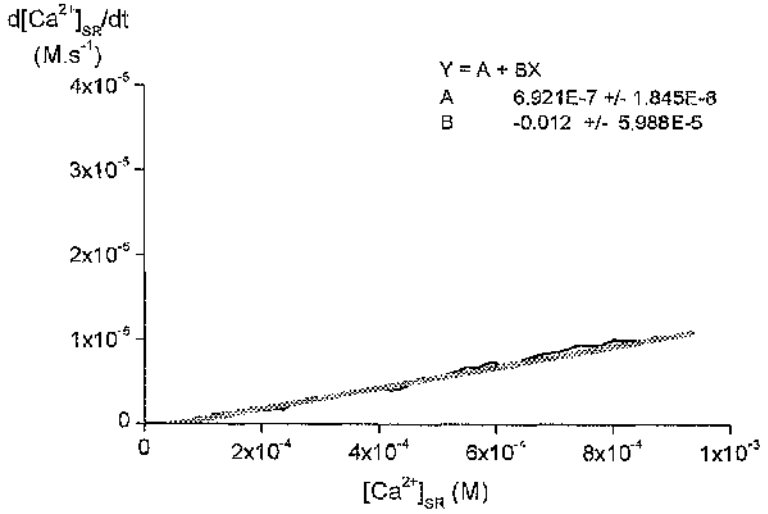

Figure 6.13. Leak profile.

The raw data is shown in black and the linear fit is shown by the grey trace. The parameters of the fit and their error are shown on the curve.

Application of this analysis technique to a number of leak phases revealed average leak characteristics shown in figure 6.14 where the mean slope has a value of 0.012 and the intercept on the y-axis is close to zero.

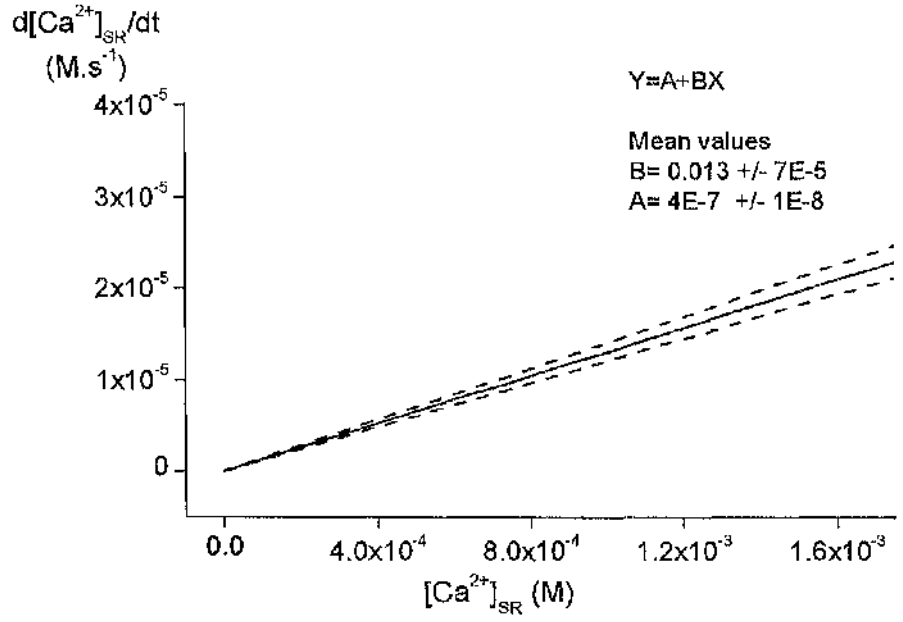

Figure 6.14. Mean leak curve. The relationship between $[Ca^{2+}]_{SR}$ and the rate of Ca^{2+} leak.

Dashed lines denote the standard error on the curve. (n=16)

Uptake data

After the leak analysis for a particular experiment the leak was subtracted from the corresponding uptake differential to reveal the relationship between SERCA2a Ca^{2+} uptake rate and $[Ca^{2+}]_{SR}$ using the parameters from the leak curve using the equation for the linear fit y=a+bx, where $x=[Ca^{2+}]_{SR}$. The values ascertained for a and b for each experiment were used and subtracted from the uptake rate (y).

The rate of change of $[Ca^{2+}]_{SR}$ with respect to time was fitted to a logistic curve. A curve from a representative experiment is shown in figure 6.15 with the corresponding logistic fit.

The curve parameters from each fit were noted. Mean values for each were calculated and used to generate a mean curve shown in figure 6.16.

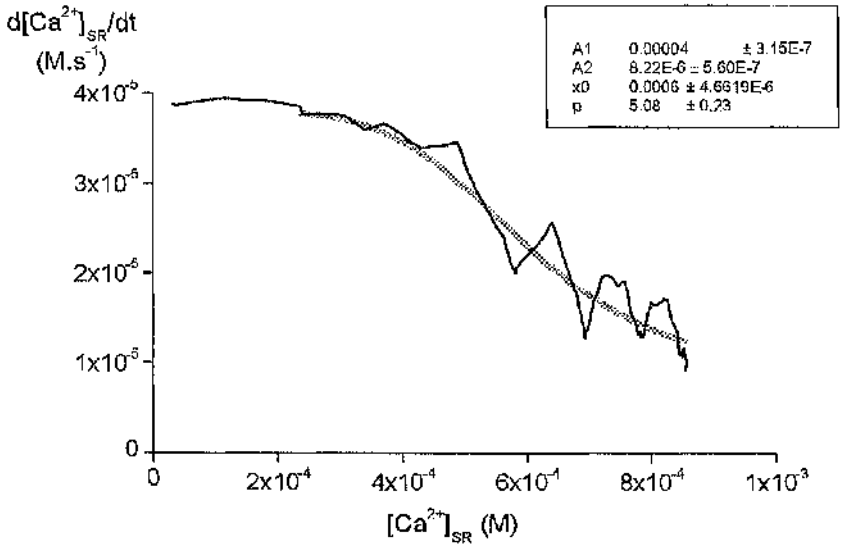

Figure 6.15. Leak rate vs. $[Ca^{2+}]_{SR}$ in the presence of 5μM ruthenium red.
The grey curve is the logistic fit to the data shown in black. A1 is the curve maximum, A2 the curve minimum, x_0 is the K_d value and p is the slope of the curve.

The logistic equation used for the curve fit is as follows:

$$d[Ca^{2+}]_{SR}/dt = \frac{A1-A2}{(1+[Ca^{2+}]_{SR}/x_0)^p)}$$

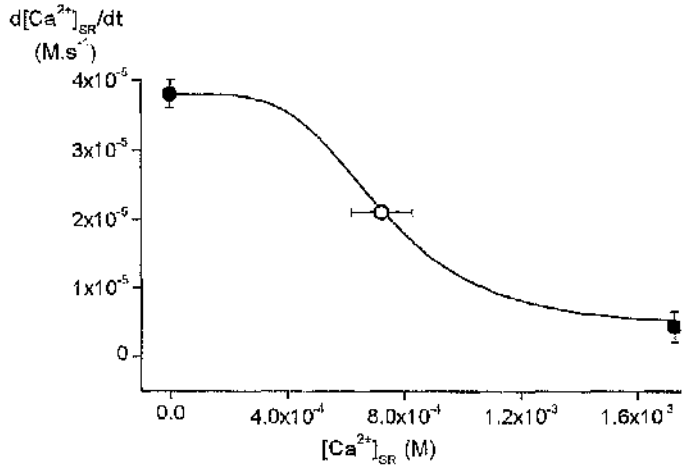

Figure 6.16. Mean uptake curve. The relationship between $[Ca^{2+}]_{SR}$ and the rate of Ca^{2+} uptake.

The closed black circles denote mean A1 and A2 values respectively and the open circle denotes the x_0 or K_d value. Error bars are also shown.

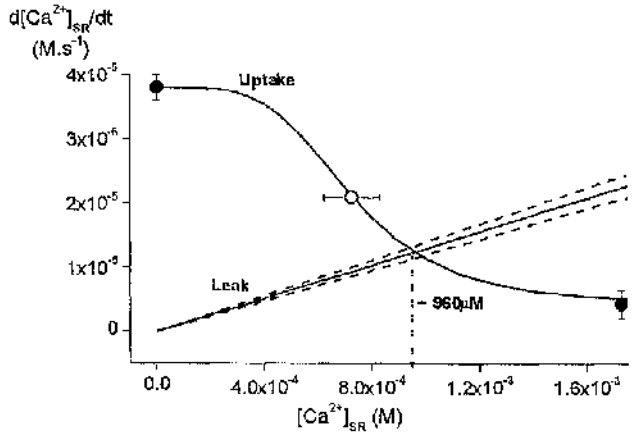

Figure 6.17. Relationship between apparent Ca^{2+} transport rates and $[Ca^{2+}]_{SR}$

Derived from mean parameters for both the uptake and the leak curves. The red dotted arrow denotes the point of interception of the two curves and therefore the equilibrium $[Ca^{2+}]_{SR}$. Uptake rate is leak corrected. Leak and uptake measured in the presence of 5µM ruthenium red. Leak measured also in the presence of 25µM thapsigargin.

Figure 6.17 shows the mean relationship between the apparent Ca^{2+} transport rates and $[Ca^{2+}]_{SR}$ derived from mean data.

6.4 Discussion

The results in this chapter represent the first direct measurement of $[Ca^{2+}]_{SR}$ within adult cardiac muscle. This has been possible by the generation of a protein-based Ca^{2+} indicator targeted to the SR.

6.4.1 Selectivity of probe

The selectivity of the probe was confirmed using an inhibitor to specifically inhibit Ca^{2+} accumulation by SR, namely thapsigargin. The results from studies carried out in the presence and absence of thapsigargin are shown in figure 6.9. The absence of any change in $[Ca^{2+}]_{SR}$ on raising the $[Ca^{2+}]_{CYT}$ from <1nM to 380nM in the presence of 25μM thapsigargin compared to the control experiment indicates that the Ca^{2+} sensitive signal can be solely attributed to SR.

6.4.2 Steady state $[Ca^{2+}]_{SR}$ in the absence of RyR_2 activity

RyR_2 was inhibited by the sustained presence of 5μM ruthenium red. There is a marked difference between the measured $[Ca^{2+}]_{SR}$ with the $[Ca^{2+}]_{CYT}$ clamped at two values in the absence and presence of RyR_2 inhibitor. Mean $[Ca^{2+}]_{SR}$ values derived from this data is shown in figure 6.10 and table 6.2. At both $[Ca^{2+}]_{CYT}$ values, in the absence of ruthenium red, the mean $[Ca^{2+}]_{SR}$ is lower compared to the mean $[Ca^{2+}]_{SR}$ in the presence of ruthenium red.

The lower $[Ca^{2+}]_{SR}$ observed in the absence of ruthenium red can be explained by a balance between SERCA-mediated Ca^{2+} uptake and RyR-mediated Ca^{2+} release which results in a steady state value of $[Ca^{2+}]_{SR}$.

The $[Ca^{2+}]_{SR}$ is more than two fold greater in the presence of ruthenium red at both values of $[Ca^{2+}]_{CYT}$. This can be accounted for by inhibition of flux through the RyR. This is consistent with the existence of a significant leak through RyR. Therefore blocking RyR-mediated Ca^{2+} leak with ruthenium red will increase the free $[Ca^{2+}]_{SR}$. The turnover of SERCA will remain high, but we assume that the leak observed is not RyR-mediated, but is a background leak which is present even in the absence of RyR-mediated Ca^{2+} leak. This decrease in leak can explain how the higher $[Ca^{2+}]_{SR}$ is attained as a new steady state $[Ca^{2+}]_{SR}$ is reached.

The values of $[Ca^{2+}]_{SR}$ observed are close to values reported by Shannon and Bers using SR vesicles. This group estimated that the $[Ca^{2+}]$ within the vesicles was in the range 0.7-1mM ((Shannon & Bers, 1997). Given that these studies were carried out with a vesicle preparation with a different surface area/volume ratio to native SR and the number of functional RyR_2 entities present was unknown, the values obtained in my own studies can be said to be in close agreement.

6.4.3 Studies in the sustained presence of ruthenium red

In addition to the above experiments, studies were also carried out in the maintained presence of ruthenium red. Figure 6.11 depicts the results obtained under such conditions. The primary effect of ruthenium red addition is clear in figure 6.11A. This effect is to increase the $[Ca^{2+}]_{SR}$ when $[Ca^{2+}]_{CYT}$ is clamped. This effect was also observed in the presence of 100μM tetracaine (data not shown as n=2).

However, on prolonged incubation with 5μM ruthenium red shown in figure 6.11B. There appears to be a biphasic effect. The initial rapid rise in $[Ca^{2+}]_{SR}$ is followed by a decline with a slower time course than the rise. This cannot be easily explained. Two possible scenarios could provide an explanation. The first involves a direct effect of ruthenium red on SERCA. Previously it has been demonstrated that ruthenium red decreases the Ca^{2+} sensitivity of SR Ca^{2+} uptake in a dose dependent manner but the V_{max} and Hill coefficient remain unchanged (Kargarcin, Ali & Kargacin 1998). Partial inhibition of SERCA would explain the slow time course compared to the decline in $[Ca^{2+}]_{SR}$ when thapsigargin is added (figure 6.11A). One of the conclusions from this study was that it was unlikely that the effect of ruthenium red on the Ca^{2+} sensitivity of SR uptake was mediated through the ryanodine receptor, as experimental conditions did not favour ryanodine receptor opening. Thus this effect on Ca^{2+} uptake is most likely to result from direct action of ruthenium red on SERCA and occurs independently of the effect on the ryanodine receptor.

It has also been demonstrated that ruthenium red inhibits SERCA reversal by P_i and ADP (Alves and de Meis 1986).

An alternative to the above explanation would be that ruthenium red in some way activates an as yet unidentified Ca^{2+} leak pathway from SR. This has not yet been reported and evidence from oxalate loaded SR with ruthenium red addition indicates an increase in the rate of uptake consistent with inhibition of RyR-mediated leak and no increased leak. However the intra-SR concentration has not been measured under these conditions, and since oxalate is used as a trapping ion to clamp $[Ca^{2+}]_{SR}$ at a low level. If another leak pathway is being activated by ruthenium red the $[Ca^{2+}]_{SR}$ may not be sufficiently high for such a leak to occur.

6.4.4 Analysis of SR Ca^{2+} leak and uptake in the absence of RyR_2 activity

The mean relationship between the leak and uptake rates and $[Ca^{2+}]_{SR}$ is shown in figure 6.17.

6.4.4.1 Uptake characteristics

The leak-corrected uptake curve appears to be non-linear and was fitted to a logistic curve. On examination of the mean uptake curve shown in figure 6.16 the first striking observation is the steep dependence of the rate of Ca^{2+} transport into the SR on the $[Ca^{2+}]_{SR}$. The apparent rate of uptake is very high when $[Ca^{2+}]_{SR}$ is low. The value from the mean curve of the maximum uptake rate is 38μM s^{-1} that corresponds to of 2.3mM min^{-1}. The rate decreases as $[Ca^{2+}]_{SR}$ increases and hence the store refills. At $[Ca^{2+}]_{SR}$ values > 1.2mM

there is virtually no Ca^{2+} uptake and the rate tends towards zero. The results suggest a form of lumenal regulation of SERCA2a activity. The result would suggest that this negative feedback of Ca^{2+} in the lumen of the store on SERCA2a controls SR Ca^{2+} content.

A simple lumenal dependence on $[Ca^{2+}]$ would not explain the relationship between $[Ca^{2+}]_{SR}$ and the rate of Ca^{2+} uptake. If this were the case the relationship would be linear. Another factor that could explain the observed result could be the presence of the Ca^{2+} buffering protein calsequestrin. In the $[Ca^{2+}]_{SR}$ range 0-0.4mM the rate of Ca^{2+} uptake does not alter much and looks relatively constant. There is a similar scenario between the concentration ranges 1.2-1.8mM where the rate tends towards zero and reaches a plateau.

Within the intermediate $[Ca^{2+}]_{SR}$ between 0.4-1.2mM, as $[Ca^{2+}]_{SR}$ is increased the rate of uptake decreases sharply, before tending towards zero at $[Ca^{2+}]_{SR}$ <1.2mM. It is conceivable that the buffering capacity of calsequestrin lies within this intermediate range of $[Ca^{2+}]_{SR}$ therefore as the buffer becomes saturated, the free $[Ca^{2+}]_{SR}$ rises and has a negative feedback effect on SERCA2a. Alternatively the rapid decrease in the rate of Ca^{2+} uptake may be due to a direct inhibition by $[Ca^{2+}]_{SR}$ on SERCA2a. This direct effect was suggested by Hasselbach for work carried out with skeletal SR vesicles (Katz *et al.*, 1977) & (Hasselbach, 1978).

6.4.4.2 Leak characteristics

In contrast to the uptake, the apparent rate of leak in the absence of ryanodine receptor activity, shows an inverse dependence on $[Ca^{2+}]_{SR}$. At very low $[Ca^{2+}]_{SR}$ values and thus the store depleted, the apparent leak rate is negligible. As the store refills, the $[Ca^{2+}]_{SR}$ value increases as does the apparent rate of leak. There exists a linear relationship between the leak rate and the $[Ca^{2+}]_{SR}$.

The kinetics of the leak suggests a simple leak channel. This has not been observed before. It represents a background Ca^{2+} leak. Previous work on SR Ca^{2+} leak suggests that in the absence of RyR_2 activity one of the major routes for Ca^{2+} extrusion from SR occurs via SERCA2a pump reversal (Hasselbach, 1978). However, the leak studied here was carried out in the presence of thapsigargin. It has been demonstrated that thapsigargin presence blocks pump reversal (Smith *et al.*, 2000) and yet a substantial Ca^{2+} leak remains. It is unlikely that the extrusion occurs via a population of RyR_2 due to incomplete inhibition as one would expect the dependence of the leak rate on $[Ca^{2+}]_{SR}$ to be non-linear under this condition.

Studies carried out by Pessah and colleagues (1997) suggest the existence of a Ca^{2+} leak channel in skeletal muscle. The pathway is unmasked by thapsigargin addition. The 'channel' is insensitive to inhibition by ruthenium red and high concentrations of ryanodine. Addition of the protein bastadin 5 in conjunction with high concentrations of ryanodine or ruthenium red eliminates

this ryanodine insensitive leak. The group suggest the identity of 'channel' as RyR_1 that is somehow dysfunctional and permanently open, but there has been no evidence of such a channel existing in cardiac muscle.

6.4.4.3 Equilibrium value of $[Ca^{2+}]_{SR}$

The equilibrium value for $[Ca^{2+}]_{SR}$ occurs when the rate of uptake and rate of leak are apparently balanced to maintain a steady state value. This value is when both the leak and uptake curves intercept. From the mean curves shown in figure 6.17, the equilibrium value is shown by the dotted red line and is occurs at a $[Ca^{2+}]_{SR}$ of approximately 0.96mM. This is similar to the mean values calculated from the steady state $[Ca^{2+}]_{SR}$ at a $[Ca^{2+}]_{CYT}$ of 380nM shown in figure 6.10 where $[Ca^{2=}]_{SR}$=1.21mM and also estimates using MgFura-2 entrapped vesicle preparations (Shannon and Bers, 1997) This group estimated that at a cytosolic $[Ca^{2+}]$ of 100-150nM, which is a good estimate of end diastolic $[Ca^{2+}]$ in the cytoplasmic compartment, the intra-vesicular $[Ca^{2+}]$ was in the range of 0.7-1mM.

Chapter 7
General Conclusions

Chapter 7-General Conclusions

The original aim was to measure the [Ca^{2+}] within the different organelles of cardiac muscle.

7.1 Use of fluorescent Ca^{2+} indicators to study organelle Ca^{2+} dynamics

Incubating populations of cells with acetoxoymethyl ester (AM) derivatives of FURA based dyes was used to introduce Ca^{2+} sensitive indicators inside the organelles. The use of indicators with very different Ca^{2+} affinities should allow the differentiation of signals from SR, mitochondria and any other passive compartment. The results from this part of the study indicated that this approach could not be used to measure Ca^{2+} within the SR lumen. However, good signals from mitochondria were achieved. Furthermore, a large passive, slowly exchanging compartment was unmasked. The cellular structure represented by this is unclear.

Work in isolated SR and mitochondria confirmed the ability of mitochondria to cleave acetoxoymethyl derivatives of FURA indicators. Isolated SR did not accumulate indicator suggesting low intrinsic esterase activity.

The general conclusion from this work is that AM loading of fluorescent indicators is not a feasible approach for studying SR Ca^{2+} dynamics in cardiac muscle. However, excellent mitochondrial signals were obtained suggesting that this may be a minimally invasive technique to study mitochondrial Ca^{2+} dynamics.

7.2 $[Ca^{2+}]_{SR}$ studies using a targeted probe

An adenovirus was generated which allowed successful expression and targeting of aequorin to SR. This generated the first direct measurement of $[Ca^{2+}]$ within a native SR structure using a bioluminescent Ca^{2+} indicator. A major limitation of this technique is the relatively short time period over which measurements can be made. This work also revealed the lumenal dependence of Ca^{2+} uptake and leak from the SR.

7.3 Future directions

There is clearly further scope for work in the areas of organelle Ca^{2+} dynamics explored in cardiac muscle. Future studies include determination of the cellular structure(s) responsible for the slow, passive exchange of Ca^{2+}. Also identification of the RyR_2-independent Ca^{2+} leak from the SR and determination of the mechanism underlying the lumenal Ca^{2+} regulation of SERCA2a.

Clarification of the lumenal control processes will enhance our understanding of the functions of SR in physiological and pathophysiological conditions (e.g. heart failure)

Reference List

Alverez J, Montero M, & Garcia-Snacho J (1999). Subcellular Ca^{2+} dynamics. *News in Physiological Science* **14**, 161-168.

Alves E.W.& de Meis,L. (1996). Effect of compound 48/80 and ruthenium red on the Ca2+-ATPase of sarcoplasmic reticulum. *J. Biol. Chem* **261**, 16854-16859

Arai, Alpert, N. R., Periasamy, & M. (1991). Cloning and characterisation of the gene encoding rabbit cardiac calsequestrin. *Gene* **109**, 275-279.

Babcock, D. F. & Hille, B. (1998). Mitochondrial oversight of cellular Ca2+ signaling. *Curr.Opin.Neurobiol.* **8**, 398-404.

Baird, G. S., Zacharias, D. A., & Tsien, R. Y. (1999). Circular permutation and receptor insertion within green fluorescent proteins. *Proc.Natl.Acad.Sci.U.S.A* **96**, 11241-11246.

Barg, S., Copello, J. A., & Fleischer, S. (1997). Different interactions of cardiac and skeletal muscle ryanodine receptors with FK-506 binding protein isoforms. *Am.J.Physiol* **272** , C1726-C1733.

Baudet, S., Weisser, J., Janssen, A. P., Beulich, K., Bieligk, U., Pieske, B., Noireaud, J., Janssen, P. M., Hasenfuss, G., & Prestle, J. (2001). Increased basal contractility of cardiomyocytes overexpressing protein kinase C epsilon and blunted positive inotropic response to endothelin- 1. *Cardiovasc.Res.* **50**, 486-494.

Becker, T. C., Noel, R. J., Coats, W. S., Gomez-Foix, A. M., Alam, T., Gerard, R. D., & Newgard, C. B. (1994). Use of recombinant adenovirus for metabolic engineering of mammalian cells. *Methods Cell Biol.* **43 Pt A**, 161-189.

Berridge MJ, Bootman M.D, & Lipp P (1998). Calcium-a life and death signal. *Nature* **395**, 646-648.

Boitier E, Rea R, & Duchen MR (1999). Mitochondria exert a negative feedback on the propagation of intracellular Ca^{2+} waves in rat cortical astrocytes. *Journal of Cell Biology* **145**, 795-808.

Brierley, G. P., Davis, M., & Jung, D. W. (1987). Respiration-dependent uptake and extrusion of Mg2+ by isolated heart mitochondria. *Arch.Biochem.Biophys.* **253**, 322-332.

Brillantes, A. B., Ondrias, K., Scott, A., Kobrinsky, E., Ondriasova, E., Moschella, M. C., Jayaraman, T., Landers, M., Ehrlich, B. E., & Marks, A. R. (1994). Stabilization of calcium release channel (ryanodine receptor) function by FK506-binding protein. *Cell* **77**, 513-523.

Brini M, De Giorgi F, Murgia M, Marsault R, Massimino ML, Cantini M, Rizzuto R, & Pozzan T (1997). Subcellular analysis of Ca^{2+} homeostasis in primary cultures of skeletal muscle myotubules. *Molecular Biology of the Cell* **8**, 129-143.

Brini M, Marsault R, Bastianutto C, Alverez J, Pozzan T, & Rizzuto R (1995). Transfected Aequorin in the measurement of cytosolic Ca^{2+} concentration. *Journal of Biological Chemistry* **270**, 9896-9903.

Buntinas, L., Gunter, K. K., Sparagna, G. C., & Gunter, T. E. (2001). The rapid mode of calcium uptake into heart mitochondria (RaM): comparison to RaM in liver mitochondria. *Biochim.Biophys.Acta* **1504**, 248-261.

Cala, S. E. & Miles, K. (1992). Phosphorylation of the cardiac isoform of calsequestrin in cultured rat myotubes and rat skeletal muscle. *Biochim.Biophys.Acta* **1118**, 277-287.

Chen, S. R., Vaughan, D. M., Airey, J. A., Coronado, R., & MacLennan, D. H. (1993). Functional expression of cDNA encoding the Ca2+ release channel (ryanodine receptor) of rabbit skeletal muscle sarcoplasmic reticulum in COS-1 cells. *Biochemistry* **32**, 3743-3753.

Chiesa, A., Rapizzi, E., Tosello, V., Pinton, P., de Virgilio, M., Fogarty, K. E., & Rizzuto, R. (2001). Recombinant aequorin and green fluorescent protein as valuable tools in the study of cell signalling. *Biochem.J.* **355**, 1-12.

Colyer, J. (1998). Phosphorylation states of phospholamban. *Ann.N.Y.Acad.Sci.* **853**, 79-91.

Conklin MW, Barone V, Sorrentino V, & Coronado R (1999). Contribution of Ryanodine Receptor type 3 to Ca^{2+} sparks in embryonic mouse skeletal muscle. *Biophysical Journal* **77**, 1394-1403.

Coronado, R., Morrissette, J., Sukhareva, M., & Vaughan, D. M. (1994). Structure and function of ryanodine receptors. *American Journal of physiology* **266**, C1485-C1504.

Donahue, J. K., Kikkawa, K., Johns, D. C., Marban, E., & Lawrence, J. H. (1997). Ultrarapid, highly efficient viral gene transfer to the heart. *Proc.Natl.Acad.Sci.U.S.A* **94**, 4664-4668.

Duchen MR (1999). Contributions of mitochondria to animal physiology: from homeostatic sensor to calcium signalling and cell death. *Journal of Physiology* **516**, 1-17.

Duchen MR (2000). mitochondria and calcium: from cell signalling to cell death. *Journal of Physiology* **529**, 57-68.

Erdahl, W. L., Chapman, C. J., Wang, E., Taylor, R. W., & Pfeiffer, D. R. (1996). Ionophore 4-BrA23187 transports Zn2+ and Mn2+ with high selectivity over Ca2+. *Biochemistry* **35**, 13817-13825.

Ferrier, G. R. & Howlett, S. E. (2001). Cardiac excitation-contraction coupling: role of membrane potential in regulation of contraction. *American Journal of physiology* **280**, 1928-1944.

Fill, M., Coronado, R., Mickelson, J. R., Vilven, J., Ma, J. J., Jacobson, B. A., & Louis, C. F. (1990). Abnormal ryanodine receptor channels in malignant hyperthermia. *Biophys.J.* **57**, 471-475.

Golovina, V. A. & Blaustein, M. P. (1997). Spatially and functionally distinct Ca2+ stores in sarcoplasmic and endoplasmic reticulum. *Science* **275**, 1643-1648.

Graham, F. L., Smiley, J., Russell, W. C., & Nairn, R. (1977). Characteristics of a human cell line transformed by DNA from human adenovirus type 5. *J.Gen.Virol.* **36**, 59-74.

Greene, A. L., Lalli, M. J., Ji, Y., Babu, G. J., Grupp, I., Sussman, M., & Periasamy, M. (2000). Overexpression of SERCA2b in the heart leads to an increase in sarcoplasmic reticulum calcium transport function and increased cardiac contractility. *J.Biol.Chem.* **275**, 24722-24727.

Griffiths, E. J. (2000). Use of ruthenium red as an inhibitor of mitochondrial Ca(2+) uptake in single rat cardiomyocytes. *FEBS Lett.* **486**, 257-260.

Grynkiewicz G, Poenie M, & Tsien RY (1985). A new generation of Ca indicators with greatly improved Fluorescence properties. *Journal of Biological Chemistry* **260**, 3440-3450.

Gunter, T. E., Buntinas, L., Sparagna, G., Eliseev, R., & Gunter, K. (2000). Mitochondrial calcium transport: mechanisms and functions. *Cell Calcium* **28**, 285-296.

Gyorke I & Gyorke S (1998). Regulation of the cardiac ryanodine receptor channel by lumenal Ca involves lumenal Ca sensing sites. *Biophysical Journal* **75**, 2801-2810.

Hackett, N.R. & Crystal R.G. (2000) *Gene Therapy: therapeutic mechanisms and strategies.* eds. Templeton N.S. & Lasic, D.D. Marcel Dekker

Hajjar RJ, Schmidt U, Kang JX, Matsui T, & Rosenzweog A (1997). Adenoviral gene transfer of phospholamban in isolated rat cardiomyocytes. *Circulation Research* **81**, 145-153.

Harkins AB, Kurebayashi N, & Baylor SM (1993). Resting myoplasmic free calcium in frog skeletal muscle fibres estimated with fluo-3. *Biophysical Journal* **65**, 865-881.

Hasselbach, W. (1978). The reversibility of the sarcoplasmic calcium pump. *Biochim.Biophys.Acta* **515**, 23-53.

He, H., Meyer, M., Martin, J. L., McDonough, P. M., Ho, P., Lou, X., Lew, W. Y., Hilal-Dandan, R., & Dillmann, W. H. (1999). Effects of mutant and antisense RNA of phospholamban on SR Ca(2+)- ATPase activity and cardiac myocyte contractility. *Circulation* **100** , 974-980.

Horwitz, M.S. (1996) *Virology* eds. Fields, B.N., Knipe, D.M., & Howley, P.M. Lippencott-Raven, Philadelphia

Hove-Madsen L & Bers DM (1993). Sarcoplasmic Reticulum Ca^{2+} uptake and thapsigargin sensitivity in permeabilised rabbit and rat ventricular myocytes. *Circulation Research* **73**, 820-828.

Ichas F, Jouaville LS, & Mazat JP (1997). mitochondria are excitable organelles capable of generating and conveying electrical and calcium signals. *Cell* **89**, 1145-1153.

Ikemoto N, Ronjat M, Meszaros LG, & Koshita M (1989). Postulated Role of Calsequestrin in the regulation of calcium release from Sarcoplasmic Reticulum. *Biochemistry* **28**, 6764-6771.

Inesi G & de Meis (1989). Regulation of steady state filling in SR. *Journal of Biological Chemistry* **264**, 5929-5936.

Inouye, S., Noguchi, M., Sakaki, Y., Takagi, Y., Miyata, T., Iwanaga, S., Miyata, T., & Tsuji, F. I. (1985). Cloning and sequence analysis of cDNA for the luminescent protein aequorin. *Proc.Natl.Acad.Sci.U.S.A* **82**, 3154-3158.

Jayaraman, T., Brillantes, A. M., Timerman, A. P., Fleischer, S., Erdjument-Bromage, H., Tempst, P., & Marks, A. R. (1992). FK506 binding protein associated with the calcium release channel (ryanodine receptor). *J.Biol.Chem.* **267**, 9474-9477.

Jones LR, Suzuki YJ, Wang W, Kobayashi YM, Ramesh V, Franzini-Armstrong C, Cleeman L, & Morad M (1998). Regulation of Ca siganlling in transgenic mouse cardiac myocytes overexpressing calsequestrin. *Journal of Clinical Investigation* **101**, 1385-1393.

Jung, D. W. & Brierley, G. P. (1994). Magnesium transport by mitochondria. *J.Bioenerg.Biomembr.* **26** , 527-535.

Jung, D. W., Chapman, C. J., Baysal, K., Pfeiffer, D. R., & Brierley, G. P. (1996). On the use of fluorescent probes to estimate free Mg2+ in the matrix of heart mitochondria. *Arch.Biochem.Biophys.* **332**, 19-29.

Jung, D. W., Panzeter, E., Baysal, K., & Brierley, G. P. (1997). On the relationship between matrix free Mg2+ concentration and total Mg2+ in heart mitochondria. *Biochim.Biophys.Acta* **1320**, 310-320.

Kabbara, A. A. & Allen, D. G. (2001). The use of the indicator fluo-5N to measure sarcoplasmic reticulum calcium in single muscle fibres of the cane toad. *J.Physiol* **534**, 87-97.

Kaftan, E., Marks, A. R., & Ehrlich, B. E. (1996). Effects of rapamycin on ryanodine receptor/Ca(2+)-release channels from cardiac muscle. *Circ.Res.* **78**, 990-997.

Kargacin, G. J., Ali, Z., & Kargacin, M. E. (1998). Ruthenium red reduces the Ca2+ sensitivity of Ca2+ uptake into cardiac sarcoplasmic reticulum. *Pflugers Arch.* **436**, 338-342.

Katz, A. M., Repke, D. I., Dunnett, J., & Hasselbach, W. (1977). Dependence of calcium permeability of sarcoplasmic reticulum vesicles on external and internal calcium ion concentrations. *J.Biol.Chem.* **252**, 1950-1956.

Kohout, T. A., O'Brian, J. J., Gaa, S. T., Lederer, W. J., & Rogers, T. B. (1996). Novel adenovirus component system that transfects cultured cardiac cells with high efficiency. *Circ.Res.* **78**, 971-977.

Kurebayashi N & Ogawa Y (1998). Effect of luminal calcium on Ca release channel activity of SR in situ. *Biophysical Journal* **74**, 1795-1807.

Lai, F. A., Anderson, K., Rousseau, E., Liu, Q. Y., & Meissner, G. (1988). Evidence for a Ca2+ channel within the ryanodine receptor complex from cardiac sarcoplasmic reticulum. *Biochem.Biophys.Res.Commun.* **151**, 441-449.

Langer, G. A., Rich, T. L., & Orner, F. B. (1990). Ca exchange under non-perfusion-limited conditions in rat ventricular cells: identification of subcellular compartments. *Am.J.Physiol* **259**, H592-H602.

Levi, A. J., Brooksby, P., & Hancox, J. C. (1993). A role for depolarisation induced calcium entry on the Na-Ca exchange in triggering intracellular calcium release and contraction in rat ventricular myocytes. *Cardiovascular Research* **27**, 1677-1690.

Liu, H. S., Jan, M. S., Chou, C. K., Chen, P. H., & Ke, N. J. (1999). Is green fluorescent protein toxic to the living cells? *Biochem.Biophys.Res.Commun.* **260**, 712-717.

Lukyanenko V, Gyorke I, & Gyorke S (1996). Regulation of calcium release by calcium inside the SR in ventricular myocytes. *Pflugers Arch-European Journal of Physiology* **432**, 1047-1054.

MacLennan, D. H. & Wong, P. T. (1971). Isolation of a calcium-sequestering protein from sarcoplasmic reticulum. *Proc.Natl.Acad.Sci.U.S.A* **68**, 1231-1235.

Marx, S. O., Ondrias, K., & Marks, A. R. (1998). Coupled gating between individual skeletal muscle Ca2+ release channels (ryanodine receptors). *Science* **281**, 818-821.

Marx, S. O., Reiken, S., Hisamatsu, Y., Jayaraman, T., Burkhoff, D., Rosemblit, N., & Marks, A. R. (2000). PKA phosphorylation dissociates FKBP12.6 from the calcium release channel (ryanodine receptor): defective regulation in failing hearts. *Cell* **101**, 365-376.

McCleod, A.G.Amy, C.Y, & Campbell K.P (1991). Frog Cardiac Calsequestrin. *Circulation Research* **69**, 344-358.

Meissner, G. (1994). Ryanodine receptor/Ca^{2+}release channels and their regulation by endogenous effectors. *Annual Review of Physiology* **56**, 485-508.

Meissner, G., Rousseau, E., Lai, F. A., Liu, Q. Y., & Anderson, K. A. (1988). Biochemical characterization of the Ca2+ release channel of skeletal and cardiac sarcoplasmic reticulum. *Mol.Cell Biochem.* **82**, 59-65.

Meldolesi, J. & Pozzan, T. (1998). The endoplasmic reticulum Ca2+ store: a view from the lumen. *Trends Biochem.Sci.* **23**, 10-14.

Miyamoto, M. I., del Monte, F., Schmidt, U., DiSalvo, T. S., Kang, Z. B., Matsui, T., Guerrero, J. L., Gwathmey, J. K., Rosenzweig, A., & Hajjar, R. J. (2000). Adenoviral gene transfer of SERCA2a improves left-ventricular function in aortic-banded rats in transition to heart failure. *Proc.Natl.Acad.Sci.U.S.A* **97**, 793-798.

Miyawaki A, Llopis J, Heim R, McCaffrey JM, Adams JA, Ikura M, & Tsien RY (1997). Fluorescent Indicators for Ca based on GFP and calmodulin. *Nature* **388**, 882-887.

Mogami H, Gardner J, Gerasimento G, Camello P, Petersen O.H, & Tepikin A.V (1999). Calcium Binding capacity of the cytosol and ER Of mouse pancreatic acinar cells. *Journal of Physiology* **518**, 463-467.

Mogami H, Tepikin A.V, & Petersen O.H (1998). Termination of cytosolic Ca signals: Ca reuptake into intracellular stores is regulated by the free Ca concentraton in the store lumen. *EMBO Journal* **17**, 435-442.

Montero, M., Alonso, M. T., Albillos, A., Garcia-Sancho, J., & Alvarez, J. (2001). Mitochondrial Ca(2+)-induced Ca(2+) release mediated by the Ca(2+) uniporter. *Mol.Biol.Cell* **12**, 63-71.

Montero, M., Alonso, M. T., Carnicero, E., Cuchillo-Ibanez, I., Albillos, A., Garcia, A. G., Garcia-Sancho, J., & Alvarez, J. (2000). Chromaffin-cell stimulation triggers fast millimolar mitochondrial Ca2+ transients that modulate secretion. *Nat.Cell Biol.* **2** , 57-61.

Montero, M., Brini, M., Marsault, R., Alvarez, J., Sitia, R., Pozzan, T., & Rizzuto, R. (1995). Monitoring dynamic changes in free Ca2+ concentration in the endoplasmic reticulum of intact cells. *EMBO J.* **14**, 5467-5475.

Murayama T, Oba T, Katayama E, Oyamada H, Oguchi K, Kobayashi M, & Ogawa Y (1999). Further characterisation of the type 3 ryanodine receptor purified from rabbit diaphragm. *Journal of Biological Chemistry* **274**, 17297-17308.

Nagai, T., Sawano, A., Park, E. S., & Miyawaki, A. (2001). Circularly permuted green fluorescent proteins engineered to sense Ca2+. *Proc.Natl.Acad.Sci.U.S.A* **98**, 3197-3202.

Niggli E (1999). Localized intracellular calcium signalling in muscle:calcium sparks and quarks. *Annual Review of Physiology* **61**, 311-335.

Pessah, I. N., Molinski, T. F., Meloy, T. D., Wong, P., Buck, E. D., Allen, P. D., Mohr, F. C., & Mack, M. M. (1997). Bastadins relate ryanodine-sensitive and -insensitive Ca2+ efflux pathways in skeletal SR and BC3H1 cells. *Am.J.Physiol* **272**, C601-C614.

Pinton, P., Tsuboi, T., Ainscow, E. K., Pozzan, T., Rizzuto, R., & Rutter, G. A. (2002). Dynamics of glucose-induced membrane recruitment of protein kinase C beta II in living pancreatic islet beta-cells. *J.Biol.Chem.* **277**, 37702-37710.

Poenie, M. (1990). Alteration of intracellular Fura-2 fluorescence by viscosity: a simple correction. *Cell Calcium* **11**, 85-91.

Post, J. A. & Langer, G. A. (1992). Cellular origin of the rapidly exchangeable calcium pool in the cultured neonatal rat heart cell. *Cell Calcium* **13**, 627-634.

Pozzan T, Magalhaes P, & Rizzuto R (2000). The comeback of mitochondria to calcium signalling. *Cell Calcium* **28**, 279-283.

Pozzan, T. & Rizzuto, R. (2000). The renaissance of mitochondrial calcium transport. *Eur.J.Biochem.* **267**, 5269-5273.

Prestle, J., Janssen, P. M., Janssen, A. P., Zeitz, O., Lehnart, S. E., Bruce, L., Smith, G. L., & Hasenfuss, G. (2001). Overexpression of FK506-binding protein FKBP12.6 in cardiomyocytes reduces ryanodine receptor-mediated Ca(2+) leak from the sarcoplasmic reticulum and increases contractility. *Circ.Res.* **88**, 188-194.

Rizzuto R, Bernardi P, & Pozzan T (2000). mitochondria as all round players of the calcium game. *Journal of Physiology* **529**, 37-47.

Robert, V., De Giorgi, F., Massimino, M. L., Cantini, M., & Pozzan, T. (1998). Direct monitoring of the calcium concentration in the sarcoplasmic and endoplasmic reticulum of skeletal muscle myotubes. *J.Biol.Chem.* **273**, 30372-30378.

Robert, V., Gurlini, P., Tosello, V., Nagai, T., Miyawaki, A., Di Lisa, F., & Pozzan, T. (2001). Beat-to-beat oscillations of mitochondrial [Ca2+] in cardiac cells. *EMBO J.* **20**, 4998-5007.

Saiki, Y. & Ikemoto, N. (1997). Fluorescence probe study of the lumenal Ca2+ of the sarcoplasmic reticulum vesicles during Ca2+ uptake and Ca2+ release. *Biochem.Biophys.Res.Commun.* **241**, 181-186.

Shannon, T. R. & Bers, D. M. (1997). Assessment of intra-SR free [Ca] and buffering in rat heart. *Biophys.J.* **73**, 1524-1531.

Shmigol, A. V., Eisner, D. A., & Wray, S. (1999). The role of the sarcoplasmic reticulum as a Ca2+ sink in rat uterine smooth muscle cells. *J.Physiol* **520 Pt 1**, 153-163.

Shmigol, A. V., Eisner, D. A., & Wray, S. (2001). Simultaneous measurements of changes in sarcoplasmic reticulum and cytosolic. *J.Physiol* **531**, 707-713.

Singh Bhogal M & Colyer J (1998). Depletion of Ca from the SR of cardiac muscle prompts phosphorylation of phospholamban to stimulate store refilling. *Proceedings of the National Academy of Sciences USA* **95**, 1484-1489.

Smith, G. L., Duncan, A. M., Neary, P., Bruce, L., & Burton, F. L. (2000). P(i) inhibits the SR Ca(2+) pump and stimulates pump-mediated Ca(2+) leak in rabbit cardiac myocytes. *Am.J.Physiol Heart Circ.Physiol* **279**, H577-H585.

Szegedi C, Sarkozi S, Herzog A, Jona I, & Varsany M (1999). Calsequestrin: more than 'only' a luminal Ca^{2+} buffer inside the SR. *Biochemical Journal* **337**, 19-22.

Tada, M. & Toyofuku, T. (1996). SR Ca(2+)-ATPase/phospholamban in cardiomyocyte function. *J.Card Fail.* **2**, S77-S85.

Timerman, A. P., Onoue, H., Xin, H. B., Barg, S., Copello, J., Wiederrecht, G., & Fleischer, S. (1996). Selective binding of FKBP12.6 by the cardiac ryanodine receptor. *J.Biol.Chem.* **271**, 20385-20391.

Tripathy, A. & Meissner, G. (1996). Sarcoplasmic reticulum lumenal Ca2+ has access to cytosolic activation and inactivation sites of skeletal muscle Ca2+ release channel. *Biophys.J.* **70**, 2600-2615.

Tsien RY (1998). The Green Fluorescent Protein. *Annual Review of Physiology* **67**, 509-544.

Valdivia, H. H. (1998). Modulation of intracellular Ca2+ levels in the heart by sorcin and FKBP12, two accessory proteins of ryanodine receptors. *Trends Pharmacol.Sci.* **19**, 479-482.

Villarreal, F. J., Lee, A. A., Dillmann, W. H., & Giordano, F. J. (1996). Adenovirus-mediated overexpression of human transforming growth factor-beta 1 in rat cardiac fibroblasts, myocytes and smooth muscle cells. *J.Mol.Cell Cardiol.* **28**, 735-742.

Westfall, M. V., Rust, E. M., & Metzger, J. M. (1997). Slow skeletal troponin I gene transfer, expression, and myofilament incorporation enhances adult cardiac myocyte contractile function. *Proc.Natl.Acad.Sci.U.S.A* **94**, 5444-5449.

Williams, A. J. & Ashley, R. H. (1989). Reconstitution of cardiac sarcoplasmic reticulum calcium channels. *Ann.N.Y.Acad.Sci.* **560**, 163-173.

Xiao, R. P., Valdivia, H. H., Bogdanov, K., Valdivia, C., Lakatta, E. G., & Cheng, H. (1997). The immunophilin FK506-binding protein modulates Ca2+ release channel closure in rat heart. *J.Physiol* **500 (Pt 2)**, 343-354.

Xin, H. B., Rogers, K., Qi, Y., Kanematsu, T., & Fleischer, S. (1999). Three amino acid residues determine selective binding of FK506-binding protein 12.6 to the cardiac ryanodine receptor. *J.Biol.Chem.* **274**, 15315-15319.

Xu L & Meissner G (1998). Regulation of cardiac muscle Ca release channel by sarcoplasmic reticulum lumenal Ca. *Biophysical Journal* **75**, 2302-2312.

Zhou, Z., Matlib, M. A., & Bers, D. M. (1998). Cytosolic and mitochondrial Ca2+ signals in patch clamped mammalian ventricular myocytes. *J.Physiol* **507 (Pt 2)**, 379-403.